The Dissertation Committee for Thomas David Novlan
certifies that this is the approved version of the following dissertation:

Fractional Frequency Reuse for Multi-Tier Cellular Networks

Committee:

Jeffrey G. Andrews, Supervisor

Arunabha Ghosh

Todd E. Humphreys

Theodore S. Rappaport

Gustavo de Veciana

Fractional Frequency Reuse for Multi-Tier Cellular Networks

by

Thomas David Novlan, B.S.E.E., M.S.E.

DISSERTATION

Presented to the Faculty of the Graduate School of

The University of Texas at Austin

in Partial Fulfillment

of the Requirements

for the Degree of

DOCTOR OF PHILOSOPHY

THE UNIVERSITY OF TEXAS AT AUSTIN

May 2012

In loving memory of my grandparents John and Lucille Novlan and Dennis and Mary Jo Hulse.

Acknowledgments

I would first like to thank my supervisor Prof. Jeffrey Andrews for inspiring me to pursue a Ph.D. in wireless communications from the beginning in his undergraduate Signals and Systems course, opening the door for countless rewarding opportunities, and for his encouragement during my time at UT. I also would like to thank the members of my committee, Dr. Arunabha Ghosh, Prof. Todd E. Humphreys, Prof. Theodore S. Rappaport, and Prof. Gustavo de Veciana, for their helpful advice and constructive feedback on my research. I would like to acknowledge AT&T Labs for supporting my research over the past three years and thank David Wolter for bringing me on as an intern during 2011-12. Also I thank Arunabha Ghosh, Arvind Raghavan, Milap Majmundar, and Rich Kobylinski for making me feel welcome as part of the Radio Technology Group and for sharing their practical perspectives on wireless communications engineering. Thanks to all my many friends and colleagues at UT over the years for insightful discussions, fruitful collaborations, and camaraderie. I would like to thank my parents, David and Linda Novlan, for their unconditional love and for fostering in me a spirit of creativity and curiosity. Special thanks and appreciation are for my wonderful wife and best friend Sarah for her continual patience, love, and encouragement these past 5 years, I could not have accomplished this without her. Finally, this is done in humble acknowledgment of Colossians 3:17, "'And whatever you do, whether in word or deed, do it all in the name of the Lord Jesus, giving thanks to God the Father through him."'

Fractional Frequency Reuse for Multi-Tier Cellular Networks

Publication No. _____

Thomas David Novlan, Ph.D.
The University of Texas at Austin, 2012

Supervisor: Jeffrey G. Andrews

Modern cellular systems feature increasingly dense base station deployments, augmented by multiple tiers of access points, in an effort to provide higher network capacity as user traffic, especially data traffic, increases. The primary limitation of these dense networks is co-channel interference. The primary source of interference is inter-cell and cross-tier interference, which is especially limiting for users near the boundary of the cells. Inter-cell interference coordination (ICIC) is a broad umbrella term for strategies to improve the performance of the network by having each cell allocate its resources such that the interference experienced in the network is minimized, while maximizing spatial reuse. Fractional frequency reuse (FFR) has been proposed as an ICIC technique in modern wireless networks. The basic idea of FFR is to partition the cell's bandwidth so that (i) cell-edge users of adjacent cells do not interfere with each other and (ii) interference received by (and created by) cell-interior users is reduced, while (iii) improving spectral reuse compared to conventional frequency reuse. It is attractive for its intuitive implementation and relatively low network coordination requirements compared to other ICIC strategies including interference cancellation, network MIMO, and opportunistic scheduling. There are

two common FFR deployment modes: Strict FFR and Soft Frequency Reuse (SFR). This dissertation identifies and addresses key technical challenges associated with fractional frequency reuse in modern cellular networks by utilizing an accurate yet tractable model of both the downlink (base station to mobile) and uplink (mobile to base station) based on the Poisson point process for modeling base station locations. The resulting expressions allow for the development of system design guidelines as a function of FFR parameters and show their impact on important metrics of coverage, rate, power control, and spectral efficiency. This new complete analytical framework addresses system design and performance differences in the uplink and downlink. Also, this model can be applied to cellular networks with multiple tiers of access points, often called heterogeneous cellular networks. The model allows for analysis as a function of system design parameters for users under Strict FFR and SFR with closed and open access between tiers.

Table of Contents

List of Tables

List of Figures

Chapter 1

Introduction

As wireless network traffic, especially web and video data traffic, exponentially increases, expectations of ubiquitous coverage and quality-of-experience are also growing, and system designers are faced with the challenge of balancing fairness with demands for high spectral efficiency. As a result, modern cellular systems feature increasingly dense base station deployments, augmented by multiple tiers of access points, in an effort to provide higher network capacity. These smaller cells, along with so-called hotspot-aided architectures, allow for greater spatial reuse of spectrum [23]. The primary limitation of these dense networks is co-channel interference [45]. Because of the soon ubiquitous use of Orthogonal Frequency Division Multiple Access (OFDMA) in these networks, the intra-cell users are assumed to be orthogonal to each other and the primary source of interference is inter-cell and cross-tier interference, which is especially limiting for users near the boundary of the cells. Inter-cell interference coordination (ICIC) is a broad umbrella term for strategies to improve the performance of the network by having each cell allocate its resources such that the interference experienced in the network is minimized, while maximizing spatial reuse [18].

We start this introduction chapter with a brief description of different ICIC approaches in modern cellular networks and motivate the use of one technique in particular, Fractional Frequency Reuse (FFR). We then discuss the challenges of

accurately modeling these networks, in particular the interference, for the purpose of FFR system design which is the primary focus of this dissertation. Finally, a summary of the contributions of this dissertation is provided along with chapter organization.

1.1 ICIC Techniques

Mitigating interference through resource allocation has been an aspect of even some of the earliest cellular networks [39]. Per-cell frequency reuse in the case of frequency-division multiple access (FDMA) or time-slot reuse in the case of time-division multiple access (TDMA) are the two most notable examples [37]. A resource allocation plan could be developed for a network such that neighboring base stations would operate using orthogonal time or frequency resources. The number of available resources is determined by the reuse factor. A higher reuse factor would allow a greater number of cells to operate orthogonally from one another, drastically reducing the amount of inter-cell interference in the network [90]. However as data rate requirements and user traffic grow exponentially especially in urban areas, network operators are under pressure to utilize as much bandwidth in each cell as possible and universal frequency reuse is the default deployment strategy [96].

1.1.1 Interference Cancellation

Another approach for for managing interference is not to avoid it, but to exploit knowledge of the interfering signals at the receiver. The concept of multi-user detection and interference cancellation has been a well-studied topic for wireless communication systems for over 20 years [9, 83, 105]. The basic idea requires base stations to acquire or estimate the channel response and data for an interfering user, regenerating the interfering signal, and then subtract it from the desired signal.

A drawback of interference cancellation is the high complexity and cost of implementation. This arises from the exponential scaling with the number of users and the high sensitivity to the accuracy of channel and interfering signal estimation. Another non-trivial consideration is the requirement for real-time exchange of information between cooperating base stations or mobiles which places limits on the potential gains due to delay [9, 49]. As a result interference cancellation in modern standards such as 3GPP LTE is proposed to be for deterministic signals known *a priori*, such as pilot signals used for synchronization and channel estimation [5, 18].

1.1.2 CoMP

The use of multiple-input multiple-output (MIMO) antenna techniques have served as one of the major enabling technologies for wireless communication networks in the past decade, both in terms of improving link reliability and increasing potential data rates. While initially MIMO techniques were mostly applied to single-link scenarios, in cellular networks they can also be applied at the network level. The idea of multiple base stations coordinating their transmissions in order to simultaneously serve multiple users has been given different names including Network MIMO, Multi-Cell MIMO, and in the context of the 3GPP LTE-Advanced standard, Coordinated Multiple Point Transmission and Reception (CoMP). Using the optimal technique of dirty paper coding (DPC) or even a suboptimal linear precoding technique, if base stations have complete information about the users' channels they can jointly design their MIMO codebooks to eliminate or greatly reduce inter-cell interference [57, 60, 100] with the strongest gains for users typically at the cell edge now at the center of the coordinating base station cluster [119].

The main challenges are centered around very low latency and high bandwidth

backhaul required for CoMP to be realized, which is a constraint that is compounded even further in heterogeneous networks where macrocell base stations and potentially a much larger number of lower-tier base stations need to be interconnected in order to share channel and user data information [65]. Also the achievable gains are highly sensitive to channel environment/estimation and were found to be very modest in recent field trials compared to theory [56].

1.1.3 Dynamic/Opportunistic Resource Allocation

One very significant feature of modern networks based on standards such as WiMAX and LTE is in the very flexible time/frequency resource allocation afforded through the use of OFDMA. Users in LTE for example can be assigned different resource blocks every millisecond and algorithms take past performance, different traffic classes, and current channel conditions in account to maximize throughput [45, 92]. Extending these algorithms from a single base station to the network context with significant inter-cell coordination has been shown to theoretically provide gains, especially for the users at the cell-edge since resources can be allocated to minimize interference from the coordinating base stations or users [27, 64, 71, 96].

These techniques are an important component of future wireless standards such as 3GPP LTE-Advanced as a component of self-organizing networks envisioned to manage the complexity of operation as the number of active access points grows dramatically [2]. For example, mechanisms for sharing basic information about users or base stations receiving strong interference is being standardized in 3GPP-LTE for use in future networks [1]. However fully dynamic and opportunistic techniques still face challenges in practical systems due to imperfections in channel estimation and feedback [32] and latency/throughput requirements on backhual networks [73,

116], similar to the challenges faced by other coordination-based ICIC techniques like CoMP [65]. Promising research on the use of machine-learning techniques for ICIC may in the future lead to more scalable and distributed approaches [16, 42, 86].

1.2 Fractional Frequency Reuse

Fractional frequency reuse (FFR) is a modification of the traditional per-cell frequency reuse used extensively in cellular networks [15, 102]. The basic idea of FFR is to partition the cell's bandwidth so that (i) cell-edge users of adjacent cells do not interfere with each other and (ii) interference received by (and created by) cell-interior users is reduced, while (iii) improving spectral reuse compared to conventional frequency reuse. Due to its intuitive implementation and relatively low network coordination requirements compared to other ICIC strategies [18], it has been accepted as part of the 4G cellular standards IEEE 802.16m (WiMAX) and Third Generation Partnership Program Long Term Evolution (3GPP-LTE) [45, 52, 96].

The use of FFR leads to natural tradeoffs between improvement in rate and coverage for cell-edge users and sum network throughput and spectral efficiency. These are important metrics to consider, especially for users at the cell-edge since modern cellular networks are increasingly required to provide users with high data-rate and guaranteed quality-of-service, regardless of their geographic location, instead of simply a minimum SINR which may be acceptable for applications like voice traffic.

There are two common FFR deployment modes: *Strict FFR* and *Soft Frequency Reuse* (SFR).

Strict FFR: Fig. 1.1(a) illustrates a Strict FFR deployment with a cell-edge reuse factor of $\Delta = 3$ and cells modeled as a hexagonal grid. Users in a pre-defined

cell-interior are allocated a common sub-band of frequencies while cell-edge users' bandwidth is partitioned across cells based on a reuse factor of Δ. In total, Strict FFR thus requires a total of $\Delta+1$ sub-bands. Interior users do not share any spectrum with edge users, which reduces interference for both interior users and cell-edge users.

SFR: Fig. 1.1(b) illustrates a SFR deployment with a reuse factor of $\Delta = 3$ on the cell-edge. SFR employs the same cell-edge bandwidth partitioning strategy as Strict FFR, but the interior users are allowed to share sub-bands with edge users in other cells. Because cell-interior users share the bandwidth with neighboring cells, they typically transmit at lower power levels than the cell-edge users [55, 70]. While SFR is more bandwidth efficient than Strict FFR, it results in more interference to both cell-interior and edge users [78].

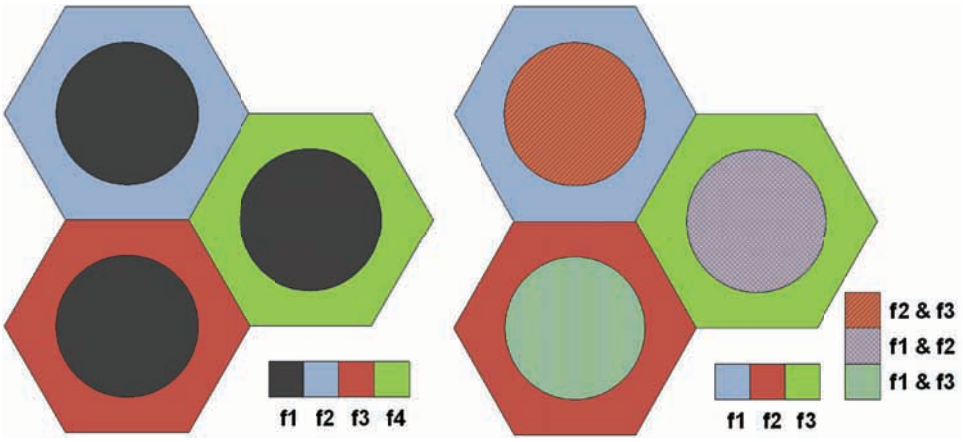

Figure 1.1: Strict FFR (left) and SFR (right) deployments with $\Delta = 3$ cell-edge reuse factor in a standard hexagonal grid model.

1.3 Modeling of cellular networks

Modeling the downlink and uplink of cellular networks poses significant technical challenges due to the interdependence between mobile and base station locations, transmit powers, and the resulting interference distribution. One approach for analysis of the uplink has been to use the Wyner model [110]. It is attractive for its analytical simplicity, wherein gains between users and base stations are normalized by the desired link and inter-cell interference is either a constant value or a single random variable. Historically popular for evaluating CDMA-based networks, this model is still used to evaluate performance from an information-theory perspective [69, 82, 95, 98, 99]. However, in [115] the applicability and accuracy of the model is shown to be limited to scenarios where the interference can be spatially averaged, for example a CDMA network uplink under high load. This type of interference averaging approach wherein inter-cell interference is assumed to be fixed is not a valid assumption for modern cellular systems where typically only a single user per cell (or sector) is active in a given resource block.

On the other extreme from the Wyner model, BSs are commonly modeled in a deterministic grid-based deployment, e.g. the popular hexagonal grid model. This approach does not lead to a tractable framework and results are based upon several simplifying approximations followed by exhaustive Monte Carlo simulations. Perhaps more importantly, the grid model does not reflect modern network topologies, which have highly variable cell sizes and opportunistic placement of new infrastructure due to topographic, demographic, or economic reasons [14], [19], [47].

The inadequacy of existing approaches has led to an increased interest in the use of random spatial models for the network topology [47]. An advantage of this new

approach is the ability to derive tractable expressions leading to more general performance characterizations and intuition for single-tier and multi-tier wireless communication networks [10, 14, 19, 30, 44, 54, 76, 81]. Recently [10] showed that a completely random (Poisson) placement of base stations was about as accurate as a grid model, and sometimes more so, when compared to a large modern cellular network.

Figs. 1.2(a)-1.2(c) compare a hexagonal grid model and a realization of Poisson distributed base stations with actual location data of an urban 4G deployment provided by a major service provider. This visual comparison exemplifies the non-uniformity of modern deployments and provides intuition and motivation for the use of the PPP model as opposed to the grid model.

Under the grid model assumption, contours of constant coverage probability can be defined as concentric circles around the central base station when averaged over the fading distribution of user signals, leading to a homogeneous experience throughout the network. However, in practice coverage areas of different cells are non-uniform in area which significantly impact the distribution of the desired signal and the interference. The ability of a random spatial model to capture this disparity is evident in Fig. 1.3 which presents a realization of a Poisson distributed cellular network with base stations centered in their respective Voronoi cells. Darker and lighter coverage regions (averaged over fading) are defined by SINR thresholds of 5 dB and 0 dB respectively. As will be discussed throughout this dissertation, this non-uniformity in coverage influences the percentage of users at the cell-edge who experience the most serious interference which in turn has significant implications on the performance of FFR in the uplink and downlink.

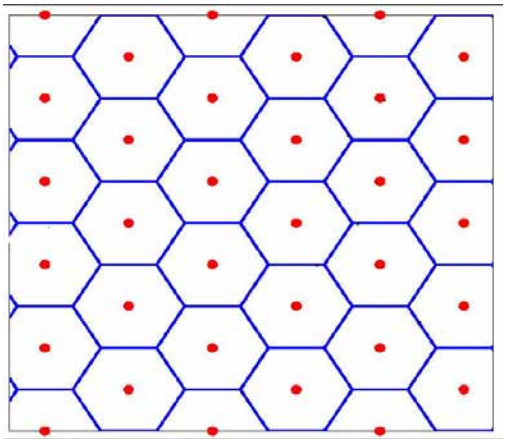

(a) Grid

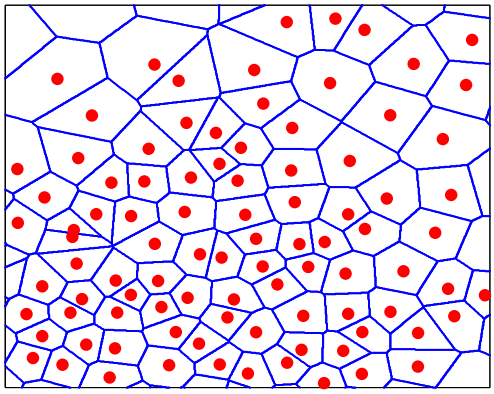

(b) Actual locations

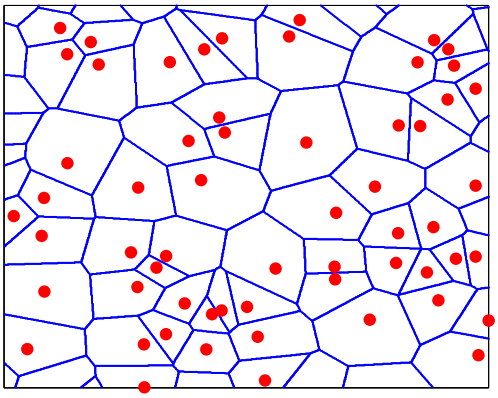

(c) PPP

Figure 1.2: Voronoi cell-based coverage regions for (a) grid, (b) Actual base station locations, and (c) PPP.

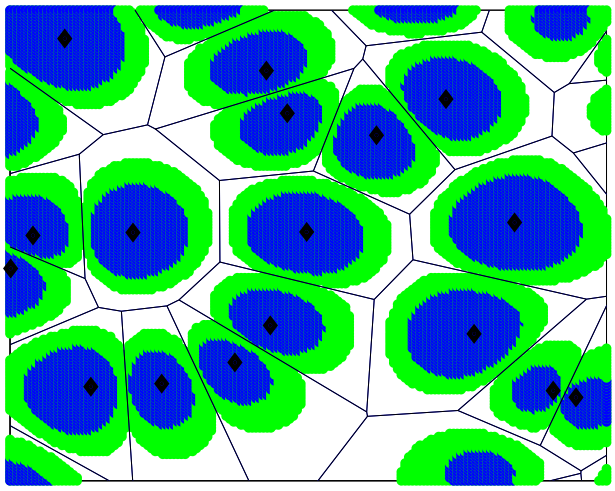

Figure 1.3: A realization of a Poisson distributed cellular network. Darker and lighter coverage regions are defined by SINR thresholds of 5 dB and 0 dB respectively.

1.4 Contributions

This dissertation addresses key technical challenges associated with utilizing fractional frequency reuse in modern heterogeneous cellular networks. An accurate yet tractable model of both the downlink and uplink allows for fundamental research on the system design challenges facing modern cellular networks. The following are the contributions of my dissertation:

Fractional frequency reuse for downlink cellular networks: The derivation of a tractable analytical model for analyzing FFR in the OFDMA cellular downlink wherein the base station locations are modeled as a Poisson point process. The resulting SINR distributions allow us to derive system design guidelines as a function of FFR design parameters and show their impact on important metrics of coverage, rate, and spectral efficiency. Also the analytical expressions are compared with

simulations utilizing the traditional grid model as well as those of actual network deployments.

FFR in multi-tier network downlinks: Next, the model is extended to the downlink of cellular networks with multiple tiers of access points, often called heterogeneous cellular networks. We derive the SINR distributions for users under Strict FFR and SFR with closed and open access models. Again, the tractable model allows for analysis as a function of the system design parameters of these networks. In particular we highlight the interdependence between user association and FFR parameters.

Analytical modeling of the cellular uplink: To complete the analytical framework we extend the Poisson model to model the uplink of cellular networks. There are several fundamental differences relative to the downlink, including practical considerations of power control, user mobility. How the system design guidelines change compared to the downlink is addressed and the expressions are compared with other modeling approaches.

FFR in for uplink cellular networks: Finally, the analytical model of the previous chapter is extended to allow the evaluation of uplink cellular networks utilizing fractional power control and FFR through the derivation of the SINR distribution of cell-edge and cell-interior users as a function of network and FFR system parameters. General insights are presented for the metrics of coverage probability, average rate, resource allocation, transmit power, and the interdependence of system design parameters.

1.5 Organization

Chapter 2 describes a framework for the analysis of the relative merits of FFR strategies and the development of system design guidelines for cellular networks. Chapter 3 proposes an extension of the framework for analysis of downlink coverage and rate for FFR strategies in multi-tier cellular networks. In Chapter 4 a new analytical model for the cellular uplink is presented and evaluated for networks not utilizing FFR. Chapter 5 then applies the model of Chapter 4 to FFR in the uplink and evaluates the metrics of coverage, rate, and transmit power. The dissertation concludes with a summary and discussion of future work in Chapter 6.

Chapter 2

FFR in the Downlink of OFDMA Cellular Networks

Faced with increased traffic demands in interference limited cellular networks, fractional frequency reuse is an attractive strategy due to its low complexity of implementation and significant gains in performance it provides for the bottom percentile of network users. This chapter presents a new model for FFR which allows for tractable analysis of the coverage and rate for average users in networks utilizing the two most common FFR deployments: Strict FFR and SFR. The key feature is that using a random, Poisson distribution for base station location overcomes the challenges faced by analysis using a deterministic grid model while also attempting to capture the non-regularity of modern deployments. We show that the Poisson model compares favorably when compared with an actual deployment and a uniform grid model. Finally this chapter presents system design guidelines for fractional frequency reuse based on the insights provided by the analysis. The insight obtained from the analysis can be used to design algorithms which efficiently allocate sub-bands to provide increased coverage to edge users for given traffic load or coverage requirements.

2.1 Related Work

Recent research on FFR has focused on the optimal design of FFR systems by utilizing advanced techniques such as graph theory [24], Markov processes [34],

and convex optimization [12, 13] to maximize network throughput. Additional work considers scheduling [6, 38, 88] of users for the different sub-bands and the authors determine the frequency partitions in a two-stage heuristic approach. Joint load-balancing and Strict FFR design, termed partial frequency reuse by the authors in [101], considers the metric of expected throughput rather than solely signal strength to develop a user association algorithm. The authors present numerical simulations for a hexagonal network to illustrate the significant throughput gains from this strategy, especially for non-uniform traffic loads.

The authors of [114] analyze the capacity and empirical pdfs of the SINR in the uplink and downlink of cellular networks utilizing a modified SFR strategy termed enhanced fractional frequency reuse (EFFR) which allows for more than two user classifications, a similar approach to [51]. They create a third partition of middle-users to allow increased control over the power control to mitigate interference.

A comparison in [103] of two dynamic SFR algorithms for the downlink, Multi-sector Gradient (MGR) and Sector Autonomous (SA), is done via system simulation. The MGR algorithm utilizes inter-BS coordination to improve the user subband selection, while the SA algorithm uses a more involved heuristic for scheduling, but requires no coordination. Both algorithms are shown to outperform universal reuse, with the MGR algorithm providing the greatest throughput improvement for uniform or non-uniform user distributions.

However these along with other related works [7, 26, 40, 63, 112] utilize the standard equally-spaced grid model for the base stations which do not result in closed or intuitive expressions for SINR, probability of coverage (or outage), or rate, and numerical simulations are used to validate the proposed model or algorithm.

Actual data from a cellular network deployment in Berlin, Germany and Lisbon, Portugal is used as the basis for a numerical evaluation of FFR in [26]. They note the heterogeneous nature of the coverage regions and how it differs from the standard hexagonal grid model. They focus on determining the resource partitions between edge and inner users similar to [12, 78] on a per-cell basis. However no tractable analysis is provided and the simulation results provided are dependent on the network realization and does not give general insight into system design.

2.2 Contributions

As previously mentioned, most prior work resorted to simulations to evaluate the performance of FFR, primarily because of the intractability of the hexagonal grid model of base station locations. This includes my initial work on FFR which evaluated the system design of Strict FFR and SFR on the basis of a grid model and numerical results [78]. In this chapter, instead, we model the BS locations as a Poisson point process (PPP). One advantage of this approach is the ability to capture the non-uniform layout of modern cellular deployments due to topographic, demographic, or economic reasons [14], [19], [47]. Additionally, tractable expressions can be drawn from the Poisson model, leading to more general performance characterizations and intuition [8].

The two key contributions of this chapter can be summarized as:

Analytical model for coverage and rate: First we present a new analytical framework to evaluate coverage probability and average rate in Strict FFR and SFR systems. Through a comparison with an actual urban base station deployment, we show that the grid model provides an upper bound for actual performance since

it idealizes real network geometry, while our framework, based on the Poisson model is a lower bound.

System design guidelines: In addition, by considering a special case relevant to interference-limited networks, the analytical expressions for the SINR distributions reduce to simple expressions, from which we develop system guidelines which show that while Strict FFR provides better coverage probability for edge users than SFR for low power control factors, a SFR system can improve its coverage performance by increasing the cell-edge user power control factor, without the loss in spectral efficiency that is inherent in Strict FFR. Finally, this chapter presents a strategy for allocating frequency sub-bands to edge users for SFR and FFR based on a chosen threshold T_{FR}, which can be related to network traffic load or coverage requirements.

2.3 System Model

In a OFDMA cellular downlink, we assume a user y is served by its closest base station. Without loss of generality, we assume this typical mobile user y to be at the origin. The associated Signal to Interference Plus Noise Ratio (SINR) is given as

$$\mathrm{SINR} = \frac{P g_y r^{-\alpha}}{\sigma^2 + P I_{\mathcal{Z}}}, \tag{2.1}$$

where for an interfering BS set $\mathcal{Z}$,

$$I_{\mathcal{Z}} = \sum_{z \in \mathcal{Z}} G_z {R_z}^{-\alpha}. \tag{2.2}$$

The locations of the base stations are modeled as independent spatial Poisson point processes (PPP) [104] of density λ. The nearest BS is at a distance r. From the

properties of PPPs, it follows that r is Rayleigh distributed [104]. We assume that all the BSs transmit with an equal power P and σ^2 is the noise power. We consider distance dependent path loss $|x|^{-\alpha}$ with path loss exponent α. We assume that the small-scale fading between any pair of nodes is i.i.d exponentially distributed with mean μ (corresponds to Rayleigh fading). This assumption provides greater clarity for the following analysis, however as in [8], these results can be extended to other general fading distributions including log-normal shadowing. The set of interfering APs in the k^{th} tier is $\mathcal{Z}_k$, i.e. access points that use the same sub-band as the mobile user. We denote the distance between the interfering AP and the mobile node in consideration by R_z. Lower case random variables are those associated with the serving AP, while their capital counterparts represent the terms associated with the interference.

Additionally, Strict FFR and SFR classify two types of users: *edge* and *interior* users. These classifications come from the typical grid model assumption for the base stations in which constant SINR contours can be defined as concentric circles around the central base station [51]. In this chapter however, since the BSs are distributed as a PPP, the term edge or interior user does not necessarily have the same geographic interpretation. Each cell is a Voronoi region with a random area [47] which, as noted in [19], more closely reflects actual deployments which are highly non-regular and provides a lower bound on performance metrics due to the lack of repulsion between base stations, which may be arbitrarily close together. Instead, a more general case is considered, in which a base station classifies users with average SINR less than a pre-determined threshold T_{FR} as edge users, while users with average SINR greater than the threshold are classified as interior users. This also does not require knowledge of the user locations. Thus the FFR threshold T_{FR} is a design parameter analogous to

the grid-based interior radius [78].

2.3.1 Resource Allocation for FFR

Much of the research on FFR system design has focused on how to determine the size of the frequency partitions [7, 12, 26, 78]. For example, in a typical LTE system with a bandwidth of 10 MHz, 50 sub-bands may be available to simultaneously serve up to 50 users per cell, each one with a bandwidth of 200 kHz [45], further divided into a smaller number of OFDM subcarriers based on the FFT size. Given a reuse factor of Δ and N_{band} total sub-bands available to the cell and assuming one sub-band per user, the allocation of sub-bands for interior users N_{int} and edge users N_{edge} is given as

$$N_{\text{edge}} = \lfloor (N_{\text{band}} - N_{\text{int}})/\Delta \rfloor \tag{2.3}$$

For SFR, all the sub-bands are reallocated in the cell, although the partitioning of sub-bands between edge and interior users is given as

$$N_{\text{int}} = N_{\text{band}} - N_{\text{edge}} \tag{2.4}$$

$$\text{where } N_{\text{edge}} \leq N_{\text{band}}/\Delta \tag{2.5}$$

From these equations we note that one of the advantages of SFR over Strict FFR is the ability to achieve 100% allocation, the same as universal reuse, due to the sharing of resources between interior and edge users. However, this results in a tradeoff between SINR improvement for edge users and network spectral efficiency.

2.4 Coverage Probability and Rate

This section presents general coverage probability expressions and numerical results for the two FFR systems. Coverage is an important metric to consider since

it can have a large impact on cell-edge user QoS and when combined with resource efficiency, can give an overall picture of cell/network capacity. In the context of this paper, we define coverage probability as the probability that a user's instantaneous SINR is greater than a value T:

$$\mathbb{P}(\text{SINR} > T) \tag{2.6}$$

This coverage probability is equivalently the CCDF of the SINR for a particular reuse strategy, which we will denote as $\bar{F}(T)$.

In the case of past work, using the grid model, base stations are assumed to be on a hexagonal or rectangular grid, allowing these expressions to be numerically computed [90]. Also, approximations using the symmetric structure of the far-out tiers in the deployment may be employed, or a worst-case user location at the edge of the cell may be considered [35]. However, the results of this section take advantage of the framework recently developed in [8]. The base station locations are instead modeled as a Poisson point process (PPP). Despite the new source of randomness in the model, the authors of [8] give a general expression for the coverage probability of a typical mobile as a function of the SINR threshold T for a given base station density λ, pathloss factor α and Δ number of frequency sub-bands, which we extend now to provide the distribution of SINR for Strict FFR and SFR.

For completeness, we now review the model, and state the main result of [8]. As in our model, in [8], the BSs are assumed to be distributed as a spatial PPP with density λ. Each BS is assumed to transmit in a frequency sub-band picked randomly from the set $\{1, 2, \ldots, \Delta\}$. Mobile users are associated with their nearest BS. The following Theorem provides the coverage probability of a typical mobile user in this network.

Theorem 1 (PPP, [8]). *When the BSs are distributed as a PPP of density λ and are allocated one of the Δ frequency sub-bands randomly, the coverage probability of a typical mobile user in the downlink is*

$$p_c(T,\lambda,\alpha,\Delta) = \pi\lambda \int_0^\infty e^{-\pi\lambda v(1+\frac{1}{\Delta}\rho(T,\alpha))-\mu T\frac{\sigma^2}{P}v^{\alpha/2}}\mathrm{d}v, \tag{2.7}$$

where

$$\rho(T,\alpha) = T^{2/\alpha}\int_{T^{-2/\alpha}}^\infty \frac{1}{1+u^{\alpha/2}}\mathrm{d}u. \tag{2.8}$$

Proof. Please refer to [8]. □

The coverage probability is particularly simple when $\sigma^2 = 0$, *i.e.,* an interference-limited network. In this case, the coverage probability equals $(1+\Delta^{-1}\rho(T,\alpha))^{-1}$, and we immediately observe the improvement in the coverage with increasing Δ. In [8], the average ergodic rate is also provided and shown to decrease with increasing Δ, further validating the model.

In this chapter, we extend this model to analyze FFR in cellular systems. Without FFR, a mobile tries to connect to its nearest BS and is in coverage if it is connected. With FFR, a mobile computes its SINR to the nearest BS, and if it is less than the threshold T_{FR}, then the BS chooses to transmit in a different FFR band randomly picked from Δ sub-bands reserved for the FFR users. If such a shift occurs, we term the mobile as a cell-edge user and as an interior user otherwise. Observe that the coverage (especially for the cell-edge users) depends on two SINR values, first the SINR on the common sub-band to determine its status (cell-edge or not), and second the actual SINR on the newly allocated sub-band. These two values of SINR are correlated since the interference is generated by the same set of nodes,

and this makes the analysis challenging. In the next subsection, we now provide the distribution of SINR for Strict FFR and SFR.

2.4.1 Probability of coverage with Strict FFR

The first result using the Poisson model focuses on the SINR distribution of cell edge users. In the case of Strict FFR, an edge user y with SINR $< T_{\mathrm{FR}}$ on the common sub-band is instead assigned a FFR sub-band δ_y, where $\delta \in \{1, ..., \Delta\}$ with uniform probability $\frac{1}{\Delta}$, and experiences new fading power $\hat{g_y}$ and out-of-cell interference $\hat{I_{\mathcal{Z}}}$, instead of g_y and $I_{\mathcal{Z}}$.

Theorem 2 (Strict FFR, edge user)**.** *The CCDF of the edge user* SINR *is given by*

$$\begin{aligned}\bar{\mathrm{F}}_{\mathrm{FFR,e}}(T) &= \mathbb{P}\left(\frac{P\hat{g}_y r^{-\alpha}}{\sigma^2 + P\hat{I_{\mathcal{Z}}}} > T \;\middle|\; \frac{Pg_y r^{-\alpha}}{\sigma^2 + PI_{\mathcal{Z}}} < T_{\mathrm{FR}}\right) \\ &= \frac{p_c(T,\lambda,\alpha,\Delta) - \pi\lambda \int_0^\infty e^{-\pi\lambda v(1+2\xi(T,T_{\mathrm{FR}},\alpha,\Delta)) - \mu(T+T_{\mathrm{FR}})\frac{\sigma^2}{P}v^{\alpha/2}} \mathrm{d}v}{1 - p_c(T_{\mathrm{FR}},\lambda,\alpha,1)}, \quad (2.9)\end{aligned}$$

where

$$\xi(T, T_{\mathrm{FR}}, \alpha, \Delta) = \int_1^\infty \left[1 - \frac{1}{1 + T_{\mathrm{FR}} x^{-\alpha}} \left(1 - \frac{1}{\Delta}\left(1 - \frac{1}{1 + Tx^{-\alpha}}\right)\right)\right] x \mathrm{d}x,$$

and $p_c(T, \lambda, \alpha, \Delta)$ *is given by* (2.7)*.*

Proof. A user y with SINR $< T_{\mathrm{FR}}$ is given a FFR sub-band δ_y, where $\delta \in \{1, ..., \Delta\}$ with uniform probability $\frac{1}{\Delta}$, and experiences new fading power $\hat{g_y}$ and out-of-cell interference $\hat{I_{\mathcal{Z}}}$, instead of g_y and $I_{\mathcal{Z}}$. The CCDF of the edge user $\bar{\mathrm{F}}_{\mathrm{FFR,e}}(T)$ is conditioned on its previous SINR,

$$\bar{\mathrm{F}}_{\mathrm{FFR,e}}(T) = \mathbb{P}\left(\frac{P\hat{g}_y r^{-\alpha}}{\sigma^2 + P\hat{I_{\mathcal{Z}}}} > T \;\middle|\; \frac{Pg_y r^{-\alpha}}{\sigma^2 + PI_{\mathcal{Z}}} < T_{\mathrm{FR}}\right). \quad (2.10)$$

Using Bayes' rule we have,

$$\bar{\mathrm{F}}_{\mathrm{FFR,e}}(T) = \frac{\mathbb{P}\left(\frac{P\hat{g_y}r^{-\alpha}}{\sigma^2+P\hat{I_{\mathcal{Z}}}} > T \ , \frac{Pg_yr^{-\alpha}}{\sigma^2+PI_{\mathcal{Z}}} < T_{\mathrm{FR}}\right)}{\mathbb{P}\left(\frac{Pg_yr^{-\alpha}}{\sigma^2+PI_{\mathcal{Z}}} < T_{\mathrm{FR}}\right)}. \tag{2.11}$$

Since $\hat{g_y}$ and g_y are i.i.d. exponentially distributed with mean μ, this gives

$$\frac{\mathbb{P}\left(\frac{P\hat{g_y}r^{-\alpha}}{\sigma^2+P\hat{I_{\mathcal{Z}}}} > T \ , \frac{Pg_yr^{-\alpha}}{\sigma^2+PI_{\mathcal{Z}}} < T_{\mathrm{FR}}\right)}{\mathbb{P}\left(\frac{Pg_yr^{-\alpha}}{\sigma^2+PI_{\mathcal{Z}}} < T_{\mathrm{FR}}\right)} = \frac{\mathbb{E}\left[e^{\left(-\mu\frac{T}{P}r^{\alpha}(\sigma^2+P\hat{I_{\mathcal{Z}}})\right)}\left(1-e^{\left(-\mu\frac{T_{\mathrm{FR}}}{P}r^{\alpha}(\sigma^2+PI_{\mathcal{Z}})\right)}\right)\right]}{\mathbb{E}\left[\left(1-e^{\left(-\mu\frac{T_{\mathrm{FR}}}{P}r^{\alpha}(\sigma^2+PI_{\mathcal{Z}})\right)}\right)\right]}, \tag{2.12}$$

which equals

$$\frac{\mathbb{E}\left[e^{\left(-\mu\frac{T}{P}r^{\alpha}(\sigma^2+P\hat{I_{\mathcal{Z}}})\right)}\right] - \mathbb{E}\left[e^{\left(-\mu\frac{\sigma^2}{P}r^{\alpha}(T+T_{\mathrm{FR}})\right)}e^{\left(-\mu r^{\alpha}(T\hat{I_{\mathcal{Z}}}+T_{\mathrm{FR}}I_{\mathcal{Z}})\right)}\right]}{1-\mathbb{E}\left[\left(e^{\left(-\mu\frac{T_{\mathrm{FR}}}{P}r^{\alpha}(\sigma^2+PI_{\mathcal{Z}})\right)}\right)\right]}. \tag{2.13}$$

Now concentrating on the second term of the numerator and *conditioning on* r, *i.e.,* the distance to the nearest BS, following the general approach of [8], we observe that the noise is independent of the interference and the expectation of $\exp\left(-\mu r^{\alpha}(T\hat{I_{\mathcal{Z}}}+T_{\mathrm{FR}}I_{\mathcal{Z}})\right)$ is the joint Laplace transform of $\hat{I_{\mathcal{Z}}}$ and $I_{\mathcal{Z}}$ evaluated at $(\mu r^{\alpha}T, \mu r^{\alpha}T_{\mathrm{FR}})$. The joint Laplace transform is

$$\begin{aligned}
\mathscr{L}(s_1,s_2) &= \mathbb{E}\left[\exp\left(-s_1\hat{I_{\mathcal{Z}}} - s_2I_{\mathcal{Z}}\right)\right] \\
&= \mathbb{E}\left[\exp\left(-s_1\sum_{z\in Z}\hat{G}_zR_z^{-\alpha}\mathbf{1}(\delta_z=\delta_y) - s_2\sum_{z\in Z}G_zR_z^{-\alpha}\right)\right] \\
&= \mathbb{E}\left[\exp\left(-\sum_{z\in Z}s_1\hat{G}_zR_z^{-\alpha}\mathbf{1}(\delta_z=\delta_y) + s_2G_zR_z^{-\alpha}\right)\right] \\
&= \mathbb{E}\prod_{z\in Z}\exp\left(-(s_1\hat{G}_zR_z^{-\alpha}\mathbf{1}(\delta_z=\delta_y) + s_2G_zR_z^{-\alpha})\right) \\
&= \mathbb{E}\prod_{z\in Z}\exp(-s_2G_zR_z^{-\alpha})\left(1-\mathbb{E}\left(\mathbf{1}(\delta_z=\delta_y)\right)\left(1-\exp(-s_1\hat{G}_zR_z^{-\alpha})\right)\right),
\end{aligned}$$

where $\mathbf{1}(\delta_y = \delta_z)$ is an indicator function that takes the value 1, if base station z is transmitting to an edge user on the same sub-band δ as user y.

Since $\hat{G}_z$ and G_z are also exponential with mean μ, we can evaluate the above expression as

$$\mathbb{E}\prod_{z\in Z}\frac{\mu}{\mu+s_2R_z^{-\alpha}}\left(1-\frac{1}{\Delta}\left(1-\frac{\mu}{\mu+s_1R_z^{-\alpha}}\right)\right). \tag{2.14}$$

By using the probability generating functional (PGFL) of the PPP [104], we obtain the Laplace transform as

$$\mathscr{L}(s_1,s_2)=\exp\left(-2\pi\lambda\int_r^\infty\left[1-\frac{\mu}{\mu+s_2x^{-\alpha}}\left(1-\frac{1}{\Delta}\left(1-\frac{\mu}{\mu+s_1x^{-\alpha}}\right)\right)\right]x\mathrm{d}x\right).$$

Hence

$$\mathscr{L}(\mu r^\alpha T,\mu r^\alpha T_{\mathrm{FR}})=\exp\left(-2\pi\lambda r^2\int_1^\infty\left[1-\frac{1}{1+T_{\mathrm{FR}}x^{-\alpha}}\left(1-\frac{1}{\Delta}\left(1-\frac{1}{1+Tx^{-\alpha}}\right)\right)\right]x\mathrm{d}x\right).$$

De-conditioning on r, we have

$$\mathbb{E}\left[e^{\left(-\mu\frac{\sigma^2}{P}r^\alpha(T+T_{\mathrm{FR}})\right)}e^{\left(-\mu r^\alpha(T\hat{I_{\mathbb{Z}}}+T_{\mathrm{FR}}I_{\mathbb{Z}})\right)}\right]]=2\pi\lambda\int_0^\infty e^{-\pi\lambda r^2(1+2\xi(T,T_{\mathrm{FR}},\alpha,\Delta))-\mu(T+T_{\mathrm{FR}})\frac{\sigma^2}{P}r^\alpha}\mathrm{d}r,$$

where

$$\xi(T,T_{\mathrm{FR}},\alpha,\Delta)=\int_1^\infty\left[1-\frac{1}{1+T_{\mathrm{FR}}x^{-\alpha}}\left(1-\frac{1}{\Delta}\left(1-\frac{1}{1+Tx^{-\alpha}}\right)\right)\right]x\mathrm{d}x.$$

Plugging back into (2.13), substituting $r^2=v$, and using the definition of p_c given by (2.7), originally defined in [8], we have

$$\frac{p_c(T,\lambda,\alpha,\Delta)-\pi\lambda\int_0^\infty e^{-\pi\lambda v(1+2\xi(T,T_{\mathrm{FR}},\alpha,\Delta))-\mu(T+T_{\mathrm{FR}})\frac{\sigma^2}{P}v^{\alpha/2}}\mathrm{d}v}{1-p_c(T_{\mathrm{FR}},\lambda,\alpha,1)}.$$

□

The SINR distributions are derived from on the geometrical properties of the spatial Poisson process and its probability generating functional (PGFL) [104] along with the independence between the downlink interference sources [8, 44]. While $\xi(T, T_{\mathrm{FR}}, \alpha, \Delta)$ is reminiscent of $\rho(T, \alpha)$ given by prior results in [8], it differs due to the dependence of the user's SINR before and after the assignment of the new FFR sub-band. This is from the fact that while the interference power and the user's fading values have changed, the location of the user relative to the base stations has not changed, and the thus the dominant path loss remains the same.

Now we turn our attention to the interior users in the case of Strict FFR. The coverage probability of the inner user does not depend on Δ since the user is allocated a sub-band shared by all base stations.

Theorem 3 (Strict FFR, interior user)**.** *The coverage probability of the interior user with Strict FFR is*

$$\bar{\mathrm{F}}_{\mathrm{FFR,i}}(T) = \frac{p_c(\max\{T, T_{\mathrm{FR}}\}, \lambda, \alpha, 1)}{p_c(T_{\mathrm{FR}}, \lambda, \alpha, 1)}$$

and $p_c(T, \lambda, \alpha, \Delta)$ *is given by* (2.7)*.*

The $\max\{T, T_{\mathrm{FR}}\}$ term in the numerator is a result of interior users having SINR $\geq T_{\mathrm{FR}}$ by definition. Also, because the interior users of all the cells share the same sub-band, the SINR CCDF is closely related to the results of [8] for users with no frequency reuse.

2.4.2 Probability of coverage with SFR

There are two major differences between SFR and Strict FFR. One is the use of power control for the edge users, controlled by the design parameter β which creates

two different classes, $P_{\text{int}} = P$ and $P_{\text{edge}} = \beta P$, where P_{int} is the transmit power of the base station if user y is an interior user and P_{edge} is the transmit power of the base station if user y is a cell-edge user [70]. Typical analysis of SFR uses values of 2-20 for β, although this choice is usually based on heuristic approaches [4, 33, 55].

Additionally, the base stations can reuse all sub-bands, but apply β to only one of the δ sub-bands. Thus, the inter-cell interference no longer comes from disjoint sets of interior and edge downlinks and the interference power is given by $\eta I_{\mathcal{Z}}$, where $\eta = (\Delta - 1 + \beta)/\Delta$ is the effective interference power factor, consolidating the impact of interference from the higher and lower power downlinks. We now consider the CCDF for SFR starting again with edge users, followed by the interior users.

Theorem 4 (SFR, edge user)**.** *The coverage probability of an SFR edge user whose initial* SINR *is less than* T_{FR} *is*

$$\begin{aligned}\bar{\text{F}}_{\text{SFR,e}}(T) &= \mathbb{P}\left(\frac{\beta P \hat{g}_y r^{-\alpha}}{\sigma^2 + \eta P \hat{I_{\mathcal{Z}}}} > T \;\middle|\; \frac{P g_y r^{-\alpha}}{\sigma^2 + \eta P I_{\mathcal{Z}}} < T_{\text{FR}}\right) \\ &= \frac{p_c(\frac{\eta T}{\beta}, \lambda, \alpha, \Delta) - \pi\lambda \int_0^\infty e^{-\pi\lambda v(1+2\zeta(T,T_{\text{FR}},\alpha,\eta,\beta)) - \mu\eta(\frac{T}{\beta}+T_{\text{FR}})\frac{\sigma^2}{\beta P} v^{\alpha/2}} \mathrm{d}v}{1 - p_c(T_{\text{FR}}, \lambda, \alpha, \Delta)},\end{aligned}$$

where

$$\zeta(T, T_{\text{FR}}, \alpha, \eta, \beta) = \int_1^\infty \left[1 - \frac{1}{1 + \eta T_{\text{FR}} x^{-\alpha}} \left(\frac{1}{1 + \frac{\eta T}{\beta} x^{-\alpha}}\right)\right] x \mathrm{d}x.$$

Proof. A user y with SINR $< T_{\text{FR}}$ is given a SFR sub-band δ, where $\delta \in \{1, ..., \Delta\}$, transmit power βP and experiences new transmit power βP, fading power $\hat{g_y}$ and out-of-cell interference $\hat{I_{\mathcal{Z}}}$, instead of g_y and $I_{\mathcal{Z}}$. The CCDF of the edge user $\bar{\text{F}}_{\text{SFR,e}}(T)$ is now conditioned on its previous SINR,

$$\bar{\text{F}}_{\text{SFR,e}}(T) = \mathbb{P}\left(\frac{\beta P \hat{g}_y r^{-\alpha}}{\sigma^2 + \eta P \hat{I_{\mathcal{Z}}}} > T \;\middle|\; \frac{P g_y r^{-\alpha}}{\sigma^2 + \eta P I_{\mathcal{Z}}} < T_{\text{FR}}\right). \tag{2.15}$$

Using Bayes' rule we have,

$$\bar{\mathrm{F}}_{\mathrm{SFR,e}}(T) = \frac{\mathbb{P}\left(\frac{\beta P \hat{g_y} r^{-\alpha}}{\sigma^2+\eta P \hat{I_{\mathcal{Z}}}} > T \ , \frac{P g_y r^{-\alpha}}{\sigma^2+\eta P I_{\mathcal{Z}}} < T_{\mathrm{FR}}\right)}{\mathbb{P}\left(\frac{P g_y r^{-\alpha}}{\sigma^2+\eta P I_{\mathcal{Z}}} < T_{\mathrm{FR}}\right)}. \tag{2.16}$$

Since $\hat{g_y}$ and g_y are exponentially distributed with mean μ, we have

$$\mathbb{P}\left(\frac{\beta P \hat{g_y} r^{-\alpha}}{\sigma^2 + \eta P \hat{I_{\mathcal{Z}}}} > T \ , \frac{P g_y r^{-\alpha}}{\sigma^2 + \eta P I_{\mathcal{Z}}} < T_{\mathrm{FR}}\right) = \mathbb{E}\left[e^{\left(-\mu \frac{T}{\beta P} r^{\alpha}(\sigma^2+\eta P \hat{I_{\mathcal{Z}}})\right)}\left(1 - e^{\left(-\mu \frac{T_{\mathrm{FR}}}{P} r^{\alpha}(\sigma^2+\eta P I_{\mathcal{Z}})\right)}\right)\right]. \tag{2.17}$$

and as before in Theorem 1 we have,

$$\bar{\mathrm{F}}_{\mathrm{SFR,e}}(T) = \frac{p_c(\eta \frac{T}{\beta}, \alpha, \Delta) - \mathbb{E}\left[\exp\left(-\mu r^{\alpha} \frac{\sigma^2}{P}(\frac{T}{\beta} + T_{\mathrm{FR}})\right) \exp\left(-\mu r^{\alpha} \eta (\frac{T}{\beta} \hat{I_{\mathcal{Z}}} + T_{\mathrm{FR}} I_{\mathcal{Z}})\right)\right]}{1 - p_c(\eta T_{\mathrm{FR}}, \alpha, 1)}.$$

Following the method of Theorem 1, concentrating on the second term and *conditioning on* r, *i.e.,* the distance to the nearest BS, we observe that the expectation of $\exp\left(-\mu r^{\alpha} \eta (\frac{T}{\beta} \hat{I_{\mathcal{Z}}} + T_{\mathrm{FR}} I_{\mathcal{Z}})\right)$ is the joint Laplace transform of $\hat{I_{\mathcal{Z}}}$ and $I_{\mathcal{Z}}$ evaluated at $(\mu r^{\alpha} \eta \frac{T}{\beta}, \mu r^{\alpha} \eta T_{\mathrm{FR}})$. The steps to evaluate the joint Laplace transform are the same as Theorem 2 with the exception that we know that the structure of $\hat{I_{\mathcal{Z}}}$ and $I_{\mathcal{Z}}$ includes all base stations not just those associated with the user's sub-band δ. This can equivalently thought of as setting $\Delta = 1$ in (2.14). Thus,

$$\mathscr{L}(s_1, s_2) = \mathbb{E} \prod_{z \in Z} \frac{\mu}{\mu + s_2 R_z^{-\alpha}} \left(\frac{\mu}{\mu + s_1 R_z^{-\alpha}}\right). \tag{2.18}$$

Using the PGFL, we obtain the Laplace transform as

$$\mathscr{L}(s_1, s_2) = \exp\left(-2\pi\lambda \int_r^{\infty} \left[1 - \frac{\mu}{\mu + s_2 x^{-\alpha}} \left(\frac{\mu}{\mu + s_1 x^{-\alpha}}\right)\right] x \mathrm{d}x\right).$$

Hence

$$\mathscr{L}\left(\mu r^{\alpha} \eta \frac{T}{\beta}, \mu r^{\alpha} \eta T_{\mathrm{FR}}\right) = \exp\left(-2\pi\lambda r^2 \int_1^{\infty} \left[1 - \frac{1}{1 + \eta T_{\mathrm{FR}} x^{-\alpha}} \left(\frac{1}{1 + \eta \frac{T}{\beta} x^{-\alpha}}\right)\right] x \mathrm{d}x\right).$$

Finally, de-conditioning on r, we have

$$\mathbb{E}\left[\exp\left(-\mu r^{\alpha}(\eta\frac{T}{\beta}\hat{I}_{\mathcal{Z}}+\eta T_{\mathrm{FR}}I_{\mathcal{Z}})\right)\right]=2\pi\lambda\int_0^{\infty}e^{-\pi\lambda r^2(1+2\zeta(T,T_{\mathrm{FR}},\alpha,\eta,\beta))-\mu(\eta\frac{T}{\beta}+\eta T_{\mathrm{FR}})\frac{\sigma^2}{P}r^{\alpha}}\mathrm{d}r,$$

where

$$\zeta(T,T_{\mathrm{FR}},\alpha,\eta,\beta)=\int_1^{\infty}\left[1-\frac{1}{1+\eta T_{\mathrm{FR}}x^{-\alpha}}\left(\frac{1}{1+\eta\frac{T}{\beta}x^{-\alpha}}\right)\right]x\mathrm{d}x.$$

Plugging back into (2.16), substituting $r^2=v$, and using the definition of p_c given by (2.7) we have

$$\frac{p_c(\frac{\eta T}{\beta},\lambda,\alpha,\Delta)-\pi\lambda\int_0^{\infty}e^{-\pi\lambda v(1+2\zeta(T,T_{\mathrm{FR}},\alpha,\eta,\beta))-\mu\eta(\frac{T}{\beta}+T_{\mathrm{FR}})\frac{\sigma^2}{\beta P}v^{\alpha/2}}\mathrm{d}v}{1-p_c(T_{\mathrm{FR}},\lambda,\alpha,\Delta)}.$$

□

The expressions only differ slightly from Strict FFR. The inclusion of η and β can be viewed as creating effective SINR and FFR thresholds $\frac{\eta T}{\beta}$ and ηT_{FR} respectively.

For SFR, the CCDF of the interior user, $\bar{\mathrm{F}}_{\mathrm{i}}(T)$ is found in the same manner as Strict FFR.

Theorem 5 (SFR,interior user)**.**

$$\bar{\mathrm{F}}_{\mathrm{SFR,i}}(T)=\frac{p_c(\eta\max\{T,T_{\mathrm{FR}}\},\alpha,1)}{p_c(\eta T_{\mathrm{FR}},\lambda,\alpha,1)}.$$

Proof. Follows from the definition of $\mathrm{F}_{\mathrm{SFR,i}}(T)$, and Theorem 3. □

Again, the CCDF is similar in structure to the Strict FFR case. Also, since for interior users there is no extra β power control in their transmit power, only the effective interference power factor η remains in the expressions.

2.5 Discussion of the Model

While our results in Section 2.4 hold for general pathloss exponents α and different noise powers σ^2, in this section we present a special case where $\alpha = 4$ and $\sigma^2 = 0$. For this case the coverage probability results reduce to simple closed-form expressions, allowing clear insight into the performance of cell-edge users, something not previously possible with the grid model. This choice of pathloss exponent is in the range of commonly used values in practice. Furthermore, most urban cellular networks - where FFR is of the most interest - are interference-limited and noise is negligible compared to the background interference from the adjacent BSs. We also provide a discussion of intuitive lower and upper bounds of the SINR distribution for edge users under SFR and conclude this section with a numerical comparison of the Poisson model against the standard grid model and an actual base station deployment for the different reuse strategies.

2.5.1 Strict FFR: No-noise and $\alpha = 4$

In the case of Strict FFR, for $\alpha = 4$ and no noise, the edge user coverage probability is given by,

$$\bar{\mathrm{F}}_{\mathrm{FFR,e}}(T) = \frac{1+\rho(T_{\mathrm{FR}},4)}{\rho(T_{\mathrm{FR}},4)}\left(\frac{1}{1+\frac{1}{\Delta}\rho(T,4)} - \frac{1}{1+2\xi(T,T_{\mathrm{FR}},4,\Delta)}\right) \tag{2.19}$$

where $\xi(T,T_{\mathrm{FR}},4,\Delta) =$

$$\frac{2T^{3/2}\arctan(\frac{1}{\sqrt{T}}) - \left(2\arctan(\frac{1}{\sqrt{T_{\mathrm{FR}}}})\right)\left({T_{\mathrm{FR}}}^{3/2}\Delta - \left(T\sqrt{T_{\mathrm{FR}}}\right)(1+\Delta)\right)}{4\Delta(T_{\mathrm{FR}}-T)} - \frac{\pi({T}^{3/2}+{T_{\mathrm{FR}}}^{3/2})\Delta + (\pi T\sqrt{T_{\mathrm{FR}}})(1-\Delta)}{4\Delta(T_{\mathrm{FR}}-T)}. \tag{2.20}$$

We also note that for $\alpha = 4$ and no noise, $\rho(T,4) = \sqrt{T}\arctan(T)$, and is in closed form as well [8]. However, when $T = T_{\mathrm{FR}}$, the expression has an indeterminate form.

By evaluating the limit $T \to T_{\mathrm{FR}}$, this simplifies to

$$\xi(T, T_{\mathrm{FR}}, 4, \Delta) = \frac{\sqrt{T_{\mathrm{FR}}}\pi(2\Delta+1)}{8\Delta} + \frac{2T_{\mathrm{FR}}}{8(T_{\mathrm{FR}}+1)\Delta} - \frac{\sqrt{T_{\mathrm{FR}}}(2\Delta+1)\cot^{-1}\left(\sqrt{T_{\mathrm{FR}}}\right)}{4\Delta}. \tag{2.21}$$

We see that the SINR distribution of Strict FFR edge users are simply a function of the SINR threshold T, the reuse factor Δ, and the reuse threshold T_{FR}. The reuse threshold determines whether a user is switched to a reuse-Δ sub-band. Although not given here, it is clear that the same applying this special case to the interior users would result in similarly closed form and simple expressions.

2.5.2 SFR: No-noise and $\alpha = 4$

Likewise for the SFR case,

$$\bar{\mathrm{F}}_{\mathrm{SFR,e}}(T) = \frac{1+\rho(\eta T_{\mathrm{FR}}, 4)}{\rho(\eta T_{\mathrm{FR}}, 4)}\left(\frac{1}{1+\rho(\frac{\eta}{\beta}T, 4)} - \frac{1}{1+2\zeta(T, T_{\mathrm{FR}}, 4, \eta, \beta)}\right) \tag{2.22}$$

where

$$\rho(T, 4) = \sqrt{T}\arctan(T) \tag{2.23}$$

and

$$\begin{aligned}\zeta(T, T_{\mathrm{FR}}, 4, \eta, \beta) \;=\; & \frac{\eta^{3/2}T\beta}{4\sqrt{T_{\mathrm{FR}}}(T - T_{\mathrm{FR}}\beta)} - \frac{\eta\beta T^3\left(2\arctan\left(\sqrt{\frac{\beta}{\eta T}}\right)+\pi\right)}{(T-T_{\mathrm{FR}}\beta)} + \\ & \frac{\eta T^{3/2}{T_{\mathrm{FR}}}^{3/2}\beta^{5/2}\left(2\arctan\left(\frac{1}{\sqrt{\eta T_{\mathrm{FR}}}}\right)-\pi\right)}{(T-T_{\mathrm{FR}}\beta)}.\end{aligned} \tag{2.24}$$

When $T_{\mathrm{FR}} = T$, the limit $T_{\mathrm{FR}} \to T$ simplifies as $\zeta(T, T_{\mathrm{FR}}, 4, \eta, \beta) =$

$$\frac{\sqrt{\eta T_{\mathrm{FR}}}\left(2\arctan\left(\frac{\beta}{\sqrt{(\eta(T_{\mathrm{FR}})\beta)}}\right)-\pi\right)}{4\sqrt{\beta}\,(\beta-1)} - \frac{2\beta\sqrt{\eta T_{\mathrm{FR}}}\arctan\left(\frac{1}{\sqrt{\eta T_{\mathrm{FR}}}}\right)+\pi}{4\,(\beta-1)}. \tag{2.25}$$

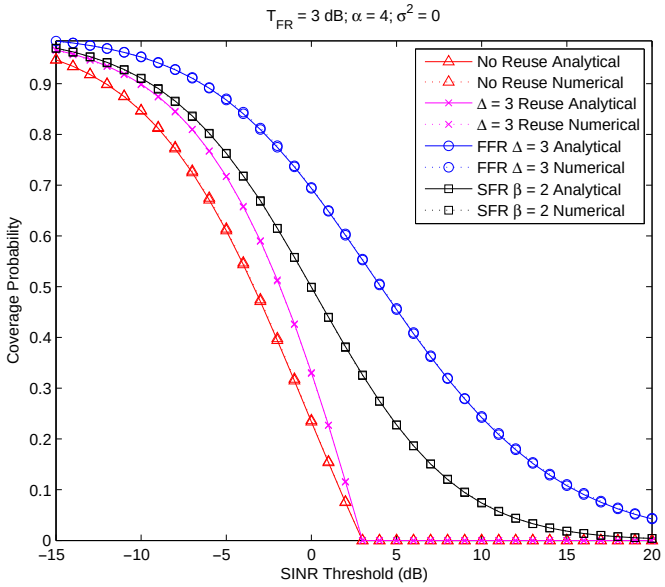

Figure 2.1: Comparison of analytical coverage probability for edge users with different reuse strategies versus Monte-Carlo simulations.

Once the again, the SINR distribution in (2.22) is only a function of the SINR threshold T and in this case, the two SFR design parameters, the reuse threshold T_{FR} and the power control factor β, which influences the effective interference factor η. In the next several sections, we will exploit this simple structure to compare Strict FFR and SFR with other reuse strategies and evaluate their relative performance as a function of the design parameters.

2.5.3 Comparison of resource allocation strategies

Comparing the SINR distributions derived in Section 2.5.1 and 2.5.2 for edge users with those of a no-frequency reuse and standard reuse-Δ system as derived in [8] provides insight into the relative merits and tradeoffs associated with FFR. In Fig. 2.1 we plot the four systems with $\sigma^2 = 0$, $\alpha = 4$, and $T_{\mathrm{FR}} = 1$ dB and compare the

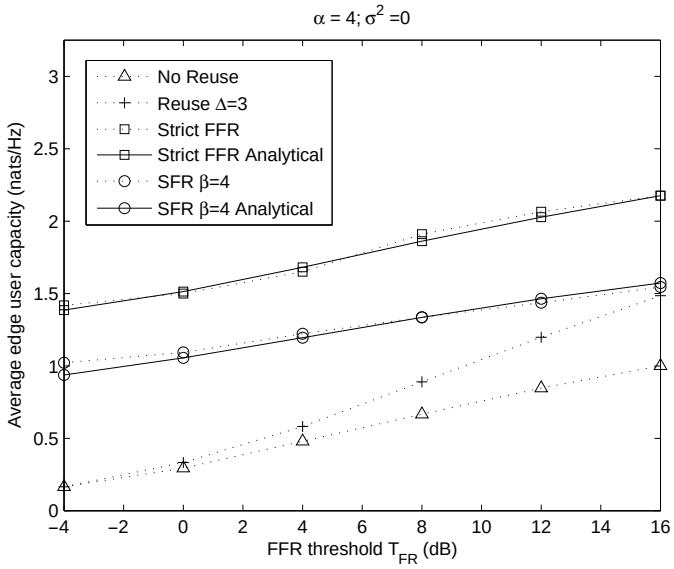

Figure 2.2: Analytical and Monte-Carlo results for average edge user capacity with different reuse strategies as a function of T_{FR}.

analytical expressions with Monte-Carlo simulations. In particular we see that Strict FFR provides better coverage than SFR to edge users. Intuition for these results can be seen from the proofs of Theorems 2 and 4. Since the probability is degraded multiplicatively by the interfering downlinks, the number of sources of interference drives the outage. When $\Delta = 3$, we see that only 33% of the base stations causing downlink interference to edge users under universal frequency reuse are active on the same resources under Strict FFR. However, SFR allows adjacent base stations to serve interior users on the same sub-bands used by adjacent edge users, increasing interference and lowering coverage. The reason for the sharp cutoffs in the coverage curves for no reuse and reuse-Δ users in Fig. 2.1 is because unlike FFR, edge users under those strategies do not get allocated a new sub-band and by definition their SINR must be below the reuse threshold T_{FR}.

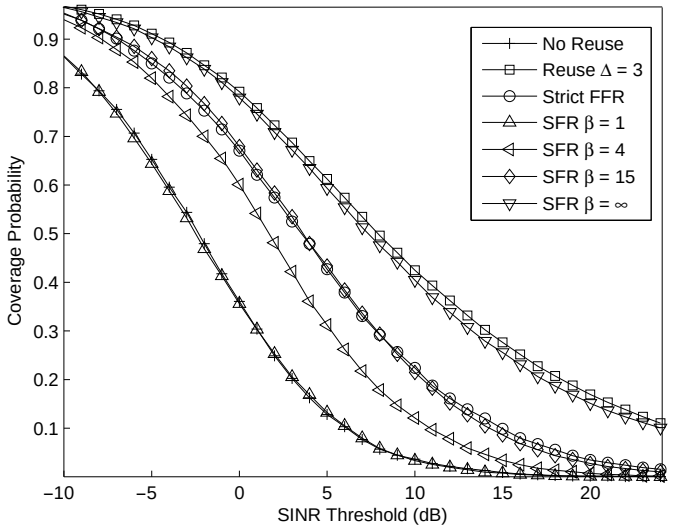

Figure 2.3: Comparison of the SINR distribution of cell-edge users of SFR with different β power-control factors, $T_{\mathrm{FR}} = 1$dB, no noise, and $\alpha = 4$ with Strict FFR and the derived lower and upper bounds.

2.5.4 Lower and Upper Bounds for SFR

One question arising from Theorem 4 is how the power control factor β influences the distribution of the SINR. Fig. 2.3 compares the coverage probability of SFR for increasing β factors with Strict FFR. As β increases, SFR performance approaches and then surpasses Strict FFR when $\beta \geq 15$, which is equivalent to a 12 dB power increase for cell-edge downlinks over interior user downlinks.

Next, we show that the performance of an SFR system is bounded by two other reuse systems, namely reuse-1 (a.k.a no frequency reuse) when $\beta \to 1$ and reuse-Δ when $\beta \to \infty$.

2.5.4.1 $\beta \to 1$

As $\beta \to 1$ then $\eta \to 1$ as well and the CCDF of the edge user SINR is given as

$$\bar{\mathrm{F}}_{\mathrm{SFR},e}(T) \;=\; \mathbb{P}\left(\frac{P\hat{g}_y r^{-\alpha}}{\sigma^2 + P\hat{I}_{\mathcal{Z}}} > T \;\middle|\; \frac{Pg_y r^{-\alpha}}{\sigma^2 + PI_{\mathcal{Z}}} < T_{\mathrm{FR}}\right). \tag{2.26}$$

This is the same as a no frequency reuse strategy where a user with SINR $\leq T_{\mathrm{FR}}$ is given a new frequency sub-band. The only benefit would be from the fading and random placement of the base stations, but the number of interfering base stations would be the same.

2.5.4.2 $\beta \to \infty$

As $\beta \to \infty$ then $\eta \to \frac{1}{3}$. From (2.1) this means the SINR of the inner user is 0 (in linear units), while the SINR for the edge user must be evaluated using L'Hopital's rule and is

$$\mathrm{SINR} = \frac{g_y r^{-\alpha}}{\sum\limits_{z \in \mathcal{Z}_{\mathrm{edge}}} G_z {R_z}^{-\alpha}}. \tag{2.27}$$

However, because only $\frac{1}{\Delta}$ of the base stations are using β for their transmit power, and are randomly chosen from the realization of the PPP with total density λ, this can be equivalently thought of as having interference from a thinned distribution with $\hat{\lambda} = \frac{\lambda}{\Delta}$. Thus we can utilize the result from [8] which showed that this is the same as the reuse-Δ case.

Fig. 2.3 compares the computed lower and upper bounds with simulated SFR systems utilizing $\beta = 1$ and β approaching ∞ respectively and shows that the bounds are quite tight in both cases.

2.6 Discussion of the Model

As noted previously, the majority of work on the design of systems using fractional frequency reuse has focused on utilizing a grid model. The distance to the BS was used to classify the edge and interior users determine resource allocation strategies for the FFR sub-bands. In this section we compare the coverage results obtained using the spatial Poisson model with a uniformly spaced rectangular grid of base stations as well as with simulations utilizing the base station locations of an urban deployment by a major service provider.

2.6.1 Comparison with the grid model

In Figs. 2.4 and 2.5 we compare the CCDFs of the SINR obtained using the PPP model with distributions obtained using Monte-Carlo simulations of a grid model as well as locations from an actual urban base station deployment for Strict FFR and SFR respectively. The grid model, as expected, is more optimistic in terms of coverage probability than the results based on the actual deployment [19], [8]. This is primarily due to the minimum distance between the interfering base stations and the typical edge user, resulting in well-defined fixed-sized tiers of interference, with the outlying tiers much less important to calculating the overall performance due to the exponentially decaying nature of the pathloss.

With the PPP model, the number of interfering base stations within a region, *i.e.,* the size of a cellular tier, is random and the distances are not lower bounded, except for the fact that the edge user is assumed to be closer to the serving base station than any of the interfering base stations. However, despite this difference, the distributions for Strict FFR and SFR follow a similar sloping shape. The comparisons

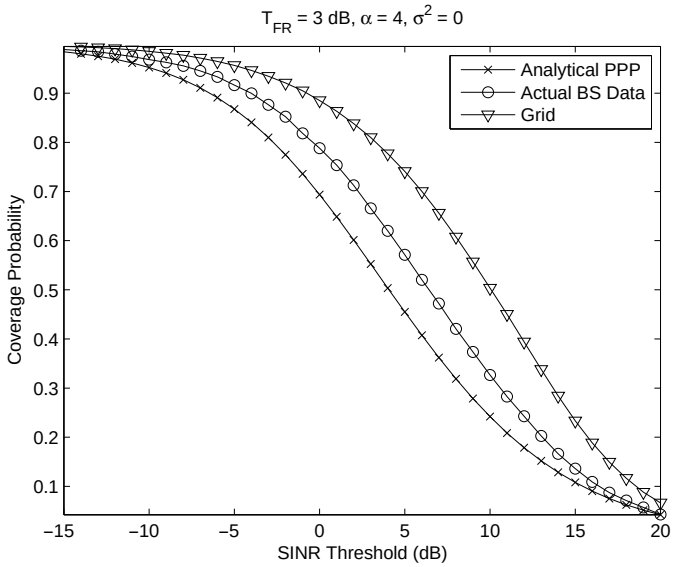

Figure 2.4: Strict FFR edge user coverage probability with Poisson-model, grid model, and actual urban base station locations.

of Figs. 2.4 and 2.5 verify the claim that the PPP model serves as a lower bound on performance in a real deployment.

We also compare the performance of the PPP model against the grid model and three additional sets of base station locations with a 25% lower density of $\lambda \approx .19$ base stations per km^2. Interestingly in Fig. 2.6 we note that for Strict FFR, the PPP model is a closer fit than the grid for the first two sets, while the third set is closer at lower SINR thresholds to the PPP model and approaches the grid model at higher SINR thresholds. In Fig. 2.7 we see that for SFR, the SINR thresholds of the models and the actual locations are bounded more closely. Intuition for this behavior is that the grid model provides a hardcore upper bound on the interference which mimicks the dependence between base station placement in real deployments essential to providing the highest SINR values. However the grid model does not capture the non-regular cell size or clustered placement of base stations which creates strong interference and

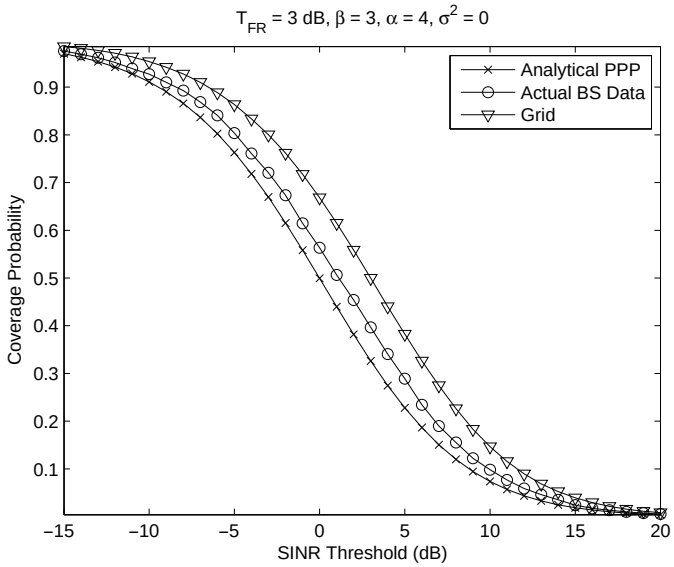

Figure 2.5: SFR edge user coverage probability with Poisson-model, grid model, and actual urban base station locations.

thus lower coverage probability at the lower SINR thresholds.

2.6.2 Impact of Lognormal Shadowing

Although the results of Section 2.4 assume an exponential fading distribution for the fast-fading experienced by the desired signal as well as the interference. However, the larger scale effect of shadowing induced by pathloss obstructions including buildings or terrain is typically modeled as a log-normal random variable. Although the expressions in Theorem 2 and 4 assume an exponential distribution they can be generalized to accommodate other fading distributions. In this section we briefly discuss the impact of considering log-normal shadowing on the coverage expressions.

In the case of Strict FFR, following the approach of Theorem 2 the Laplace transforms of the interference on the original and FFR subbands given by (2.14) takes

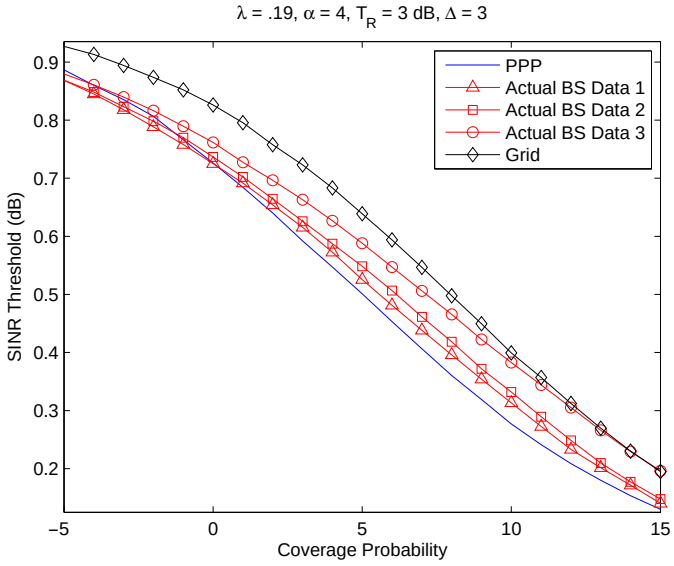

Figure 2.6: Strict FFR edge user coverage probability with the PPP model and simulations using the grid model, and three sets of suburban base station locations with $\lambda = .19$ and $\alpha = 4$.

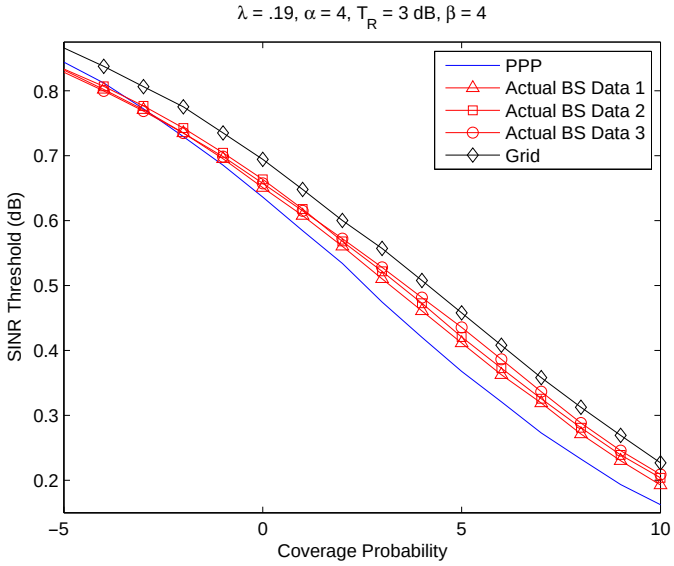

Figure 2.7: SFR edge user coverage probability with the PPP model and simulations using the grid model, and three sets of suburban base station locations with $\lambda = .19$ and $\alpha = 4$.

the form

$$\mathbb{E}_{G_z,R_z} \prod_{z\in Z} \exp(-s_2 G_z R_z^{-\alpha}) \left(1 - \mathbb{E}\left(\mathbf{1}(\delta_z = \delta_y)\right)\left(1 - \exp(-s_1 \hat{G}_z R_z^{-\alpha})\right)\right). \quad (2.28)$$

If the interference fading power G_z is taken to have a general distribution $f(G)$ the Laplace transform can be written as $\mathscr{L}(\mu r^\alpha T, \mu r^\alpha T_{\mathrm{FR}}) =$

$$\exp\left(-2\pi\lambda r^2 \int_0^\infty \left(\int_r^\infty \left[1 - e^{-\mu r^\alpha T_{\mathrm{FR}} G x^{-\alpha}} \left(1 - \frac{1}{\Delta}(1 - e^{-\mu r^\alpha T \hat{G} x^{-\alpha}})\right)\right] x \mathrm{d}x\right) f(G)\mathrm{d}G\right). \quad (2.29)$$

Applying the same approach for SFR gives the following expression for the joint Laplace transform of the interference $\mathscr{L}\left(\mu r^\alpha \eta \frac{T}{\beta}, \mu r^\alpha \eta T_{\mathrm{FR}}\right) =$

$$\exp\left(-2\pi\lambda r^2 \int_0^\infty \left(\int_r^\infty \left[1 - e^{-\mu r^\alpha \eta T_{\mathrm{FR}} G x^{-\alpha}} e^{-\mu r^\alpha \eta \frac{T}{\beta} \hat{G} x^{-\alpha}}\right] x \mathrm{d}x\right) f(G)\mathrm{d}G\right). \quad (2.30)$$

In Fig. 2.8 the coverage probability expressions of Section 2.4 are compared with the general expressions of (2.29) and (2.30) assuming log-normal shadowing with standard deviation of 6 dB. We note that the shadowing induces an almost constant shift of the SINR. As a result, the insights provided by the more tractable expressions without shadowing into relative performance between FFR strategies is maintained.

We also compare coverage probability for Strict FFR and SFR given by the Poisson model with the grid model and urban BS locations also including log-normal shadowing with standard deviation of 6 dB in Fig. 2.9 and Fig. 2.10. Interestingly, the coverage expressions for Strict FFR and SFR are closer to the simulations based on the actual data than was even the case in Figs. 2.4 and 2.5. One way of interpreting this result is that shadowing can be viewed as displacing the locations of the interfering base stations in a random fashion which favors the Poisson model which already induces a non-uniform topology.

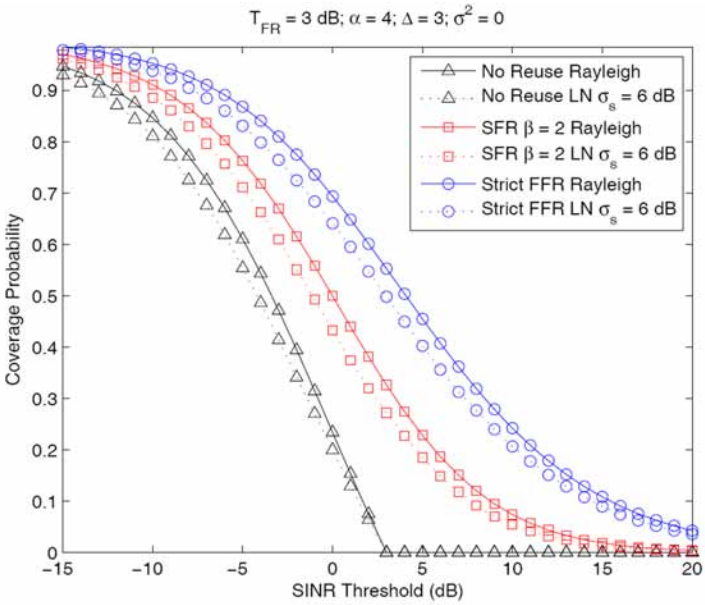

Figure 2.8: Comparison of the SINR distribution of cell-edge users with full-reuse, Strict FFR, and SFR with $\beta = 2$, no noise, $\alpha = 4$, and log-normal shadowing with standard deviation of 6 dB.

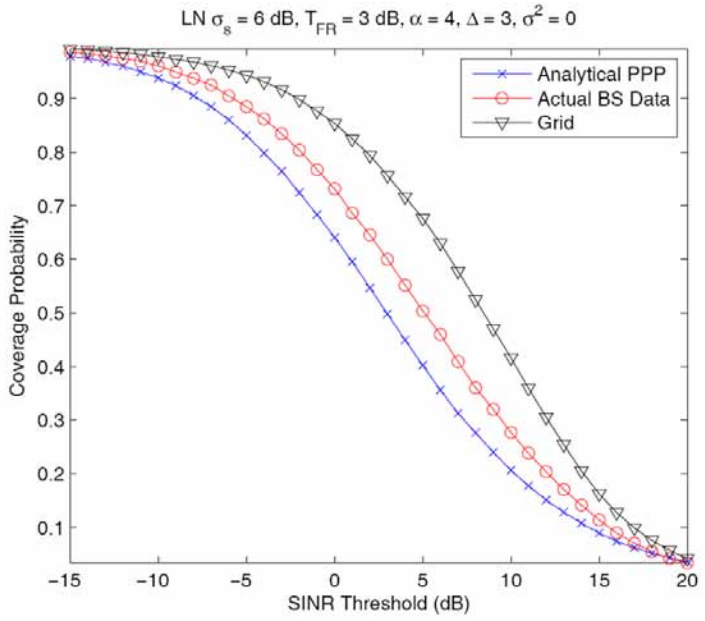

Figure 2.9: Strict FFR edge user coverage probability with Poisson-model, grid model, and actual urban base station locations with log-normal shadowing with standard deviation of 6 dB.

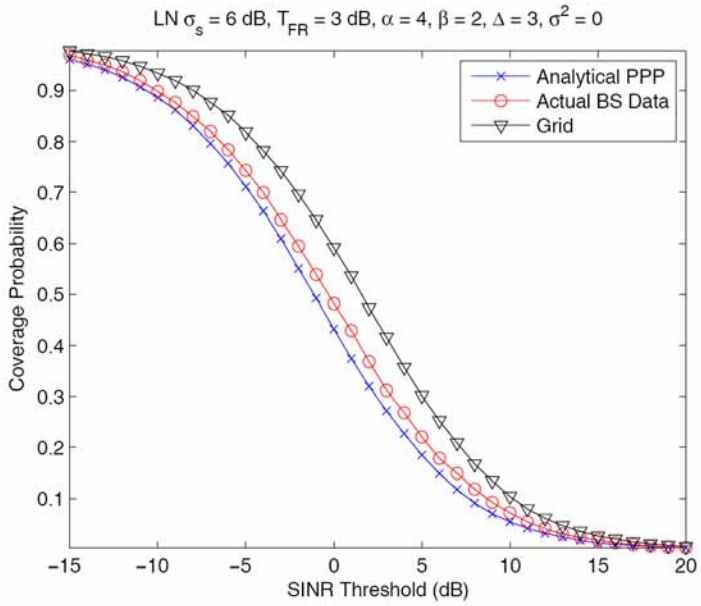

Figure 2.10: SFR edge user coverage probability with Poisson-model, grid model, and actual urban base station locations with standard deviation 6 dB.

2.7 Average Edge User Rate

In modern cellular networks utilizing OFDMA, user rate is directly related to average SINR and the system's resource allocation algorithm. Again as with the SINR distributions, most prior work utilizing the grid model relied on simulations to analyze the performance. The coverage results derived in Section 2.4 can be extended to develop average user rate expressions under Strict FFR or SFR, creating a new set of system design tools for general and hybrid FFR strategies. Additionally, this allows for greater insight into the joint optimization of coverage and rate.

Adaptive modulation and coding is assumed such that users are able to achieve the average data rate and the expressions are given in terms of nats/Hz, where 1 bit $= \log_e(2)$ nats. We define the average rate of a edge user to be

$$\bar{\tau} = \mathbb{E}[\ln(1 + \text{SINR})], \tag{2.31}$$

averaging over the base station locations and the fading distributions [8]. In [81] we show that these results can be evaluated using numerical integration and reduce to simple expressions for the same special cases as presented for the coverage probability.

2.7.0.1 Strict FFR

First we consider the typical edge user given a Strict FFR sub-band.

Theorem 6 (Strict FFR, edge user)**.** *The average rate of an edge user under Strict FFR is*

$$\bar{\tau}_{FFR}(T_{\mathrm{FR}},\lambda,\alpha,\Delta)=\int_{t>0}\frac{p_c\left((e^t-1),\lambda,\alpha,\Delta\right)-\xi\left(e^t-1,T_{\mathrm{FR}},\alpha,\Delta\right)}{1-p_c(T_{\mathrm{FR}},\lambda,\alpha,1)}\mathrm{d}t \qquad (2.32)$$

where

$$\xi\left(e^t-1,T_{\mathrm{FR}},\alpha,\Delta\right)=\int_1^\infty\left[1-\frac{1}{1+T_{\mathrm{FR}}x^{-\alpha}}\left(1-\frac{1}{\Delta}\left(1-\frac{1}{1+(e^t-1)x^{-\alpha}}\right)\right)\right]x\mathrm{d}x$$

and $p_c\left((e^t-1),\lambda,\alpha,\Delta\right)$ *is given by* (2.7)*.*

Proof. The average rate of an edge user, $\bar{\tau}_{FFR}(T_{\mathrm{FR}},\lambda,\alpha)$, is determined by integrating over the SINR distribution derived in Theorem 2. Starting from (2.31) we have

$$\begin{aligned}\bar{\tau}_{FFR}(T_{\mathrm{FR}},\lambda,\alpha,\Delta) &= \mathbb{E}\left[\ln\left(1+\mathrm{SINR}\right)\right]\\ &= \int_{r>0}e^{-\pi\lambda r^2}\mathbb{E}\left[\ln\left(1+\frac{P\hat{g}_y r^{-\alpha}}{\sigma^2+P\hat{I}_{\mathcal{Z}}}\right)\right]2\pi\lambda r\mathrm{d}r, \qquad (2.33)\end{aligned}$$

where we use the fact that since the rate $\tau=\ln(1+\mathrm{SINR})$ is a positive random variable, $E[\tau]=\int_{t>0}P(\tau>t)\mathrm{d}t$. Following the approach of Theorem 1, we condition the edge user's new SINR based on the previous value, guaranteed to be below T_{FR} and have $\bar{\tau}_{FFR}(T_{\mathrm{FR}},\lambda,\alpha,\Delta)=$

$$\int_{r>0}e^{-\pi\lambda r^2}\int_{t>0}\mathbb{P}\left[\ln\left(1+\frac{P\hat{g}_y r^{-\alpha}}{\sigma^2+P\hat{I}_{\mathcal{Z}}}\right)>t\;\middle|\;\frac{Pg_y r^{-\alpha}}{\sigma^2+PI_{\mathcal{Z}}}<T_{\mathrm{FR}}\right]2\pi\lambda\mathrm{d}t\;r\mathrm{d}r.$$

Applying Bayes' rule gives,

$$\begin{aligned}
&\mathbb{P}\quad\left[\ln\left(1+\frac{P\hat{g_y}r^{-\alpha}}{\sigma^2+P\hat{I_{\mathcal{Z}}}}\right)>t\;\middle|\;\frac{Pg_yr^{-\alpha}}{\sigma^2+PI_{\mathcal{Z}}}<T_{\mathrm{FR}}\right]\\
&=\quad\frac{\mathbb{P}\left(\ln\left(1+\frac{P\hat{g_y}r^{-\alpha}}{\sigma^2+P\hat{I_{\mathcal{Z}}}}\right)>t\;,\frac{Pg_yr^{-\alpha}}{\sigma^2+PI_{\mathcal{Z}}}<T_{\mathrm{FR}}\right)}{\mathbb{P}\left(\frac{Pg_yr^{-\alpha}}{\sigma^2+PI_{\mathcal{Z}}}<T_{\mathrm{FR}}\right)}
\end{aligned}\tag{2.34}$$

Following the method of Theorem 2 gives $\bar{\tau}_{FFR}(T_{\mathrm{FR}},\lambda,\alpha)$

$$\begin{aligned}
&=\quad\int_{t>0}2\pi\lambda\int_{r>0}e^{-\pi\lambda r^2}\frac{\mathbb{E}\left[e^{-\mu r^\alpha\frac{e^t-1}{P}\left(\sigma^2+P\hat{I_{\mathcal{Z}}}\right)}\right]}{1-\mathbb{E}\left[e^{\left(-\mu r^\alpha\frac{T_{\mathrm{FR}}}{P}(\sigma^2+PI_{\mathcal{Z}})\right)}\right]}\mathrm{d}t\;r\mathrm{d}r\\
&\quad-\int_{t>0}2\pi\lambda\int_{r>0}e^{-\pi\lambda r^2}\frac{\mathbb{E}\left[e^{\left(-\mu r^\alpha\frac{\sigma^2}{P}(e^t-1+T_{\mathrm{FR}})\right)}e^{\left(-\mu r^\alpha((e^t-1)\hat{I_{\mathcal{Z}}}+T_{\mathrm{FR}}I_{\mathcal{Z}})\right)}\right]}{1-\mathbb{E}\left[e^{\left(-\mu r^\alpha\frac{T_{\mathrm{FR}}}{P}(\sigma^2+PI_{\mathcal{Z}})\right)}\right]}\mathrm{d}t\;r\mathrm{d}r\\
&=\quad\int_{t>0}\frac{p_c(e^t-1,\alpha,\Delta)-\xi(e^t-1,T_{\mathrm{FR}},\alpha,\Delta)}{1-p_c(T_{\mathrm{FR}},\lambda,\alpha,1)}\mathrm{d}t,
\end{aligned}\tag{2.35}$$

where

$$\xi(e^t-1,T_{\mathrm{FR}},\alpha,\Delta)=\int_1^\infty\left[1-\frac{1}{1+T_{\mathrm{FR}}x^{-\alpha}}\left(1-\frac{1}{\Delta}\left(1-\frac{1}{1+(e^t-1)x^{-\alpha}}\right)\right)\right]x\mathrm{d}x,$$

and $p_c\left(e^t-1,\lambda,\alpha,\Delta\right)$ is given by (2.7). □

These results are clearly related to the coverage probability for Strict FFR given in Theorem 2. As a result, these results can be evaluated using numerical integration and reduce to simple expressions for the same special cases as presented in Section 2.4.

2.7.0.2 SFR

The case for SFR edge users follows similarly to Theorem 6.

Theorem 7 (SFR, edge user)**.** *The average rate of an edge user under SFR is*

$$\bar{\tau}_{SFR}(T_{\rm FR},\lambda,\alpha,\eta,\beta)=\int_{t>0}\frac{p_c\left(\frac{\eta}{\beta}(e^t-1),\lambda,\alpha,\Delta\right)-\zeta\left(e^t-1,T_{\rm FR},\alpha,\eta,\beta\right)}{1-p_c(\eta T_{\rm FR},\lambda,\alpha,1)}{\rm d}t \quad (2.36)$$

where

$$\zeta\left(e^t-1,T_{\rm FR},\alpha,\eta,\beta\right)=\int_1^\infty\left[1-\frac{1}{1+\eta T_{\rm FR}x^{-\alpha}}\left(\frac{1}{1+\frac{\eta}{\beta}(e^t-1)x^{-\alpha}}\right)\right]x{\rm d}x$$

and $p_c\left(\frac{\eta}{\beta}(e^t-1),\lambda,\alpha,\Delta\right)$ *is given by* (2.7).

Proof. Starting from (2.31) and integrating over the edge user SINR distribution for SFR derived in Theorem 4 we have

$$\begin{aligned}\bar{\tau}_{SFR}(T_{\rm FR},\lambda,\alpha,\eta,\beta) &= \mathbb{E}\left[\ln\left(1+{\rm SINR}\right)\right]\\ &= \int_{r>0}e^{-\pi\lambda r^2}\mathbb{E}\left[\ln\left(1+\frac{P\beta\hat{g}_y r^{-\alpha}}{\sigma^2+P\eta\hat{I}_{\mathcal{Z}}}\right)\right]2\pi\lambda r{\rm d}r\end{aligned}$$

$$= \int_{r>0}e^{-\pi\lambda r^2}\int_{t>0}\mathbb{P}\left[\ln\left(1+\frac{P\beta\hat{g}_y r^{-\alpha}}{\sigma^2+P\eta\hat{I}_{\mathcal{Z}}}\right)>t\;\middle|\;\frac{Pg_y r^{-\alpha}}{\sigma^2+P\eta I_{\mathcal{Z}}}<T_{\rm FR}\right]2\pi\lambda{\rm d}t\;r{\rm d}r.$$

Following the method of Theorem 4 gives $\bar{\tau}_{SFR}(T_{\rm FR},\lambda,\alpha,\eta,\beta)$

$$\begin{aligned}&= 2\pi\lambda\int_{r>0}e^{-\pi\lambda r^2}\int_{t>0}\frac{\mathbb{E}\left[e^{\left(-\mu r^\alpha\frac{e^t-1}{P\beta}(\sigma^2+\eta\beta\hat{I_{\mathcal{Z}}})\right)}\right]}{1-\mathbb{E}\left[e^{\left(-\mu r^\alpha\frac{T_{\rm FR}}{P}(\sigma^2+P\eta\beta I_{\mathcal{Z}})\right)}\right]}{\rm d}t\;r{\rm d}r\\ &\quad -2\pi\lambda\int_{r>0}e^{-\pi\lambda r^2}\int_{t>0}\frac{\mathbb{E}\left[e^{\left(-\mu r^\alpha\frac{\sigma^2}{P\beta}(e^t-1+\beta T_{\rm FR})\right)}e^{\left(-\mu r^\alpha\eta((e^t-1)\hat{I_{\mathcal{Z}}}+T_{\rm FR}I_{\mathcal{Z}})\right)}\right]}{1-\mathbb{E}\left[e^{\left(-\mu r^\alpha\frac{T_{\rm FR}}{P}(\sigma^2+P\eta\beta I_{\mathcal{Z}})\right)}\right]}{\rm d}t\;r{\rm d}r\\ &= \int_{t>0}\frac{p_c(\frac{\eta}{\beta}(e^t-1),\alpha,1)}{1-p_c(\eta T_{\rm FR},\lambda,\alpha,1)}-\frac{\zeta(e^t-1,T_{\rm FR},\alpha,\eta,\beta)}{1-p_c(\eta T_{\rm FR},\lambda,\alpha,1)}{\rm d}t, \qquad (2.37)\end{aligned}$$

where

$$\zeta\left(e^t-1,T_{\rm FR},\alpha,\eta,\beta\right)=\int_1^\infty\left[1-\frac{1}{1+\eta T_{\rm FR}x^{-\alpha}}\left(\frac{1}{1+\frac{\eta}{\beta}(e^t-1)x^{-\alpha}}\right)\right]x{\rm d}x,$$

and $p_c\left(\frac{\eta}{\beta}(e^t-1),\lambda,\alpha,\Delta\right)$ is given by (2.7). □

Fig. 2.11 compares the average rates for edge users under Strict FFR and SFR with $\beta = 4$ with no reuse and reuse-3 as a function of the threshold T_{FR}. We note that Strict FFR provides the highest average rates since it is also the strategy that provides the highest coverage for edge users. Also, the average rate increases linearly as T_{FR} is increased because users with increasingly higher initial SINR are provided a FFR sub-band. As with coverage probability, as β increases, edge users under SFR can have a higher rate than Strict FFR. However, since η also increases with β, this gain in rate for edge users is a tradeoff with decreasing average rates for interior users.

2.8 Rate and Resource Allocation for FFR

Systems under various traffic loads and channel conditions may have different priorities in regards to which metrics are most important. For example, networks experiencing high traffic loads may wish to optimize spectral efficiency, however in another circumstance, providing peak data rates for interference-limited edge users may be the desired goal. Since optimizing one metric for FFR systems usually leads to sub-optimal performance in regards to the other metrics, designers may additionally consider a hierarchy for the tradeoffs, by fixing thresholds for multiple metrics and optimizing the remaining ones in order to compromise between improving throughput and maintaining resource efficiency. This section explores these tradeoffs and compares the performance of SFR and FFR using the Poisson model and proposes a resource allocation strategy utilizing the analytical SINR distributions for maximizing sum-rate and balancing resource efficiency based on traffic load.

2.8.1 System Design Guidelines

Systems under various traffic loads and channel conditions may have different priorities in regards to which metrics are most important. For example, networks experiencing high traffic loads may wish to optimize spectral efficiency, however in another circumstance, providing peak data rates for interference-limited edge users may be the desired goal. Since optimizing one metric for FFR systems usually leads to sub-optimal performance with regard to the other metrics, designers may additionally consider a hierarchy for the tradeoffs, by fixing thresholds for multiple metrics and optimizing the remaining ones in order to compromise between improving throughput and maintaining resource efficiency. This section explores these tradeoffs and compares the performance of SFR and FFR using the Poisson model and proposes a resource allocation strategy utilizing the analytical SINR distributions for maximizing sum-rate and balancing resource efficiency based on traffic load.

We present system design guidelines for SFR and Strict FFR based on the analytical SINR distributions which are verified by Monte-Carlo simulations. The total number of sub-bands in the system under consideration is 48, comparable to a 10MHz LTE deployment. The user snapshots are taken over a 10 km^2 area with 25 uniformly spaced grid base stations, while the PPP base stations are modeled with a corresponding density of $\lambda = 1/(4000\pi^2)$ base stations per m^2.

Coverage. From the shape of the curves in Fig. 2.1 it is noted that at low values of β, SFR provides lower coverage probability compared to Strict FFR. However, if β is sufficiently large, SFR will surpass Strict FFR in terms of coverage as it approaches the performance of reuse-Δ. This tradeoff is achieved when there is approximately a 12 dB difference between downlink transmit power to edge and interior

users. Increasing β beyond this results in diminishing performance gain compared to the substantially increased required transmit powers.

Spectrum Utilization. However, under high traffic loads, interference avoidance may not outweigh the cost of reserving bandwidth for the partitioning structures of the reuse systems, especially reuse-Δ, or Strict FFR with a high number of sub-bands allocated to edge users. Reduction in resource efficiency additionally hurts the peak throughput of the cell, since users with high rate requirements may not be able to be allocated sufficient number of sub-bands. One benefit of SFR is the ability to balance the SINR gains experienced under Static FFR while utilizing more of the available sub-bands in every cell.

Sum Rate. Network sum rate performance was evaluated by running simulations of the various systems using $T_{\mathrm{FR}} = 3$ dB. The number of sub-bands available to edge users was varied from 2 - 16, representing the maximum number of edge user sub-bands since $\Delta = 3$ and $N_{band}/3 = 16$. This is analogous to varying the interior radius of FFR systems under the grid model [78]. Fig. 2.11 indicates that SFR with $\beta = 2$ is able to provide higher sum-rate than standard systems without sensitivity to the number of sub-bands allocated because when $N_{ext} \leq N_{band}/\Delta$, all the available sub-bands are allocated.

However, in the case of Strict FFR, as the number of sub-bands is increased, the total sum rate of Strict FFR decreases. This is because of Strict FFR's fundamental tradeoffs between spectral efficiency and the improved performance provided to edge users. Also note that when $N_{ext} = N_{band}/\Delta$, Strict FFR does not converge to reuse-Δ. Instead it has lower sum-rate. This is because although both systems allocate the same number of sub-bands in this case, reuse-Δ gives resources to inte-

rior and edge users, while Strict FFR only allocates resources to edge users, who by definition have smaller received power due to path loss and interference, reducing the achievable rate.

SINR**-proportional Resource Allocation**. Under the grid model, the frequency reuse partitions are based on the geometry of the network, and the resource allocation between interior and cell-edge users is proportional to the square of the ratio of the interior radius and the cell radius. In the case of the Poisson based model, geometric intuition for sub-band allocation does not apply, and instead allocation should be made based on SINR distributions from Section 2.4, improving the sum-rate for Strict FFR and SFR over that shown in Fig. 2.11.

Based on a chosen FFR threshold T_{FR}, the number of sub-bands can then be chosen by evaluating the CCDF at T_{FR} and choosing N_{edge} to be proportional to that value. In other words,

$$N_{edge} = \lfloor \left(1 - \bar{\mathrm{F}}_{FFR,e}(T_{\mathrm{FR}})\right) N_{band} \rfloor. \tag{2.38}$$

The threshold T_{FR} may be set as a design parameter, or may be alternatively chosen based on traffic load by inverting the CCDF (*i.e.,* low T_{FR} represents low edge user traffic and high T_{FR} when there are a large number of edge users). Fig. 2.12 presents the results of simulations of this SINR-proportional algorithm as function of T_{FR}. Both SFR and Strict FFR outperform the standard reuse strategies. SFR outperforms Strict FFR for smaller values of T_{FR}, due to the the loss in spectral efficiency of Strict FFR. As T_{FR} increases, Strict FFR provides greater sum-rate, due to larger gain in coverage for edge users when the number of allocated sub-bands for edge users is large.

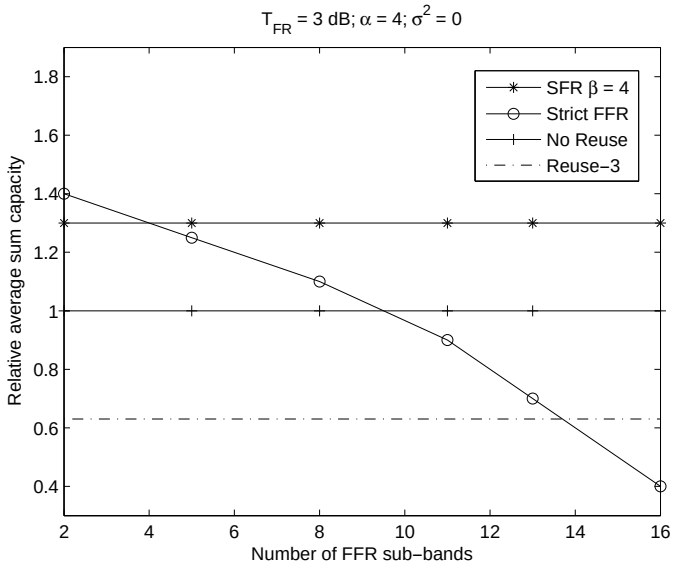

Figure 2.11: Average sum capacity for different reuse strategies as a function of the number of FFR sub-bands allocated for edge users.

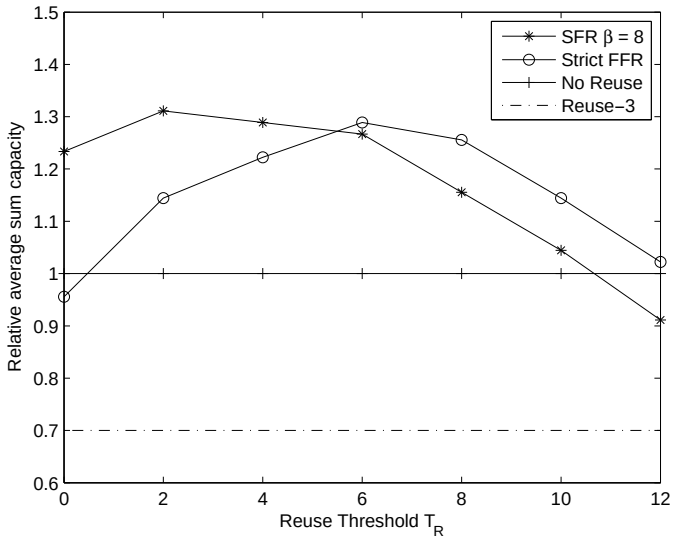

Figure 2.12: Average sum capacity for different reuse strategies using SINR-proportional sub-band allocation as a function of T_{FR}.

2.9 Conclusion

This chapter has presented a new analytical framework to evaluate coverage probability and average rate in cellular networks utilizing Strict FFR and SFR systems, leading to tractable expressions. The resulting system design guidelines highlighted the merits of those strategies as well as the tradeoffs between the superior interference reduction of Strict FFR and the greater resource efficiency of SFR.

In the next chapter this model for a single-tier cellular network is extended to heterogeneous networks with multiple-tiers of access points each applying the same or potentially different user association and FFR strategies. Tractable expressions for coverage and rate are developed as well as insights with regards to the impact of various interdependent network and system parameters.

Chapter 3

FFR in the Multi-Tier Cellular Downlink

Modern cellular network deployments are currently transitioning from homogeneous voice-centric deployments to highly heterogeneous data-centric networks made of different classes of access points [87]. These include operator deployed picocells and distributed antenna systems [84, 93, 118]. Additionally, in the case of home user-deployed femtocells, planning is not done in conjunction with the network operator [23]. Performance analysis of these networks becomes much more involved than for a single-tier network because of the need to account for inter-cell and cross-tier interference. While at the same time, practical interference coordination strategies like FFR become even more relevant and attractive in this context.

A further complication arises from different user association policies that can be implemented in multi-tier networks. The simplest is closed access, in which mobiles are restricted from connecting with certain tiers of access points. The reasons for selecting closed access may not solely be based on system performance metrics, but economic or legal factors in some cases [23]. Open access instead allows users in a multi-tier network to connect to APs of different tiers based on the association policy, which may be measured Signal to Interference Ratio (SIR) or traffic load. Open access is advantageous as an interference management technique since a macro user close by to a femtocell may be the source of significant interference to femtocell users or vice versa in the case of closed access, but if the user can instead connect to the femtocell,

the cross-tier interference is removed [111]. As a result, we propose to model and analyze the use of FFR systems for closed and open multi-tier networks.

This chapter extends the model of FFR in the downlink of a cellular network with a single-tier of base stations developed in the Chapter 2 to a general multi-tier network with closed and open access between the tiers. This allows for tractable expressions for the SINR distributions to be derived as a function of the FFR parameters which can be utilized for the system design of these networks.

3.1 Related Work

Early work on frequency partitioning for two-tier networks is found in [22]. Their proposed strategy maximizes the spectral efficiency for a minimum QoS requirement and the number of users per tier. They model the femtocells as uniformly distributed and characterize the macrocell interference using a hexagonal grid model. They highlight the importance of a decentralized approach to resource allocation in heterogeneous deployments as well as the importance of avoiding dominant intra and inter-tier interferers by allocating orthogonal resources to those users whenever possible.

The authors in [66] consider an adaptive FFR strategy for mitigating inter-femtocell interference while keeping spectral efficiency as high as possible. They vary the size of FFR partitions and transmit power based on the amount of estimated interference. However they use a deterministic model for the femtocells inside of a single building and neglect macrocell or femtocell interference outside of the building.

Very recent work in [67] considers a deterministic model analysis of the spectral efficiency of femtocells as a function of the femtocell's location in a two-tier network

with base stations modeled as a hexagonal grid and femtocells uniformly deployed in each cell. They fix the macrocell FFR sub-band allocations and then consider the spectral efficiency of a femtocell as a function of its distance from the cell center. Not surprisingly, they find that the performance of the femtocells improves when they use subbands not also utilized by macrocells. This is similar to the approach in [68] except that the authors consider the performance for different densities of femtocells and propose allocating femtocells in the cell-interior different subbands than those in the cell-edge region of the macrocell.

Frequency partitioning between macrocells and femtocells is revisited in [11]. They propose a model where some sub-bands are reserved for only macrocell or femtocell users in addition to a common group of sub-bands, similar in concept to the Strict FFR model. They also alternately consider partitioning in the time domain. They provide a large number of simulation results based on a deterministic model for the AP locations and motivate a dynamic partitioning based on measured interference levels by users in either tier.

The authors in [59] consider performance tradeoffs for closed and open femtocell networks. Their analysis uses stochastic geometry tools from [43] in order to derive SINR distributions for different deployment scenarios at the cell edge or interior and for varying femtocell densities. However their analysis is constrained to the interior of a single macrocell and does not consider the effect of inter-cell interference or the use of FFR on the SINR distributions.

3.2 Contributions

We consider the two common FFR deployments Strict FFR and SFR in the context of general K-tier cellular network downlinks for closed access and two-tiers for open access. In the case of Strict FFR, inter-cell and cross-tier interference is present on the common sub-band allocated to all macrocells, while the FFR sub-band is reserved for macrocell users and does not experience cross-tier interference, only inter-cell interference thinned with a reuse factor of Δ. For SFR, due to reuse of all sub-bands in every cell, the edge user FFR sub-bands are also utilized by the other tiers, however edge users are allocated a higher transmit power on that sub-band.

Performance analysis of these networks is much more involved than for a single-tier network because of the need to account for inter-cell and cross-tier interference and the non-uniformity of the access point deployments arising from both topographic and economic reasons. A further complication in heterogeneous network analysis arises from different user association policies. As a result, there is a need for new and general models for analyzing the important metrics of coverage and rate in the context of these multi-tier networks. While prior work has relied on simulations based on deterministic models of AP locations, these have not led to general or tractable solutions. Instead, we extend the model of Chapter 2 for a single tier to multiple tiers of AP locations modeled as Poisson point processes [14, 19, 47]. This modeling approach has been recently applied to the analysis of cellular networks due to the ability to derive tractable expressions for coverage and rate both for one-tier [8] and very recently, heterogeneous networks [30, 31, 74, 75]. This allows the development of tractable expressions for the SINR distributions to be derived as a function of the FFR parameters which can be utilized for the system design of these networks. The

three contributions of this chapter are as follows:

SINR **distributions for closed access:** We extend the framework of Chapter 2 to evaluate the SINR distributions for users in a general K-tier network downlinks utilizing Strict FFR and SFR. We consider closed access, which limits users to associate with APs in only one tier, with all the other tiers contributing interference.

SIR **distributions for open access:** We propose a new framework for analyzing open access downlinks under Strict FFR and SFR in which users may associate with APs in more than one tier. We evaluate coverage probability and average rate for users in a two-tier network.

System design guidelines: Applications to system design for closed and open access networks are given based on the prior analysis. The models give insight into how the FFR parameters and resource partitions change based on the densities, transmit powers, and resource allocation strategies of the tiers.

3.3 System Model

We consider an OFDMA cellular downlink with K-tiers of access points (APs). The locations of the access points are modeled as independent spatial Poisson point processes (PPP) [104] of density λ_k with independence between the tiers. In other words, for a given PPP, the number of points in a bounded area is a Poisson-distributed random variable and those points are uniformly-distributed within the area. A realization of a three-tier network with Poisson distributed APs and Voronoi cell coverage regions based on a SINR threshold of 1 dB is given in Fig. 3.2.

Without loss of generality, we assume a typical mobile user at the origin and

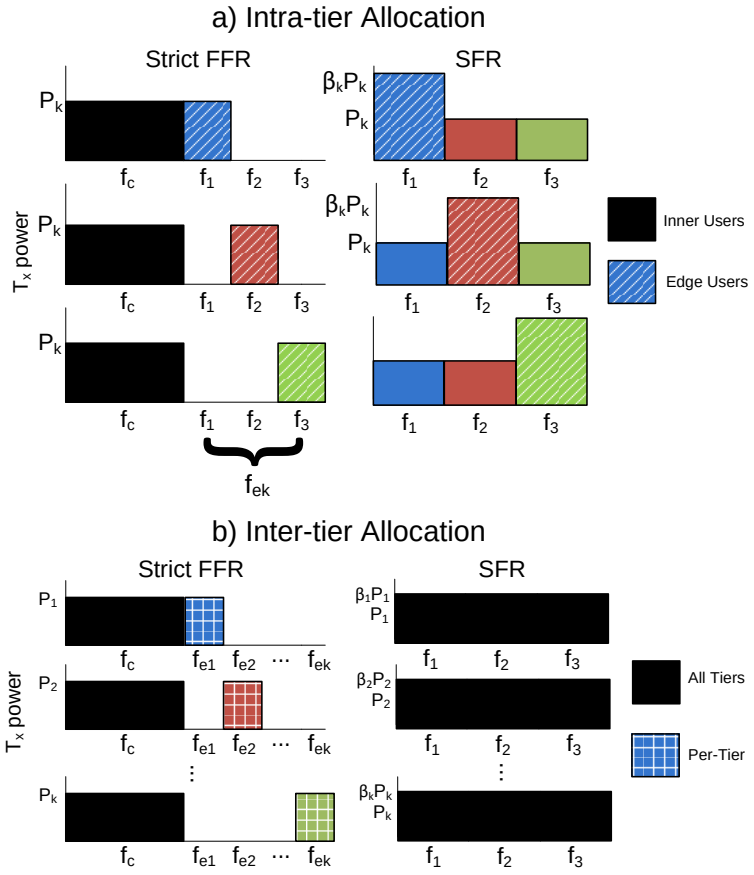

Figure 3.1: a) Intra-tier Strict FFR and SFR subband and transmit power allocations. b) Inter-tier subband allocations. For simplicity of illustration the cell-edge frequency reuse factor for all tiers is set to $\Delta = 3$.

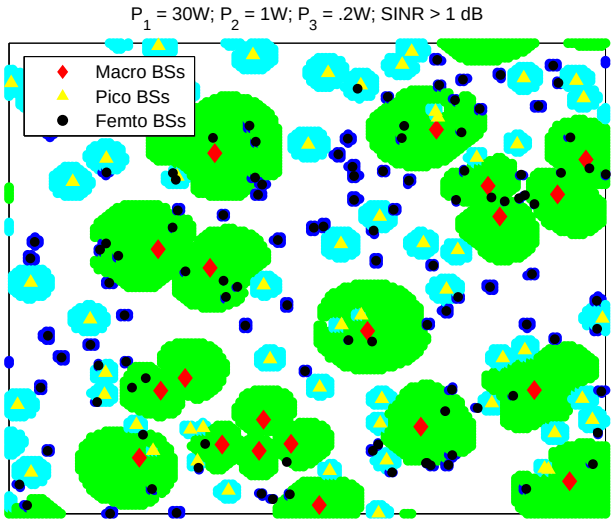

Figure 3.2: A realization of a Poisson distributed three-tier cellular network with coverage regions defined by an SINR threshold of 1 dB.

compute the SINR for this typical mobile. We assume that the mobile user is served by only one tier at a time and by the closest AP of that tier, which is at a distance r_k. Since the underlying APs are distributed as PPPs, it follows that r_k is Rayleigh distributed [104]. We assume that all the access points of the k^{th} tier transmit with an equal power P_k. The path loss exponent is given by α, and σ^2 is the noise power. We assume that the small-scale fading between any interfering AP and the typical mobile in consideration, denoted by G_z, is i.i.d exponentially distributed with mean μ (corresponds to Rayleigh fading). The set of interfering APs in the k^{th} tier is $\mathcal{Z}_k$, i.e. access points that use the same subband as the mobile user. We denote the distance between the interfering AP and the mobile node in consideration by R_z. Fig. 3.2 shows a realization of three-tier network with Poisson distributed APs and Voronoi cell coverage regions based on strongest received power.

The associated signal-to-interference-plus-noise-ratio (SINR) is given as

$$\text{SINR} = \frac{P_k g_k {r_k}^{-\alpha}}{\sigma^2 + \sum_{k=1}^{K} P_k I_k}, \tag{3.1}$$

where for an interfering set of k^{th} tier APs $\mathcal{Z}_k$,

$$I_k = \sum_{z \in \mathcal{Z}_k} G_z {R_z}^{-\alpha}. \tag{3.2}$$

In the above expression, we have assumed that the nearest AP to the mobile in the k^{th} tier is at a distance r_k, which is a random variable. Also the fading between the nearest AP in consideration is denoted by g_k.

We will consider the two most common types of FFR: *Strict FFR* and *Soft Frequency Reuse* (SFR). Under Strict FFR, which extends the traditional frequency reuse used extensively in current cellular networks [15, 102], users in the interior of a cell are allocated a common subband of frequencies f_c while at the cell-edge, users are allocated separate subbands partitioned across cells with a reuse factor of Δ. The left sub-figure in Fig. 3.1a illustrates potential Strict FFR allocations with $\Delta = 3$ in which edge users are given frequency resources corresponding to subbands f_1, f_2, or f_3. The primary advantage of Strict FFR is the significant reduction in interference for edge users, although there is a loss in spectral efficiency since each cell cannot fully utilize all $\Delta + 1$ subbands [78].

The right sub-figure in Fig. 3.1a illustrates the frequency and transmit power allocation for SFR. Edge users are allocated bandwidth subbands with a reuse factor of Δ, but the main difference vs. Strict FFR is that each cell utilizes all Δ subbands since interior users are allowed to share subbands with edge users in other cells. Because cell-edge users share the bandwidth with neighboring cells, their downlinks are typically transmitted with higher power levels in order to reduce the impact of

the inter-cell interference [55, 70]. To accomplish this, a transmit power control factor $\beta \geq 1$ is introduced to create two different classes, $P_{\text{int}} = P$ and $P_{\text{edge}} = \beta P$, where P_{int} is the transmit power of the base station if user y is an interior user and P_{edge} is the transmit power of the base station if user y is a cell-edge user. The increased interference for edge users under SFR is traded off for greater spectral utilization [33].

With FFR, a mobile user first determines its SINR to the nearest AP of the k^{th} tier and checks if it is less than the tier's FFR threshold T_k. If so, then the user is classified as an *edge* user and the AP transmits its downlink on the reserved FFR band, randomly picked from Δ_k subbands available. Otherwise we classify the mobile as an *interior* user. These classifications arise differently than prior work utilizing the typical grid model assumption which defines an interior radius [78], since constant SINR contours can no longer be defined as concentric circles around the AP [51]. In fact the edge or interior user classifications does not necessarily have the same geographic interpretation for each cell. As noted in [19], this consequence of the spatial PPP more closely reflects non-regular deployments and typically corresponds to a lower performance bound compared to the upper bound provided by the grid model.

To accommodate the difference between SFR and Strict FFR in terms of the use of power control, we introduce the design parameter β. Typical ranges for β are 0-20 dB [4, 33]. On the edge subbands, this extra downlink power is applied by $1/\Delta_k$ of the base stations of each tier and the interference power is given by $\sum_{k=1}^{K} \eta_k P_k I_k$, where $\eta_k = (\Delta_k - 1 + \beta_k)/\Delta_k$ consolidates the edge and interior downlinks into a single effective interference term.

3.4 Coverage Probability with Closed Access

We initially consider coverage probability the downlink of a multi-tier network with closed access between the tiers. For example, in the context of a two-tier network with macrocells and underlaid femtocells, a mobile user connected to the macrocell may be in range of a femtocell, but is unable to connect to that femtocell, potentially resulting in cross-tier interference.

Coverage probability is the probability that a user's SINR is greater than a threshold T, equivalently the CCDF of the SINR for a particular reuse strategy, denoted as

$$\bar{F}(T) = \mathbb{P}(\text{SINR} > T). \tag{3.3}$$

The results of the prior chapter and further elaborated upon in [80, 81] take advantage of the framework recently developed in [8] utilizing the Poisson point process (PPP) model for base station locations. In this section this model is extended to provide the exact distribution of SINR for cell-edge users with Strict FFR and SFR under closed access user association.

3.4.1 Multi-tier coverage with Strict FFR

In the case of Strict FFR, we assume that inter-cell and cross-tier interference is present on the common subband allocated to all tiers, while the FFR subbands are reserved for edge users of each tier and do not experience cross-tier interference, only inter-cell interference thinned with a reuse factor of Δ_k. Edge users of a given tier are those who have SINR less than the macrocell's FFR threshold T_k on the common subband shared by all cells and are therefore selected by the reuse strategy to have a new subband allocated to them from the Δ_k total available subbands reserved for

the edge users.

Theorem 8 (Strict FFR, closed access, edge user)**.** *The coverage probability of a k^{th}-tier edge user in a strict FFR system, assigned a FFR subband is* $\bar{\mathrm{F}}_{\mathrm{FFR,cl}}(k,T) =$

$$\frac{\pi\lambda_1 \int_0^\infty e^{-\pi\lambda_1 v\left(1+\frac{\rho(T,\alpha)}{\Delta}\right)-\mu T\frac{\sigma^2}{P_k}v^{\alpha/2}}\mathrm{d}v}{1-\pi\lambda_k\int_0^\infty e^{-\pi\lambda_1 v\left(1+\rho(T_k,\alpha)+2\sum_{j\neq k}^K \kappa_{j,k}\psi(\gamma_{j,k}T_k,\alpha)\right)\Theta(\alpha,\sigma,)\mathrm{d}v}} - \frac{e^{-\pi\lambda_k v\left(1+2\xi(T,T_k,\alpha,\Delta)+2\sum_{j\neq k}^K \kappa_{j,k}\psi(\gamma_{j,k}T_k,\alpha)\right)\Theta(\alpha,\sigma,)\mathrm{d}v}}{1-\pi\lambda_k\int_0^\infty e^{-\pi\lambda_1 v\left(1+\rho(T_k,\alpha)+2\sum_{j\neq k}^K \kappa_{j,k}\psi(\gamma_{j,k}T_k,\alpha)\right)\Theta(\alpha,\sigma,)\mathrm{d}v}}, \tag{3.4}$$

$$\textit{where } \rho(z,\alpha) = z^{2/\alpha}\int_{z^{-2/\alpha}}^\infty \frac{1}{1+u^{\alpha/2}}\mathrm{d}u, \tag{3.5}$$

$$\xi(T,T_k,\alpha,\Delta_k) = \int_1^\infty \left[1-\frac{1}{1+T_k x^{-\alpha}}\left(1-\frac{1}{\Delta_k}\left(1-\frac{1}{1+Tx^{-\alpha}}\right)\right)\right]x\mathrm{d}x, \tag{3.6}$$

$$\Theta\left(\alpha,\sigma,\right) = e^{-\mu(T+T_k)\frac{\sigma^2}{P_k}v^{\alpha/2}}, \tag{3.7}$$

$$\textit{and } \psi(z,\alpha) = csc\left(\frac{2\pi}{\alpha}\right)\frac{\pi z^{2/\alpha}}{\alpha}\ ,\ \gamma_{j,k} = \frac{P_j}{P_k}\ ,\ \kappa_{j,k} = \frac{\lambda_j}{\lambda_k}. \tag{3.8}$$

Proof. A user y connected to a kth tier AP with $\mathrm{SINR}_k < T_k$ is given a FFR subband δ_y, where $\delta \in \{1,...,\Delta_k\}$ with uniform probability $\frac{1}{\Delta_k}$, and experiences new fading power $\hat{g_k}$ and out-of-cell interference $P_k\hat{I_k}$, instead of g_k and $\sum_{j\neq k}^K P_j I_j$. The CCDF of the edge user $\bar{\mathrm{F}}_{\mathrm{FFR,cl}}(k,T)$ is now conditioned on its previous SINR. Using Bayes' rule we have,

$$\mathbb{P}\left(\frac{P_k\hat{g_k}{r_k}^{-\alpha}}{\sigma^2+P_k\hat{I_k}} > T \;\middle|\; \frac{P_k g_k {r_k}^{-\alpha}}{\sigma^2+\sum_{j\neq k}^K P_j I_j} < T_k\right) = \frac{\mathbb{P}\left(\frac{P_k\hat{g_k}{r_k}^{-\alpha}}{\sigma^2+P_k\hat{I_k}} > T\ ,\ \frac{P_k g_k {r_k}^{-\alpha}}{\sigma^2+\sum_{j\neq k}^K P_j I_j} < T_k\right)}{\mathbb{P}\left(\frac{P_k g_k {r_k}^{-\alpha}}{\sigma^2+\sum_{j\neq k}^K P_j I_j} < T_k\right)}. \tag{3.9}$$

Conditioning on r_k, the distance to the nearest kth tier AP, which is Rayleigh distributed and focusing on the numerator of (3.9), since $\hat{g_k}$ and g_k are i.i.d. expo-

nentially distributed with mean μ, gives

$$\mathbb{E}\left[e^{\left(-\mu\frac{Tr_k{}^{\alpha}}{P_k}(\sigma^2+P_k\hat{I}_k)\right)}\right] \; - \\ \mathbb{E}\left[e^{\left(-\mu\frac{Tr_k{}^{\alpha}}{P_k}(\sigma^2+P_k\hat{I}_k)\right)}e^{\left(-\mu\frac{T_kr_k{}^{\alpha}}{P_k}\left(\sigma^2+P_kI_k+\sum_{j\neq k}^{K}P_jI_j\right)\right)}\right],$$

Factoring out terms dependent on the independent noise power σ^2 we observe that the expectation of the second term with respect to $\hat{I}_k$, I_1, I_2, ... , and I_K is the joint Laplace transform $\mathscr{L}(\hat{s_k}, s_1, s_2, ..., s_K)$ of $\hat{I}_k$, I_1, I_2, ..., and I_K given by $\mathbb{E}\left[e^{\left(-\hat{s_k}\hat{I}_k-s_kI_k-\sum_{j\neq k}^{K}s_jI_j\right)}\right]$

$$= \mathbb{E}\left[e^{\left(-\hat{s_k}\sum_{z\in Z_k}\hat{G}_zR_z{}^{-\alpha}\mathbf{1}(\delta_z=\delta_y)-s_kG_zR_z{}^{-\alpha}\right)}\times \right. \\ \left. e^{\left(-\sum_{j\neq k}^{K}\left(s_j\sum_{z\in Z_j}G_jR_z{}^{-\alpha}\right)\right)}\right]$$

$$= \prod_{j\neq k}^{K}\mathbb{E}\left[\prod_{z\in Z_j}e^{\left(-s_jG_zR_z{}^{-\alpha}\right)}\right]\times$$

$$\mathbb{E}\left[\prod_{z\in Z_k}\left(1-\mathbb{E}\left[\mathbf{1}(\delta_z=\delta_y)\right](1-e^{(-\hat{s_k}\hat{G}_zR_z{}^{-\alpha})})\right)e^{\left(-s_kG_zR_z{}^{-\alpha}\right)}\right],$$

where $\mathbf{1}(\delta_y = \delta_z)$ is an indicator function that takes the value 1 if base station z is transmitting to an edge user on the same subband δ as user y, and the third step arises from the independence of I_k and $\hat{I}_k$ with respect to $I_{j\neq k}$. Since $\hat{G}_z$ and G_z are also exponential random variables with mean μ, we can evaluate the above expression as

$$\mathbb{E}\left[\prod_{z\in Z_k}\left(1-\frac{1}{\Delta_k}\left(1-\frac{\mu}{\mu+\hat{s_k}R_z{}^{-\alpha}}\right)\right)\frac{\mu}{\mu+s_kR_z{}^{-\alpha}}\right]\prod_{j\neq k}^{K}\mathbb{E}\left[\prod_{z\in Z_j}\frac{\mu}{\mu+s_jR_z{}^{-\alpha}}\right].$$

By using the probability generating functional (PGFL) of the PPP [104] we obtain $\mathscr{L}(\hat{s_k}, s_1, s_2, ..., s_K) =$

$$e^{\left(-2\pi\lambda_1\int_{r_1}^{\infty}\left[1-\frac{\mu}{\mu+s_kx^{-\alpha}}\left(1-\frac{1}{\Delta}\left(1-\frac{\mu}{\mu+\hat{s_k}x^{-\alpha}}\right)\right)\right]x\mathrm{d}x\right)}\prod_{j\neq k}^{K}e^{\left(-2\pi\lambda_j\left(\frac{s_j}{\mu}\right)^{2/\alpha}\frac{\pi\csc(\frac{2\pi}{\alpha})}{\alpha}\right)}.$$

Substituting for the integration variables s and de-conditioning on r_k, we have

$$2\pi r_k \lambda_k \int_0^\infty e^{-2\pi\lambda_k {r_k}^2\left(\frac{1}{2}+\xi(T,T_k,\alpha,\Delta_k)\right)} e^{-2\pi\lambda_k {r_k}^2\left(\sum_{j\neq k}^{K}\kappa_{j,k}\psi(\gamma_{j,k}T_k,\alpha)\right)} e^{-\mu(T+T_k)\frac{\sigma^2}{P_k}{r_k}^\alpha} \mathrm{d}r_k, \quad (3.10)$$

where $\xi(T,T_k,\alpha,\Delta_k) =$

$$\int_{r_k}^\infty \left[1-\frac{1}{1+T_k {r_k}^\alpha x^{-\alpha}}\left(1-\frac{1}{\Delta_k}\left(1-\frac{1}{1+T{r_k}^\alpha x^{-\alpha}}\right)\right)\right] x\mathrm{d}x,$$

$$\text{and } \psi(z,\alpha) = \csc\left(\frac{2\pi}{\alpha}\right)\frac{\pi \mathrm{z}^{2/\alpha}}{\alpha}\ ,\ \gamma_{\mathrm{j,k}} = \frac{\mathrm{P_j}}{\mathrm{P_k}}\ ,\ \kappa_{\mathrm{j,k}} = \frac{\lambda_{\mathrm{j}}}{\lambda_{\mathrm{k}}}.$$

Now we focus on the denominator of (3.9), using the independence of I_1 and I_2,...,I_K we have

$$\begin{aligned}
& 1-\mathbb{E}\left[e^{-\mu\frac{T_k}{P_k}{r_k}^\alpha(\sigma^2+\sum_{k=1}^{K}P_k I_k)}\right] \\
= \ & 1-\mathbb{E}\left[e^{\left(-\mu\frac{T_k}{P_k}{r_k}^\alpha(\sigma^2+P_k I_k)\right)}\right]\prod_{j\neq k}^{K}\mathbb{E}\left[e^{\left(-\mu\frac{T_k}{P_k}{r_k}^\alpha(P_j I_j)\right)}\right] \\
= \ & 1-2\pi r_k\lambda_k\int_0^\infty e^{-\pi\lambda_k {r_k}^2(1+\rho(T_k,\alpha))}\times \\
& e^{-\pi\lambda_k {r_k}^2\left(2\sum_{j\neq k}^{K}\kappa_{j,k}\psi(\gamma_{j,k}T_k,\alpha)\right)} e^{-\mu(T+T_k)\frac{\sigma^2}{P_k}{r_k}^\alpha}\mathrm{d}r_k. \qquad (3.11)
\end{aligned}$$

The first term of the numerator represents the SINR on the newly allocated subband and we have

$$\pi\lambda_k\int_0^\infty e^{-\pi\lambda_k v\left(1+\frac{\rho(T,\alpha)}{\Delta_k}\right)-\mu T\frac{\sigma^2}{P_k}v^{\alpha/2}}, \qquad (3.12)$$

since the received interference is only from the first tier APs due to the closed access frequency allocation for edge users and is originally given in [8].

Thus plugging (3.10) and (3.11) back into (3.9), and substituting (3.12) for the first term of the numerator and substituting ${r_k}^2 = v$ we have (3.4). □

An immediate observation of this framework is that it leads to expressions which are only a function of the relevant FFR design parameters. The intra-tier interference before and after FFR is applied are captured in the $\xi(T, T_k, \alpha, \Delta_k)$ and $\rho(z, \alpha)$ terms respectively, while the cross tier interference terms for each tier are expressed by $\psi(z, \alpha)$.

3.4.2 Multi-tier coverage with SFR

We now consider the CCDF of the SINR for edge users with SFR. In this case all the subbands overlap with those of the other tiers since SFR makes use of the entire spectrum but allocates edge users with SINR below the FFR threshold a higher transmit power determined by the β parameter.

Theorem 9 (SFR, closed access, edge user)**.** *The coverage probability of an SFR edge user whose initial* SINR *is less than* T_k *is*

$$\bar{\mathrm{F}}_{\mathrm{SFR,cl}}(k,T) = \left(f_{n1}\left(k,T\right) - f_{n2}\left(k,T\right)\right)/f_{d1}\left(k,T\right), \tag{3.13}$$

where

$$f_{n1} = \pi\lambda_k \int_0^\infty e^{-\pi\lambda_k v\left(1+\rho\left(\frac{\eta_k T}{\beta_k},\alpha\right)+2\sum_{j\neq k}^{K}\kappa_{j,k}\psi\left(\frac{T\beta_j\gamma_{j,k}}{\beta_k},\alpha\right)\right)} e^{-\frac{\mu T\sigma^2}{\beta P_k}v^{\alpha/2}}\mathrm{d}v$$

$$f_{n2}\left(k,T\right) = \pi\lambda_k \int_0^\infty e^{-\pi\lambda_k v(1+2\zeta(T,T_k,\alpha,\beta,\eta))-\mu(T+\eta T_k)\frac{\sigma^2}{P_k}v^{\alpha/2}} \times e^{-\pi\lambda_k v\left(2\sum_{j\neq k}^{K}\kappa_{j,k}\left(\psi\left(\frac{\beta_j\gamma_{j,k}}{\beta_k}T,\alpha\right)+\psi\left(\gamma_{j,k}T_k,\alpha\right)\right)\right)}\mathrm{d}v.$$

$$f_{d1}\left(k,T\right) = 1 - \pi\lambda_k \int_0^\infty e^{-\pi\lambda_k v(1+\rho(\eta T_k,\alpha))} \times e^{-2\pi\lambda_k v\sum_{j\neq k}^{K}\kappa_k\psi(\gamma_k T_k,\alpha)-\mu(\eta T_k)\frac{\sigma^2}{P_1}v^{\alpha/2}}\mathrm{d}v$$

$\zeta(T, T_k, \alpha, \beta_k, \eta_k) =$

$$\int_1^\infty 1 - \frac{1}{(1+\eta_k {T_k}^\alpha x^{-\alpha})\left(1+\frac{\eta_k}{\beta_k}T^\alpha x^{-\alpha}\right)} x \mathrm{d}x,$$

$\rho(z,\alpha)$ is given by (3.5)*, and $\psi(z,\alpha)$, $\kappa_{j,k}$ and $\gamma_{j,k}$ are given by* (3.8)*.*

Proof. A k^{th} tier connected user y with SINR $< T_k$ is assigned a FFR subband δ_y, where $\delta \in \{1, ..., \Delta_k\}$ with uniform probability $\frac{1}{\Delta_k}$, and experiences new fading power $\hat{g_k}$, transmit power $\beta_k P_k$, and out-of-cell interference $\sum_{j=1}^K \eta_j P_j \hat{I_j}$. The CCDF of the edge user $\bar{\mathrm{F}}_{\mathrm{SFR,cl}}(k,T)$ is now conditioned on its previous SINR,$\bar{\mathrm{F}}_{\mathrm{SFR,cl}}(k,T) =$

$$\mathbb{P}\left(\frac{\beta_k P_k \hat{g_k} {r_k}^{-\alpha}}{\sigma^2 + \sum_{j=1}^K \eta_j P_j \hat{I_j}} > T \;\middle|\; \frac{P_k g_k {r_k}^{-\alpha}}{\sigma^2 + \sum_{j=1}^K \eta_j P_j I_j} < T_k\right). \tag{3.14}$$

Using Bayes' rule as in Theorem 8 and focusing on the resulting numerator, since $\hat{g_k}$ and g_k are i.i.d. exponentially distributed with mean μ, this gives

$$\mathbb{E}\left[e^{\left(-\mu\frac{T}{\beta_k P_k}{r_k}^\alpha(\sigma^2+\sum_{j=1}^K \eta_j P_j \hat{I_j})\right)}\right] -$$

$$\mathbb{E}\left[e^{\left(-\mu\frac{T}{\beta_k P_k}{r_k}^\alpha(\sigma^2+\sum_{j=1}^K \eta_j P_j \hat{I_j})\right)} e^{\left(-\mu\frac{T_k}{P_k}{r_1}^\alpha(\sigma^2+\sum_{j=1}^K \eta_j P_j I_j)\right)}\right],$$

Now concentrating on the second term, factoring out terms corresponding to the independent noise power σ^2, and *conditioning on* r_k, we obtain the joint Laplace transform of $\hat{I_1}$, $\hat{I_2}$, ..., $\hat{I_K}$, and I_1, I_2, ..., I_K given by

$$\mathbb{E}\left[\prod_{z\in Z_k} \frac{\mu}{\mu+\hat{s_k}{R_z}^{-\alpha}} \frac{\mu}{\mu+s_k {R_z}^{-\alpha}}\right] \times$$
$$\prod_{j\neq k}^K \mathbb{E}\left[\prod_{z\in \hat{Z}_j} \frac{\mu}{\mu+\hat{s_j}{R_z}^{-\alpha}}\right] \mathbb{E}\left[\prod_{z\in Z_j} \frac{\mu}{\mu+s_j {R_z}^{-\alpha}}\right]. \tag{3.15}$$

Using the same method as Theorem 8 and de-conditioning on r_k we obtain

$$2\pi r_k \lambda_k \quad \int_0^\infty e^{-\pi\lambda_k {r_k}^2(1+2\zeta(T,T_k,\alpha,\beta_k,\eta_k))-\mu(\frac{T}{\beta_k}+T_k)\frac{\sigma^2}{P_k}{r_k}^\alpha}$$
$$\times \quad e^{-\pi\lambda_k {r_k}^2\left(2\sum_{j\neq k}^K \kappa_{j,k}\left(\psi(\frac{\gamma_{j,k}}{\beta_k}T,\alpha)+\psi(\gamma_{j,k}T_k,\alpha)\right)\right)} \mathrm{d}r_k, \tag{3.16}$$

where $\zeta(T, T_k, \alpha, \beta_k, \eta_k) =$

$$\int_{r_k}^{\infty} \left[1 - \frac{1}{1 + \eta_k T_k {r_k}^{\alpha} x^{-\alpha}} \frac{1}{1 + \frac{\eta_k}{\beta_k} T {r_k}^{\alpha} x^{-\alpha}} \right] x \mathrm{d}x,$$

Using the same argument and analysis for the resulting denominator of (3.14) after Bayes' rule is applied we have

$$1 - 2\pi r_k \lambda_k \int_0^{\infty} e^{-\pi \lambda_k {r_k}^2 \left(1 + \rho(\eta T_k, \alpha) + 2 \sum_{j \neq k}^{K} \kappa_{j,k} \psi(T_k, \alpha)\right)} e^{-\mu(T + \eta_k T_k) \frac{\sigma^2}{P_k} {r_k}^{\alpha}} \mathrm{d}r_k, \quad (3.17)$$

Finally, the first term of the numerator is given as

$$2\pi r_k \lambda_k \int_0^{\infty} e^{-\pi \lambda_k {r_k}^2 \left(1 + \rho(\frac{\eta_k}{\beta_k} T, \alpha) + 2 \sum_{j \neq k}^{K} \kappa_{j,k} \psi(\frac{\eta_j \gamma_{j,k}}{\beta_k} T, \alpha)\right)} e^{-\mu(T) \frac{\sigma^2}{\beta_k P_k} {r_k}^{\alpha}} \mathrm{d}r_k. \quad (3.18)$$

Thus plugging (3.16), (3.17), and (3.18) back into (3.14) and substituting ${r_k}^2 = v$ we have (3.13). □

The expressions differ from Strict FFR both due to the effective SINR and FFR thresholds shaped by the power control factor β and effective interference power η respectively.

3.4.3 Model Evaluation

While all the coverage probability results hold for general α and σ^2, we present a special case of $\alpha = 4$ and $\sigma^2 = 0$, corresponding to an interference-limited urban cellular network [90] where FFR techniques are of special interest. Additionally, in this case the expressions reduce to a simple closed-form, something that cannot be achieved with a deterministic model.

In the case of $\alpha = 4$ and no noise, for *Strict FFR*, the CCDF is given as,

$$\bar{\mathrm{F}}_{\mathrm{FFR,cl}}(k,T) = \frac{1+\rho(T_k)+\frac{\pi}{2}\sum_{j\neq k}^{K}\kappa_{j,k}\sqrt{\gamma_{j,k}T}}{\rho(T_k)+\frac{\pi}{2}\sum_{j\neq k}^{K}\kappa_{j,k}\sqrt{\gamma_{j,k}T}}\times$$
$$\left(\frac{1}{1+\frac{\rho(T)}{\Delta_k}} - \frac{1}{1+2\xi(T,T_k,4,\Delta_k)+\frac{\pi}{2}\sum_{j\neq k}^{K}\kappa_{j,k}\sqrt{\gamma_{j,k}T}}\right),$$
$$\text{where } \xi(T,T_k,4,\Delta_k) = \frac{T\rho(T)-\rho(T_k)\left(T_k\Delta_k - T\left(1+\Delta_k\right)\right)}{4\Delta_k(T_1-T)},$$
$$\text{and } \rho(x) = \sqrt{x}\arctan\left(\sqrt{x}\right).$$

In the case of $\alpha = 4$ and no noise, for *SFR*, the CCDF is given as,

$$\bar{\mathrm{F}}_{\mathrm{SFR,cl}}(k,T) = \frac{1+\rho(\eta_k T_k)+\frac{\pi}{2}\sum_{j\neq k}^{K}\sqrt{\gamma_{j,k}T}}{\rho(\eta_k T_k)+\frac{\pi}{2}\sum_{j\neq k}^{K}\sqrt{\gamma_{j,k}T}}$$
$$\times \left(\frac{1}{1+\frac{\rho(\frac{\eta_k}{\beta_k}T)}{\Delta_k}+\frac{\pi}{2}\sum_{j\neq k}^{K}\sqrt{\frac{\gamma_{j,k}}{\beta_k}T}} - \frac{1}{1+2\zeta(T,T_k,4,\beta_k,\eta_k)+\frac{\pi}{2}\sum_{j\neq k}^{K}\sqrt{\gamma_{j,k}T}}\right),$$

where $\zeta(T,T_k,4,\beta_k,\eta_k) =$

$$\frac{{\eta_k}^{3/2}T\beta_k}{4\sqrt{T_k}(T-T_k\beta)} - \frac{\eta_k\beta_k T^3\left(2\arctan\left(\sqrt{\frac{\beta_k}{\eta_k T}}\right)+\pi\right)}{(T-T_k\beta_k)}$$
$$+ \frac{\eta_k T^{3/2}{T_k}^{3/2}\beta^{5/2}\left(2\arctan\left(\frac{1}{\sqrt{\eta_k T_k}}\right)-\pi\right)}{(T-T_k\beta_k)}. \tag{3.19}$$

Fig. 3.3 shows the derived distributions for first-tier Strict FFR and SFR edge users for a three-tier network without noise, $\Delta_1 = 3$, $T_1 = 3$ dB, P_1 $\lambda_1 = 24$ APs per $10km^2$, $\kappa_2 = 4$, $\gamma_2 = .01$ $\lambda_3 = 9$, $\gamma_3 = .001$, and $\alpha = 4$. The Strict FFR and the $\beta_1 = 2$ curves are plotted with the results of Monte Carlo simulations based on the above parameters to highlight the accuracy of the mathematical model. We also see the improved coverage afforded to cell-edge users with FFR compared to

universal frequency reuse. For Strict FFR, much of the gain results in the removal of both cross-tier interference and $1/\Delta_1$ of the intra-tier interference. SFR provides a lower coverage gain, but this can be mitigated by the use of higher β_1, up to the theoretical maximum of $\beta = \infty$ which approaches Strict FFR coverage, however much lower values will more likely be used due to practical implementation constraints. Additionally when comparing Strict FFR and SFR one must take into account that more spectrum is available for SFR since each cell fully utilizes all subbands.

In Fig. 3.4 we consider the coverage probability of a typical third tier edge user. Even with a large reuse threshold of $T_3 = 10$ dB and $\beta_3 = 8$, due to the much lower transmit power and the even greater impact of cross-tier interference the relative coverage improvement of SFR is reduced compared to Fig. 3.3. As with the first tier edge users, the Strict FFR coverage probability is the greatest due to the removal of the strong cross-tier interference.

Using similar techniques we can derive the distributions for interior users using this framework. Additionally, these results are also valid for $\alpha \neq 4$, but the expressions no longer have the same simple closed-form. Instead they are integrals that can be evaluated using numerical techniques.

3.5 Coverage Probability with Open Access

In the following analysis of open access downlinks we make the following two assumptions, (i) that there are only two-tiers of access points, and (ii) we only consider the SIR, as the access metric, neglecting noise. While our general framework can accommodate an unlimited number of tiers and noise, making those assumptions greatly reduces the complexity of the expressions for the SIR distributions. The

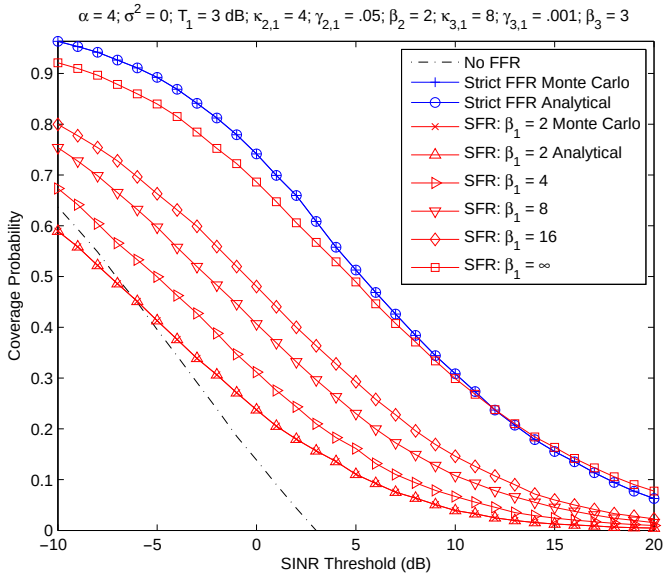

Figure 3.3: Downlink first tier edge user SINR distributions for closed access with three tiers of APs.

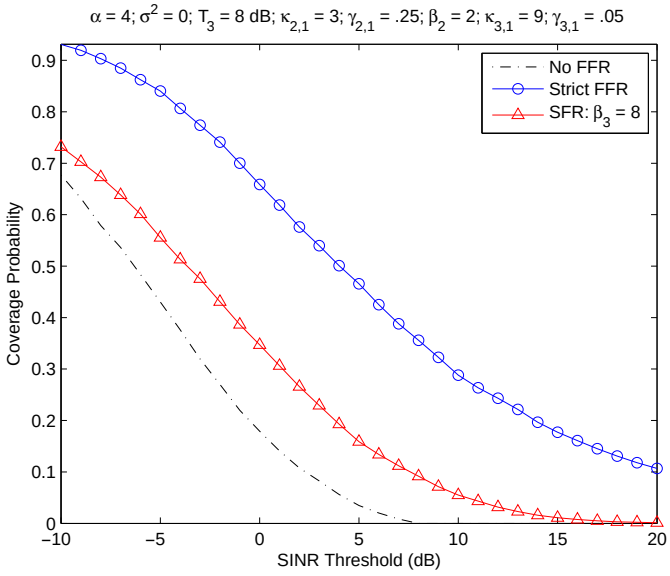

Figure 3.4: Downlink third tier edge user SINR distributions for closed access with three tiers of APs.

following SIR distributions for Strict FFR and SFR are a function of two open access thresholds, T_1 set by the first tier and T_2 set by the second tier of APs. The open access thresholds determine whether a user is switched to a reuse-Δ subband or served by a either the common band of the nearest first or second tier AP.

Let SIR_1 and SIR_2 denote the SIR at the typical mobile of the closest first and second tier AP respectively,

$$\mathrm{SIR}_1 = \frac{P_1 g_1 {r_1}^{-\alpha}}{P_1 I_1 + P_2 I_2 + P_2 g_2 {r_2}^{-\alpha}} \tag{3.20}$$

$$\mathrm{SIR}_2 = \frac{P_2 g_2 {r_2}^{-\alpha}}{P_1 I_1 + P_2 I_2 + P_1 g_1 {r_1}^{-\alpha}}. \tag{3.21}$$

Here r_1 denotes the distance of the mobile at the origin to the nearest first tier AP, and r_2 the distance to the nearest second tier AP. The interference caused by the first tier APs is denoted by I_1, while I_2 is the interference caused by the second tier APs, excluding the closest one. If for a mobile user, $\mathrm{SIR}_1 < T_1$ and $\mathrm{SIR}_2 < T_2$, then the mobile user is allocated a new FFR subband δ_y, where $\delta \in \{1, ..., \Delta\}$ with uniform probability $\frac{1}{\Delta}$ and a new SIR given by $\hat{\mathrm{SIR}}$ which is different under Strict FFR or SFR. The CCDF of the edge user SIR under open access is given by

$$\bar{\mathrm{F}}_{\mathrm{FFR,op}}(k, T) = \mathbb{P}\left(\hat{\mathrm{SIR}} > T \mid \mathrm{SIR}_1 < T_1 \ , \ \mathrm{SIR}_2 < T_2\right). \tag{3.22}$$

As we can see from (3.22) the analysis of the coverage probability is more complicated relative to closed access due to the inter-dependence of the terms SIR_1 and SIR_2. For convenience of notation in the following Theorems we explicitly consider the first-tier edge user SIR. However, this can be extended to the second tier in a straightforward manner and we present results later for that case as well.

3.5.1 Strict FFR

First we consider the distribution of (3.22) for Strict FFR. Since the mobile user is allocated a different subband, it experiences new fading power $\hat{g_1}$ and out-of-cell interference $P_1\hat{I}_1$, which does not have cross-tier interference.

Theorem 10 (Strict FFR, open access, edge user)**.** *The coverage probability of an edge user in a strict FFR system, assigned a FFR subband is* $\bar{\mathrm{F}}_{\mathrm{FFR,op}}(T) =$

$$\frac{p_c(T,\lambda_1,\alpha,\Delta)-\int_0^\infty\int_0^\infty 2\pi\lambda_1 r_1 e^{-\pi\lambda_1 {r_1}^2} 2\pi\lambda_2 r_2 e^{-\pi\lambda_2 {r_2}^2} g_n(r_1,r_2)\mathrm{d}r_1\mathrm{d}r_2}{\int_0^\infty\int_0^\infty 2\pi\lambda_1 r_1 e^{-\pi\lambda_1 {r_1}^2} 2\pi\lambda_2 r_2 e^{-\pi\lambda_2 {r_2}^2} g_d(r_1,r_2)\mathrm{d}r_1\mathrm{d}r_2}$$

$$\begin{aligned}
\textit{where } g_d(r_1,r_2) &= 1-\epsilon_1 e^{(-2\pi\lambda_1\rho_{1,1}(T_1,\alpha))} e^{(-2\pi\lambda_2\rho_{1,2}(\gamma T_1,\alpha))} \\
&\quad -\epsilon_2 e^{(-2\pi\lambda_1\rho_{2,1}(T_2/\gamma,\alpha))} e^{(-2\pi\lambda_2\rho_{2,2}(T_2,\alpha))}, \\
g_n(r_1,r_2) &= \epsilon_1 e^{-2\pi(\lambda_1\xi_{1,1}(T,T_1,\alpha,\Delta)+\lambda_2\rho_{1,2}(T_1,\alpha))} \\
&\quad +\epsilon_2 e^{-2\pi(\lambda_1\xi_{2,1}(T,T_2/\gamma,\alpha,\Delta)+\lambda_2\rho_{2,2}(T_2,\alpha))},
\end{aligned}$$

$$\xi_{a,b}(T,z,\alpha,\Delta) = \int_{r_b}^\infty 1-\frac{1}{1+zr_a^\alpha x^{-\alpha}}\left(\Delta-\frac{Tr_b^\alpha x^{-\alpha}}{1+\Delta Tr_b^\alpha x^{-\alpha}}\right)x\mathrm{d}x,$$

$$\rho_{a,b}(z,\alpha) = \int_{r_b}^\infty 1-\frac{1}{1+zr_a^\alpha x^{-\alpha}}xdx,\ \gamma=\frac{P_2}{P_1},$$

$$\epsilon_1 = \left(\frac{1}{T_1\gamma\frac{{r_1}^\alpha}{{r_2}^\alpha}+1}\right),\ \textit{and}\ \epsilon_2 = \left(\frac{1}{T_2\left(\gamma\frac{{r_1}^\alpha}{{r_2}^\alpha}\right)^{-1}+1}\right). \tag{3.23}$$

Proof. A user y with $\mathrm{SIR}_1 < T_1$ when connected to the closest first-tier AP and $\mathrm{SIR}_2 < T_2$ when connected to the closest second-tier AP is given a FFR subband δ_y, where $\delta \in \{1,...,\Delta_1\}$ with uniform probability $\frac{1}{\Delta_1}$, and experiences new fading power $\hat{g_1}$ and out-of-cell interference $P_1\hat{I}_1$. The CCDF of the edge user $\bar{\mathrm{F}}_{\mathrm{FFR,op}}(T)$ is now

conditioned on its previous SIR and r_1 and r_2, the distance to the nearest tier 1 and tier 2 AP respectively, given by

$$\mathbb{P}\left(\frac{P_1\hat{g_1}{r_1}^{-\alpha}}{P_1\hat{I}_1} > T \;\middle|\; \mathrm{SIR}_1 < T_1, \mathrm{SIR}_2 < T_2\right). \tag{3.24}$$

Using Bayes' rule and initially focusing on the denominator, the conditional term in (3.24), and conditioning on g_2 gives

$$\mathbb{P}\left[\frac{{r_1}^{\alpha}}{P_1}\left(\frac{P_2}{T_2}g_2{r_2}^{-\alpha} - (P_1I_1 + P_2I_2)\right) \;<\; g_1\right. \tag{3.25}$$

$$\left.<\;\; T_1\frac{{r_1}^{\alpha}}{P_1}\left(P_1I_1 + P_2I_2 + P_2g_2{r_2}^{-\alpha}\right) \;\middle|\; g_2\right]\mathbb{P}\left(g_2\right). \tag{3.26}$$

Since g_1 and g_2 are i.i.d. exponentially distributed with mean μ, and setting $\bar{I} = P_1I_1 + P_2I_2$, this gives

$$\mathbb{E}_{g_2}\left[\int_{\frac{{r_1}^{\alpha}}{P_1}\left(\frac{P_2}{T_2}g_2{r_2}^{-\alpha} - \bar{I}\right)^+}^{T_1\frac{{r_1}^{\alpha}}{P_1}\left(\bar{I}+P_2g_2{r_2}^{-\alpha}\right)} \mu e^{-\mu x}dx\right] =$$

$$\mathbb{E}_{g_2}\left[e^{-\mu\frac{{r_1}^{\alpha}}{P_1}\left(\frac{P_2}{T_2}g_2{r_2}^{-\alpha} - \bar{I}\right)^+} - e^{-\mu T_1\frac{{r_1}^{\alpha}}{P_1}\left(\bar{I}+P_2g_2{r_2}^{-\alpha}\right)}\right],$$

$$\text{where } (x)^+ = \begin{cases} x & : x > 0 \\ 0 & : x \leq 0 \end{cases}$$

Evaluating the expectation, collecting terms and simplifying gives,

$$1 - \epsilon_1 e^{-\bar{I}\mu T_1\frac{{r_1}^{\alpha}}{P_1}} - \epsilon_2 e^{-\bar{I}\mu T_2\frac{{r_2}^{\alpha}}{P_2}}, \tag{3.27}$$

where γ, ϵ_1, and ϵ_2 are given by (3.23).

We observe that the expectation of (3.27) with respect to I_1 and I_2 is the joint Laplace transform of I_1 and I_2 evaluated at $(\mu T_1\frac{{r_1}^{\alpha}}{P_1}, \mu T_2\frac{{r_2}^{\alpha}}{P_2})$. The joint Laplace transform denoted by

$$\begin{aligned} g_d(r_1, r_2) &= \mathbb{E}_{I_1,I_2}\left[1 - \epsilon_1 e^{-s_1\bar{I}} - \epsilon_2 e^{-s_2\bar{I}}\right] \\ &= 1 - \epsilon_1 e^{(-2\pi\lambda_1\rho_{1,1}(T_1,\alpha))}e^{(-2\pi\lambda_2\rho_{1,2}(\gamma T_1,\alpha))} \\ &\quad - \epsilon_2 e^{(-2\pi\lambda_1\rho_{2,1}(T_2/\gamma,\alpha))}e^{(-2\pi\lambda_2\rho_{2,2}(T_2,\alpha))}, \end{aligned}$$

where $\rho_{a,b}(z,\alpha)$ is given by (3.23). De-conditioning on r_1 and r_2, we have

$$\int_0^\infty \int_0^\infty 2\pi\lambda_1 r_1 e^{-\pi\lambda_1 {r_1}^2} 2\pi\lambda_2 r_2 e^{-\pi\lambda_2 {r_2}^2} g_d(r_1,r_2)\mathrm{d}r_1\mathrm{d}r_2. \tag{3.28}$$

Now we turn our attention to the numerator which equals,

$$\mathbb{E}\left[e^{\left(-\mu\hat{I}_1 T {r_1}^\alpha\right)}\left(1-\epsilon_1 e^{\left(-\bar{I}\mu T_1 \frac{{r_1}^\alpha}{P_1}\right)}+\epsilon_2 e^{\left(-\bar{I}\mu T_2 \frac{{r_2}^\alpha}{P_2}\right)}\right)\right].$$

Concentrating on the second term we observe that the expectation with respect to $\hat{I}_1$,I_1, and I_2 is the joint Laplace transform of $\hat{I}_1$, I_1, and I_2 evaluated at $(\mu T {r_1}^\alpha, \mu T_1 \frac{{r_1}^\alpha}{P_1}, \mu T_2 \frac{{r_2}^\alpha}{P_2})$. The joint Laplace transform $g_n(r_1,r_2) := \mathscr{L}_{\text{num}}\left(\mu T {r_1}^\alpha, \mu T_1 \frac{{r_1}^\alpha}{P_1}, \mu T_2 \frac{{r_2}^\alpha}{P_2}\right)$

$$= \epsilon_1 e^{-2\pi(\lambda_1 \xi_{1,1}(T,T_1,\alpha,\Delta_1)+\lambda_2\rho_{1,2}(T_1,\alpha))}$$

$$+ \epsilon_2 e^{-2\pi(\lambda_1 \xi_{2,1}(T,T_2/\gamma,\alpha,\Delta_1)+\lambda_2\rho_{2,2}(T_2,\alpha))},$$

where $\xi_{a,b}(T,z,\alpha,\Delta)$ is given by (3.23). De-conditioning on r_1 and r_2,

$$\int_0^\infty \int_0^\infty 2\pi\lambda_1 r_1 e^{-\pi\lambda_1 {r_1}^2} 2\pi\lambda_2 r_2 e^{-\pi\lambda_2 {r_2}^2} g_n(r_1,r_2)\mathrm{d}r_1\mathrm{d}r_2. \tag{3.29}$$

Finally, plugging (3.10) and (3.28) into (3.24), and substituting (3.12) for the first term of the numerator by definition and ${r_1}^2 = v$ we have (3.23). □

Compared to the closed access results, the derivations are not nearly as clean due to the dependence of the user's SIR on r_1 and r_2. The derivations require evaluating a double integral which does not have a closed form. In fact, the number of tiers under consideration determines the number of integrals which must be evaluated. Despite this, we can still obtain insight into the underlying nature of the distributions. Also, it is expected that most practical deployments would not have more than about three tiers even in dense environments, making this analysis practical through the use of numerical evaluation of the integrals.

3.5.2 SFR

As was the case for closed access, the SFR expressions differ from Strict FFR due to the power control factor and effective interference power. Additionally the full Δ-reuse of subbands with SFR results in cross-tier interference for the edge users as well as interior users. We now give the expression for coverage probability with open access and SFR based on the SIR in (3.22).

Theorem 11 (SFR, open access, edge user)**.** *The coverage probability of an SFR edge user whose initial* SIR *is less than T_1 and T_2 is* $\bar{\mathrm{F}}_{\mathrm{SFR,op}}(T) =$

$$\frac{\pi\lambda_1 \int_0^\infty e^{-\pi\lambda_1 v\left(1+\rho\left(\frac{\eta_1}{\beta_1}T,\alpha\right)+2\kappa_{2,1}\psi\left(\frac{\gamma_{2,1}}{\beta_1}T,\alpha\right)\right)}\mathrm{d}v}{\int_0^\infty\int_0^\infty\left(2\pi\lambda_1 r_1 e^{-\pi\lambda_1 {r_1}^2}\right)\left(2\pi\lambda_2 r_2 e^{-\pi\lambda_2 {r_2}^2}\right)f_d(r_1,r_2)\mathrm{d}r_1\mathrm{d}r_2} - \frac{\int_0^\infty\int_0^\infty\left(2\pi\lambda_1 r_1 e^{-\pi\lambda_1 {r_1}^2}\right)\left(2\pi\lambda_2 r_2 e^{-\pi\lambda_2 {r_2}^2}\right)f_n(r_1,r_2)\mathrm{d}r_1\mathrm{d}r_2}{\int_0^\infty\int_0^\infty\left(2\pi\lambda_1 r_1 e^{-\pi\lambda_1 {r_1}^2}\right)\left(2\pi\lambda_2 r_2 e^{-\pi\lambda_2 {r_2}^2}\right)f_d(r_1,r_2)\mathrm{d}r_1\mathrm{d}r_2}.$$

where $f_n(r_1, r_2) =$

$$\begin{aligned}&\epsilon_1 e^{-2\pi\lambda_1\left(\zeta_{1,1}(T,T_1,\alpha,\beta_1,\eta_1)+\kappa_{2,1}\left(\psi\left(\frac{\gamma_{2,1}}{\beta_1}T,\alpha\right)+\rho_{1,2}(\gamma_{2,1}T_1,\alpha)\right)\right)}\\ &+\epsilon_2 e^{-2\pi\lambda_1\left(\zeta_{2,1}\left(T,\frac{T_2}{\gamma_{2,1}},\alpha,\beta_1,\eta_1\right)+\kappa_{2,1}\left(\psi\left(\frac{\eta_2\gamma_{2,1}}{\beta_1}T,\alpha\right)+\rho_{2,2}(T_2,\alpha)\right)\right)},\end{aligned}$$

$$\begin{aligned}f_d(r_1,r_2) &= 1-\epsilon_1 e^{(-2\pi\lambda_1(\rho_{1,1}(\eta T_1,\alpha)+\kappa_{2,1}\rho_{1,2}(\gamma T_1,\alpha)))}\\ &\quad -\epsilon_2 e^{\left(-2\pi\lambda_1\left(\rho_{2,1}\left(\frac{\eta}{\gamma}T_2,\alpha\right)+\kappa_{2,1}\rho_{2,2}(T_2,\alpha)\right)\right)},\end{aligned}$$

$$\zeta_{a,b}(y,z,\beta,\eta) = \frac{1}{2(y-z)}\left(y\rho_{a,b}(y,\alpha)+z\rho_{a,b}(z,\alpha)\right), \tag{3.30}$$

and $\rho_{a,b}(z,\alpha)$ *given by* (3.23).

Proof. A user y with $\mathrm{SIR}_1 < T_1$ and $\mathrm{SIR}_2 < T_2$ given by (3.20) is allocated a FFR subband with uniform probability $\frac{1}{\Delta}$, and experiences new fading power $\hat{g_1}$, transmit

power βP_1, and out-of-cell interference $\bar{I} = \eta_1 P_1 I_1 + \eta_2 P_2 I_2$. The CCDF of the edge user $\bar{\mathrm{F}}_{\mathrm{SFR,op}}(T)$ is now given by

$$\mathbb{P}\left(\frac{\beta P_1 \hat{g_1} {r_1}^{-\alpha}}{\eta_1 P_1 \hat{I_1} + \eta_2 P_2 \hat{I_2}} > T \;\middle|\; \mathrm{SIR}_1 < T_1, \mathrm{SIR}_2 < T_2\right) \tag{3.31}$$

Using the method of Theorem 10, applying Bayes' rule we have the joint Laplace transform of I_1 and I_2 given r_1 and r_2,

$$\begin{aligned} f_d(r_1, r_2) = 1 &- \epsilon_1 e^{(-2\pi\lambda_1(\rho_{1,1}(\eta_1 T_1, \alpha) + \kappa_{2,1}\rho_{1,2}(\eta_2 \gamma 2{,}1 T_1, \alpha)))} \\ &- \epsilon_2 e^{\left(-2\pi\lambda_1\left(\rho_{2,1}\left(\frac{\eta_1}{\eta_2\gamma_{2,1}} T_2, \alpha\right) + \kappa_{2,1}\rho_{2,2}(\eta_2 T_2, \alpha)\right)\right)}, \end{aligned}$$

where ϵ_1,ϵ_2,γ_{2_1}, and $\rho_{a,b}(z, \alpha)$ are given by (3.23).

De-conditioning on r_1 and r_2, we have

$$\int_0^\infty \int_0^\infty 2\pi\lambda_1 r_1 e^{-\pi\lambda_1 {r_1}^2} 2\pi\lambda_2 r_2 e^{-\pi\lambda_2 {r_2}^2} f_d(r_1, r_2) \mathrm{d}r_1 \mathrm{d}r_2. \tag{3.32}$$

Again, following the method of Theorem 10, we observe that the numerator of (3.31) is given by

$$\begin{aligned} &\pi\lambda_1 \int_0^\infty e^{-\pi\lambda_1 v\left(1 + \rho\left(\frac{\eta}{\beta} T, \alpha\right) + 2\kappa\psi\left(\frac{\gamma}{\beta} T, \alpha\right)\right)} \mathrm{d}v - \\ &\int_0^\infty \int_0^\infty 2\pi\lambda_1 r_1 e^{-\pi\lambda_1 {r_1}^2} 2\pi\lambda_2 r_2 e^{-\pi\lambda_2 {r_2}^2} f_n(r_1, r_2) \mathrm{d}r_1 \mathrm{d}r_2, \end{aligned} \tag{3.33}$$

where $f_n(r_1, r_2) = \epsilon_1 e^{-2\pi\lambda_1\left(\zeta_{1,1}(T, T_1, \alpha, \Delta, \beta, \eta) + \kappa\psi\left(\frac{\gamma}{\beta} T, \alpha\right) + \kappa\rho_{1,2}(\gamma T_1, \alpha)\right)}$

$$+ \epsilon_2 e^{-2\pi\lambda_1\left(\zeta_{2,1}(T, T_2/\gamma, \alpha, \Delta, \beta, \eta) + \kappa\psi\left(\frac{\gamma}{\beta} T, \alpha\right) + \kappa\rho_{2,2}(T_2, \alpha)\right)}.$$

Thus plugging (3.33) and (3.32) back into (3.31) and substituting ${r_1}^2 = v$ we have (3.30). □

The expressions have a similar form but differ from Strict FFR due to the effect of η and β on the SIR and FFR thresholds. As with Strict FFR, the derivations do not reduce as simply as closed access expressions due to the dependence of the user's SIR on r_1 and r_2, but are still quickly computable with basic numerical methods.

3.5.3 Model Evaluation

Fig. 3.5 shows the derived distributions for Strict FFR and SFR edge users for a two-tier network with $\lambda_1 = 24$ APs per $10km^2$, $\lambda_2 = 5\lambda_1$, no noise, and $\alpha = 4$ compared with Monte-Carlo simulations. As with closed access, the curves match exactly. We also note that there is an upwards shift in the coverage probability curves, due to the impact of off-loading of users onto the secondary tier. With closed access, users whose SINR falls below the first tier FFR threshold $T_1 = 1$dB would be assigned a FFR band and may or may not be able to be covered due to interference or propagation challenges, however if their SINR to a second tier AP is greater than $T_2 = 5$dB, they are guaranteed coverage and affect the distribution of the users who utilize FFR.

In Fig. 3.6 we consider the coverage probability of a typical second tier edge user under open access. Due to the 20x lower transmit power and the impact of first tier users offloaded onto the second tier due to the 3dB difference in reuse thresholds, the curves have a different shape than those of Fig. 3.5. In fact we see that for SFR, the coverage probability for SINR < -2 is slightly less than for no-reuse, while for Strict FFR coverage the removal of the strong cross-tier interference clearly is the most beneficial. The interdependence of the system design parameters and the selection of the FFR thresholds is further investigated in the following section.

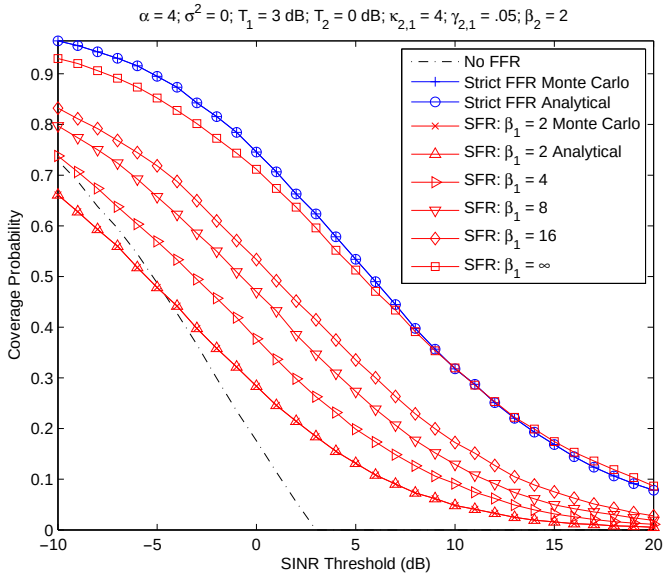

Figure 3.5: Downlink first tier edge user SINR distributions for open access with two tiers of APs.

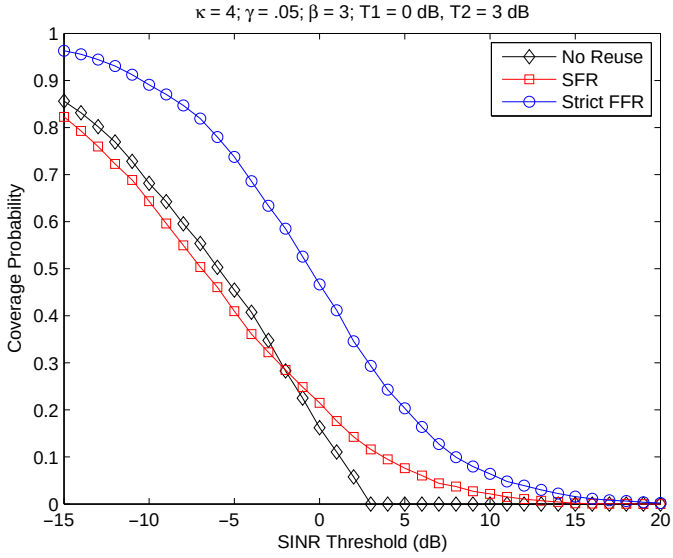

Figure 3.6: Downlink 2nd-tier edge user SINR distributions for open access with two tiers of APs.

3.6 System Design Implications

In this section we present several applications of the Strict FFR and SFR SINR and SIR distributions derived for closed and open access in Sections 3.4 and 3.5, which illustrate how they can be used to provide additional tools and insight for the system design of heterogeneous networks utilizing FFR.

3.6.1 Average Edge User Rate

In modern cellular networks, the important metric of average achievable rate can be derived from the SINR statistics. In this section we illustrate how the coverage results derived in Section 3.4 and 3.5 can be straightforwardly extended to develop average edge user rate expressions under Strict FFR or SFR.

The average data rate $\bar{\tau} = \mathbb{E}\left[\ln\left(1 + \mathrm{SINR}\right)\right]$ is achieved by the users, assuming adaptive modulation and coding, and the expressions are given in terms of nats/Hz, where 1 bit = $\log_e(2)$ nats. The average rate of an edge user is determined by integrating over the SINR distribution and fading. Due to the two-stage nature of FFR the $\mathrm{SINR_e}$ of the edge user on the new subband is conditioned on the previous $\mathrm{SINR_i}$ on the common subband. Thus we have $\bar{\tau} = \mathbb{E}\left[\ln\left(1 + \mathrm{SINR}\right)\right] =$

$$\int_0^\infty \int_0^\infty \pi\lambda e^{-\pi\lambda\mu} \mathbb{P}\left[\ln\left(1 + \mathrm{SINR_e}\right) > t \;\middle|\; \mathrm{SINR_i} < T_{\mathrm{FR}}\right] \mathrm{d}\mu.$$

where we use the fact that since the rate $\tau = \ln(1 + \mathrm{SINR})$ is a positive random variable, $E[\tau] = \int_{t>0} P(\tau > t)\mathrm{d}t$. From the above expression we see that the derivation of these terms involves substituting e^{t-1} in place of the SINR threshold T and computing an additional integral.

3.6.2 Multi-tier Interference and Closed Access

We now consider a two-tier network with Strict FFR and closed access and show the connection between the density ratio of the tiers κ and the SINR distribution. Fig. 3.7 plots the distribution for edge users as an increasing function of κ, effectively increasing the density of second-tier APs. As κ increases we see in Fig. 3.7 that the SINR increases for first tier users. This is a consequence of the use of Strict FFR, since the FFR bands are reserved for only first tier users, any user moving from the common band to the FFR band will see a reduction in interference. As the interference from the second tier increases with κ, more and more first tier users have SINR below T_1 and since they cannot connect to the second tier due to the closed access constraint, they must be moved onto a FFR subband. The implication of this result is that the size of the partitions will need to be increased, which for Strict FFR, can cause the overall sum rate of the first tier APs to decrease due to the reduction in overall spectrum usage.

3.6.3 Open access FFR thresholds

In Fig. 3.8 the SFR edge user SIR CCDF is shown for different values of T_2, the second-tier FFR threshold under open access. Decreasing T_2 increases the number of mobile users which can connect to that AP on the common subband. From Fig. 3.8 we see that this results in the overall increase of the SIR of the edge users. In other words, as T_2 increases, only the users with the worst SIR are given FFR subbands and they also are the users who can have the greatest benefit from the FFR subbands.

A related concept is called biasing, in which the access thresholds of the secondary APs are adjusted in order to increase the offload from a higher tier to a lower

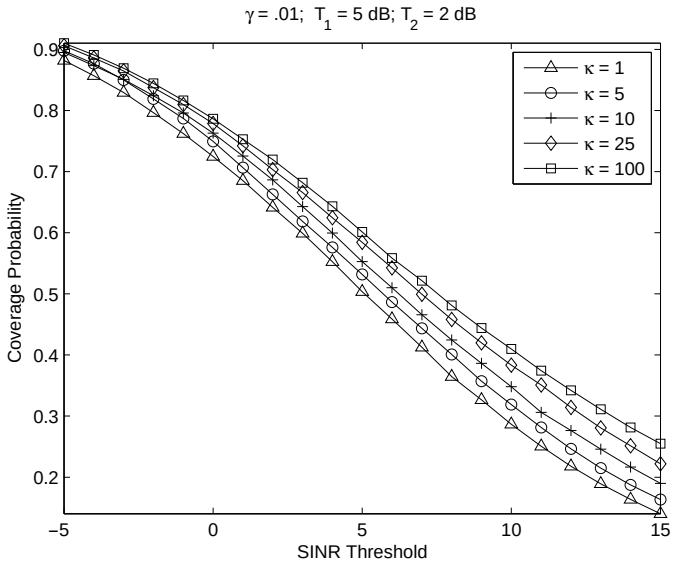

Figure 3.7: Downlink edge user SINR distributions for Strict FFR and closed access as a function of the tier density ratio κ.

one [59]. The reasons for biasing may not be solely related to the ability of an AP to provide coverage for a user, but rather to reduce traffic for especially overloaded tiers. Our framework can implicitly capture this effect in the design of T_1 and T_2. By raising T_1 and lowering T_2 we can define a middle SIR range $T_{Bias} = T_1 - T_2$, wherein a desired percentage of users are offloaded.

3.7 Conclusion

This chapter has presented a new tractable analytical framework for evaluating coverage probability in heterogeneous networks utilizing Strict FFR and SFR which captures the non-uniformity of these deployments and gives insight into the performance tradeoffs of those FFR strategies. The model presented in this chapter can be utilized as a foundation for performance analysis of heterogeneous networks utilizing dynamic FFR strategies for addressing changing channel conditions and user

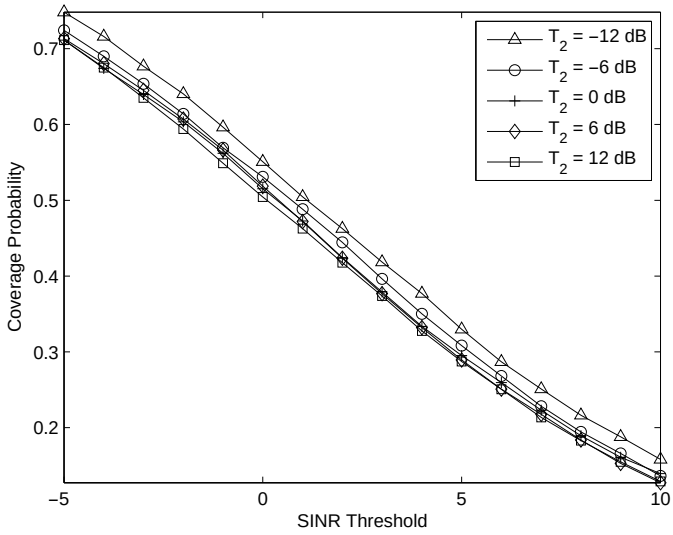

Figure 3.8: Downlink edge user SIR distributions for SFR and open access as a function of T_2.

traffic in the network [6, 101, 103]. Tractable analysis will also assist system designers in determining optimal parameters and evaluating the performance of potential algorithms in non-uniform and multi-tier deployments.

Chapter 4

Analytical Modeling of Uplink Cellular Networks

While the downlink of modern cellular networks has historically driven their bandwidth and speed requirements, improvements in uplink performance are increasingly important due to the evolution of symmetric traffic applications like social networking, video-calls, and real-time generation and sharing of media content. A complete analytical framework for the cellular uplink requires several fundamental changes to the system model compared to the downlink, nearly all of which make analysis more difficult. While interference in the downlink comes from the fixed locations, in the uplink, interference is generated by mobile devices distributed throughout the network. A second distinction is the use of location-dependent power control, which makes the transmit power highly variable, and therefore significantly changes the interference statistics compared to the downlink. Additionally, for the uplink, both a maximum power constraint and consideration of average transmit power are especially important for battery powered user devices. These constraints and their interdependence have made analysis of the uplink very challenging using traditional approaches especially when advanced ICIC techniques are also applied. While the downlink analysis in Chap. 2 took advantage of recent work in [10], no analogous framework was present for the uplink. As a result, this chapter presents a new non-trivial tractable model for determining the fundamental metric of the complete Signal to Interference Plus Noise Ratio (SINR) distribution in the uplink with universal fre-

quency reuse. Using tools from stochastic geometry and point process theory, this model can be applied to compute the performance metrics of coverage probability, rate, and implications on transmit power and lays the groundwork for analysis of FFR in the uplink as will be shown in Chap. 5.

4.0.1 Uplink Modeling Approaches

One approach for analysis of the uplink has been to use the Wyner model [110]. It is attractive for its analytical simplicity, wherein gains between users and base stations are normalized by the desired link and inter-cell interference is either a constant value or a single random variable. Historically popular for evaluating CDMA-based networks, this model is still used to evaluate performance from an information-theory perspective [69, 82, 95, 98, 99]. However, in [115] the applicability and accuracy of the model is shown to be limited to scenarios where the interference can be spatially averaged, for example a CDMA network under high load. This type of interference averaging approach wherein inter-cell interference is assumed to be fixed is not a valid assumption for modern cellular systems where typically only a single user per cell (or sector) is active in a given resource block.

Another traditional approach is to model base stations in a deterministic grid-based deployment, e.g. the popular hexagonal grid model. However as was discussed in earlier chapters, this approach does not lead to a tractable framework and results are based upon several simplifying approximations followed by exhaustive Monte Carlo simulations. Perhaps more importantly, the grid model – which was always highly idealized – is particularly out-of-touch with ongoing deployments, which have highly variable cell sizes and opportunistic placement of new towers.

The inadequacy of these existing approaches has led to research on the use of random spatial models for the network topology [47], due to the ability to derive tractable expressions leading to more general performance characterizations while capturing the non-uniformity of modern deployments [10, 14, 19, 30, 76, 81]. While this approach has mostly been applied to the downlink, recent work has also attempted to extend this to the uplink by deriving some approximate results for interference limited networks [46]. Under assumptions of multiple users per-base station transmitting on the same frequency CDMA-style and averaged transmit power for the interference the authors of [46] derive analytical expressions for average spectral efficiency as the numbers of antennas, base stations, and users grows asymptotically large.

4.0.2 Power Control

Power control in various forms has been one of the key system design features for past, current, and proposed wireless standards [108, 117]. Fast uplink power control has been an especially important feature in CDMA-based networks [3, 50, 53, 62]. One reason for this is to mitigate the "near-far" problem that occurs when a base station cannot decode the signals of cell-edge users due to the much greater received power (and thus interference) caused by cell-interior users. For modern OFDMA-based cellular networks, due to the orthogonality of per-cell resources removing inter-cell interference and the aggressive use of adaptive modulation and coding techniques, fast power control is not as important of a feature. Instead, slow power control is typically considered, which attempts to overcome pathloss and large-scale fading (shadowing). For example, the 3GPP-LTE standard supports the utilization of open and closed-loop fractional power control in the uplink [21, 36, 97]. While having an impact on coverage and rate, both by overcoming path loss and reshaping the distri-

bution of the interference power, power control is also an important factor for battery utilization. Without a tractable analytical model it is difficult to gain intuition or quantitative results from a system/network design perspective due to the complicated relationship between the relevant parameters.

Recent work on the use of power control in modern OFDMA-based networks has focused on evaluating performance of different power control algorithms for a given set of system parameters via intensive simulations. The authors of [77] evaluated the impact of the maximum transmit power on open and closed-loop algorithms. In [21], the authors investigate the use of fractional power control in the uplink as a method for maintaining constant interference power at the base station. This is of interest for many practical receiver algorithms which attempt to mitigate the impact of the interference but typically require either knowledge of the interference power or require it to be roughly constant. However a fundamental assumption of these approaches, along with several earlier ones in [89, 113] is the standard regular hexagonal model for base station locations and as a result the results are produced via simulation for only a few sets of possible design parameters.

Very recent work by the authors of [28] proposes an analytical approach to this problem, with a particular goal of giving insight into the selection of fractional power control parameters. They consider a grid deployment for the base station locations and utilize a so-called "fluid" model which approximates the interference received in the center cell as coming from outside cells with the base stations located on rings of fixed radii [61]. Under these assumptions they develop expressions for the SINR and spectral efficiency for users at relative cell-edge and cell-center locations and use these to infer optimal power control parameters.

4.0.3 Contributions

The main contribution of this chapter is the derivation of uplink coverage probability for a randomly chosen mobile user with fractional power control, which is a general power control framework that incorporates virtually all modern cellular systems. The locations of the mobile users are modeled as a realization of the Poisson Point Process (PPP) and it is assumed that the BS corresponding to each mobile user is located uniformly in its Voronoi cell [104]. The uplink analysis is significantly more involved than its downlink counterpart because the transmit power of a mobile in the uplink depends upon the distance to its associated base station due to the fractional power control. It turns out that the random variables denoting this distance for each mobile user are identically distributed but not independent in general. This dependence is not easy to model accurately and hence leads to some technical challenges in the derivation of the coverage probability. However, in this chapter we show that this dependence is weak and can be ignored, which improves the tractability of the system model with minimal impact on the accuracy of the results. We then derive the coverage probability for a randomly chosen mobile user and show that it closely matches "true" power control, which refers to the case where the independence assumption is not considered and each Voronoi cell is constrained to have exactly one MS-BS pair active at the same time. Using the same model for the user locations, coverage probability expression for "regular" BS deployments are also derived, where it is assumed that a BS is uniformly distributed in a circle around its corresponding mobile (independent of other BSs) instead of being uniformly distributed in its Voronoi cell. Interestingly, this analytical result closely approximates the coverage probability computed numerically for the hexagonal grid model.

After a discussion of the derived expressions for coverage and average rate, system design guidelines are presented compare the uplink expressions with the downlink and coverage probability and transmit power utilization is evaluated as a function of the power control parameters. These results quantify the tradeoff between improved cell-edge SINR for low and moderate values of the fractional power control factor with significant overall power reduction available if power control is more aggressively applied. The next section gives the system model and a discussion of important underlying assumptions.

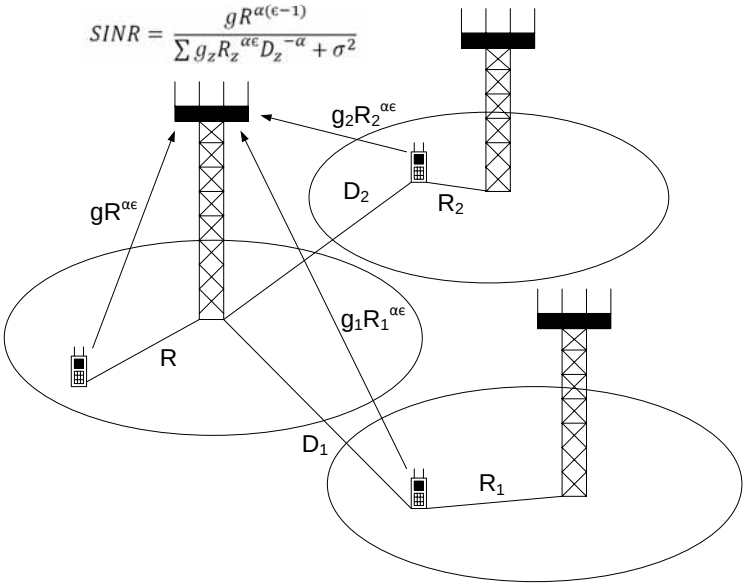

Figure 4.1: Visual system model example giving the SINR at base station 0, focusing on the serving mobile and two interfering mobiles in adjacent cells.

4.1 System Model and Relevant Tools

The uplink of a cellular network utilizes an orthogonal multiple access technique composed of a single class of base stations, macro base stations for example, and focus on the received SINR at a randomly chosen base station. Fig. 4.1 gives a visual representation of the uplink system model and relationship between parameters. The mobile user locations are assumed to form a realization of a spatial PPP [104] with density λ. We assume that a mobile user is connected to the closest BS and that each BS has an active uplink user scheduled. Under such an assumption, it is reasonable to assume that each BS is uniformly distributed in the Voronoi cell of its corresponding mobile user. We further assume that the BS chosen at random for analysis is located at the origin and that it connects to the closest mobile user, located at distance R. As discussed in detail in the sequel, there is a subtle difference between this random choice of BS and a point randomly chosen in $\mathbb{R}^2$ due to the coupling in the mobile and BS point processes. The set of interfering mobiles is $\mathcal{Z}_k$, and we denote the distance between an interfering mobile and the BS of interest by D_z and the distance of the interfering mobile to its serving BS as R_z. Path loss is inversely proportional to distance with the path loss exponent given by α, and σ^2 is the noise power. We consider small-scale Rayleigh fading between the mobiles and the BS under consideration, and a constant baseline mobile transmit power of μ^{-1}. Thus the received power is given by $gR^{-\alpha}$, where g is i.i.d exponentially distributed with mean μ^{-1}.

Next we consider the power control model. We assume that all the mobiles utilize distance-proportional fractional power control of the form $R_z^{\alpha\epsilon}$, where $\epsilon \in [0, 1]$ is the power control factor. Thus, as a user moves closer to the desired base station, the transmit power required to maintain the same received signal power decreases,

which is an important consideration for battery-powered mobile devices. Under this system model, the associated Signal to Interference Plus Noise Ratio (SINR) at a BS located at origin is

$$\text{SINR} = \frac{gR^{\alpha(\epsilon-1)}}{\sigma^2 + I_{\mathcal{Z}}}, \tag{4.1}$$

where for an interfering set of mobiles $\mathcal{Z}$,

$$I_{\mathcal{Z}} = \sum_{z \in \mathcal{Z}} (R_z^{\alpha})^{\epsilon} \, g_z D_z{}^{-\alpha}. \tag{4.2}$$

If $\epsilon = 1$, the numerator of (4.1) becomes g, with the pathloss completely inverted by the power control, and if $\epsilon = 0$ no channel inversion is performed and all the mobiles transmit with the same power. In the next section we derive the distribution of the SINR as a function of the network density, pathloss, and fractional power control factor ϵ.

Throughout this chapter comparisons of the presented model are made with various other approaches. In this section to aid discussion and provide clarity the following descriptions for the different models used throughout this paper are given.

PPP: Mobile locations are based upon a spatial PPP. In each mobile's Voronoi cell, a single BS is dropped uniformly within that cell. Due to dependence induced by the structure of Poisson-Voronoi tessellation, direct analysis of this approach is not given. Instead several reasonable approximations are made in the following two approaches based upon the main result of this paper given in Theorem 12.

PPP-Rayleigh: Mobile locations are again based upon a spatial PPP. However several approximations are made to allow for tractability: i) R, the distance of the desired user to the serving BS is assumed to be Rayleigh distributed, ii) R_z, the distance of the interfering mobiles to their BS, are assumed to be independent, and

iii) the marginal distribution of R_z is also approximated as Rayleigh. The results for this model are given in Sec. 4.2.1.

PPP-Uniform: This model differs from the Rayleigh PPP model in the third assumption, the distribution of R_z. In this case R_z is assumed to be uniformly distributed over a circle of same area as the average area of the Voronoi cells. Results are given in Sec. 4.2.2.

Grid: Base stations are located on a regular grid and users are distributed uniformly in each cell's area. Since this model does not lead to tractable expressions it is evaluated via Monte-Carlo simulations.

Wyner: The Wyner model gives a single value for the interference γ which is a function of the pathloss exponent α [115]. The resulting SIR is deterministic and given by $\text{SIR} \equiv \frac{1}{2\gamma}$.

Log-normal: This approach approximates inter-cell interference as a log-normal random variable with parameters determined through a numerical fit using simulations of the grid model.

4.2 Coverage probability

The probability of coverage can be formally defined as the complementary cumulative distribution function (ccdf) of SINR as:

$$p_c = \mathbb{P}[\text{SINR} > T], \tag{4.3}$$

which is the probability that the uplink SINR at a typical BS is greater than the target SINR T. It can also be visualized as being the average area or the average fraction of users in coverage. As noted earlier, we perform analysis on a randomly

chosen BS assumed to be located at the origin that connects to the closest mobile user. The distribution of the distance of the closest mobile from the randomly chosen BS R can be approximated by the null probability of a PPP as follows:

$$\mathbb{P}[R > r] \approx \mathbb{P}[\text{No mobile is in the circle of area } \pi r^2] = e^{-\lambda \pi r^2}. \tag{4.4}$$

The probability density function (PDF) of R can now be derived to be:

$$f_R(r) = 2\pi\lambda r e^{-\lambda \pi r^2},\ r \geq 0. \tag{4.5}$$

It should be noted that this is not the exact distribution of R because the randomly chosen BS is not the same as a randomly chosen point in $\mathbb{R}^2$ for which this distribution is exact. This difference comes due to the coupling of mobile and BS point processes. However, as we discuss in detail for R_z this approximation is tight and does not affect the accuracy of our results.

The net interference at a randomly chosen BS is the sum of the powers from all the transmitting mobiles lying farther than R. As described in the previous section, this power depends upon the distance of a mobile to its corresponding BS and the power control factor $\epsilon \in [0, 1]$. For a mobile $z \in \mathcal{Z}$, we denote its distance to the corresponding BS as R_z. It should be noted that the random variables $\{R_z\}_{z \in \mathcal{Z}}$ are identically distributed but not independent in general. The dependence is induced by the structure of Poisson-Voronoi tessellation and the restriction that only one BS can lie in each Voronoi cell. To visualize this dependence, recall a simple fact that the presence of a BS in a particular Voronoi cell forbids the presence of any other BS in this particular cell. However, as discussed in detail later in this section, this dependence is weak and we will henceforth assume each R_z to be independent and identically distributed (i.i.d.). Under this independence assumption, we first derive the coverage

probability for the general distribution of R_z and then use this general result to study two particular scenarios corresponding to non-uniform and regular coverage regions. The main uplink coverage probability result of this chapter is stated in Theorem 12.

Theorem 12 (Uplink coverage for i.i.d. R_z)**.** *The uplink coverage probability is given by:*

$$p_c(T,\lambda,\alpha,\epsilon) = 2\pi\lambda \int_{r>0} r e^{-\pi\lambda r^2 - Tr^{\alpha(\epsilon-1)}\sigma^2} \mathscr{L}_{I_z}\left(Tr^{\alpha(1-\epsilon)}\right) \mathrm{d}r, \tag{4.6}$$

where the Laplace transform of the interference is given by

$$\mathscr{L}_{I_z}(s) = \exp\left(-2\pi\lambda \int_r^{\infty} \left(1 - \mathbb{E}_{R_z}\left[\frac{1}{1+sR_z^{\alpha\epsilon}x^{-\alpha}}\right]\right) x\mathrm{d}x\right). \tag{4.7}$$

Proof. Starting from the definition of p_c and SINR,

$$\begin{aligned}
p_c(T,\lambda,\alpha,\epsilon) &= \int_{r>0} \mathbb{P}\left(\mathrm{SINR} > T\right) f_R(r)\mathrm{d}r && (4.8)\\
&= \int_{r>0} \mathbb{P}\left(\frac{g\left(r^{\alpha(\epsilon-1)}\right)}{\sigma^2 + I_{\mathcal{Z}}} > T\right) 2\pi\lambda r e^{-\pi\lambda r^2}\mathrm{d}r && (4.9)\\
&= \int_{r>0} \mathbb{P}\left(g > \frac{T(\sigma^2 + I_{\mathcal{Z}})}{r^{\alpha(\epsilon-1)}}\right) 2\pi\lambda r e^{-\pi\lambda r^2}\mathrm{d}r && (4.10)\\
&\overset{(a)}{=} \int_{r>0} 2\pi\lambda r e^{-\pi\lambda r^2} e^{-Tr^{\alpha(1-\epsilon)}\sigma^2} \mathbb{E}_{I_z}\left[e^{-Tr^{\alpha(1-\epsilon)}I_z}\right] \mathrm{d}r && (4.11)\\
&\overset{(a)}{=} \int_{r>0} 2\pi\lambda r e^{-\pi\lambda r^2} e^{-Tr^{\alpha(1-\epsilon)}\sigma^2} \mathscr{L}_{I_z}\left(Tr^{\alpha(1-\epsilon)}\right) \mathrm{d}r, && (4.12)
\end{aligned}$$

where (a) follows from the fact that $g \sim \exp(1)$ and (b) follows from the definition of Laplace transform of interference $\mathscr{L}_{I_z}(s) = \mathbb{E}_{I_z}[e^{-sI_z}]$. To complete the proof, we now derive an expression for $\mathscr{L}_{I_z}(s)$ below:

$$\mathscr{L}_{I_z}(s) = \mathbb{E}_{I_z}\left[\exp\left(-\sum_{z\in\mathcal{Z}} sR_z^{\alpha\epsilon} g_z D_z^{-\alpha}\right)\right] \tag{4.13}$$

$$= \mathbb{E}_{R_z,g_z,D_z}\left[\prod_{z\in\mathcal{Z}} \exp\left(-sR_z^{\alpha\epsilon} g_z D_z^{-\alpha}\right)\right] \tag{4.14}$$

$$\overset{(a)}{=} \mathbb{E}_{R_z,D_z}\left[\prod_{z\in\mathcal{Z}} \mathbb{E}_{g_z}\left[\exp\left(-sR_z^{\alpha\epsilon} g_z D_z^{-\alpha}\right)\right]\right] \tag{4.15}$$

$$\overset{(b)}{=} \mathbb{E}_{D_z}\left[\prod_{z\in\mathcal{Z}} \mathbb{E}_{R_z}\left[\frac{1}{1+sR_z^{\alpha\epsilon} D_z^{-\alpha}}\right]\right] \tag{4.16}$$

$$\overset{(c)}{=} \exp\left(-2\pi\lambda\int_r^\infty \left(1-\mathbb{E}_{R_z}\left[\frac{1}{1+sR_z^{\alpha\epsilon} x^{-\alpha}}\right]\right) x\mathrm{d}x\right), \tag{4.17}$$

where (a) follows from the independence of g_z, (b) follows from the independence of R_z and from the fact that $g_z \sim \exp(1)$, and (c) follows from the Probability Generating Functional (PGFL) of a PPP [104]. □

The coverage probability expression can be simplified for the full power control case ($\epsilon = 1$) in the interference-limited scenario (inter-mobile interference dominates thermal noise), which is stated as the following corollary of Theorem 12.

Corollary 1. *The uplink coverage probability for the full power control case ($\epsilon = 1$) assuming no noise ($\sigma^2 = 0$) is given by*

$$p_c(T,\lambda,\alpha,\epsilon=1) = \int_{r>0} 2\pi\lambda r e^{-\pi\lambda r^2} \mathscr{L}_{I_z}(T)\,\mathrm{d}r, \tag{4.18}$$

where $\mathscr{L}_{I_z}(s)$ is a function of r and is given by (4.17) with $\epsilon = 1$.

4.2.1 Distribution of R_z and Comments on Independence Assumption

After deriving the coverage probability expressions for general R_z, we now derive the distribution of R_z for the PPP model under the independence assumption.

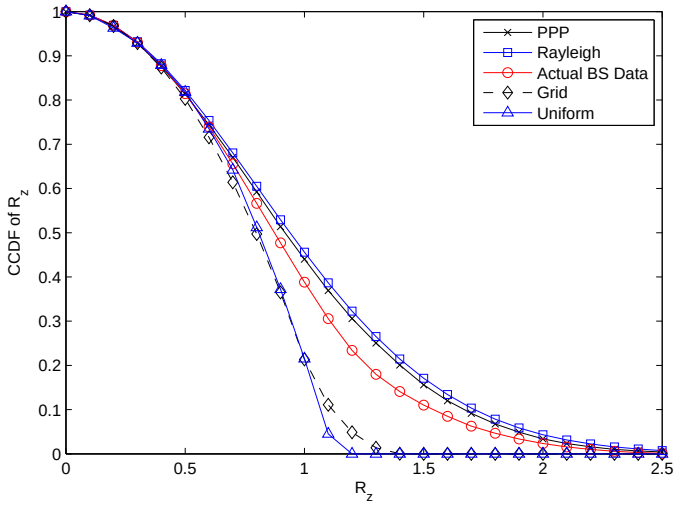

Figure 4.2: A comparison of the CCDFs of R_z both for the PPP and a grid model with their respective approximations for $\lambda = 1/4$. Also included is the CCDF of R_z for a set of real BS locations of an urban 4G network.

As mentioned in the previous section, each BS is randomly located in the Voronoi-cell of its corresponding mobile. Therefore, as was done in case of R, R_z can also be approximated by the distance of a randomly chosen point in $\mathbb{R}^2$ to its closest BS and hence its distribution can be approximated by Rayleigh distribution (as derived for R):

$$f_{R_z}(r_z) \approx 2\pi\lambda r_z e^{-\lambda\pi r_z^2} \ , \ r_z \geq 0 \tag{4.19}$$

The approximate CCDF of R_z is $\mathbb{P}[R_z > r_z] \approx e^{-\lambda\pi r_z^2}$, which is shown to be a tight fit for the numerical estimate for the PPP model in Fig. 4.2. Although it shows that our approximations for the distributions of R and R_z are tight, it does not provide any insight into the extent of dependence between random variables $\{R_z\}_{z\in\mathcal{Z}}$ which is defined by their joint distribution. Since it is hard to gain insights from the complete joint distribution of $\{R_z\}_{z\in\mathcal{Z}}$, we study a simplified case of the joint distribution of

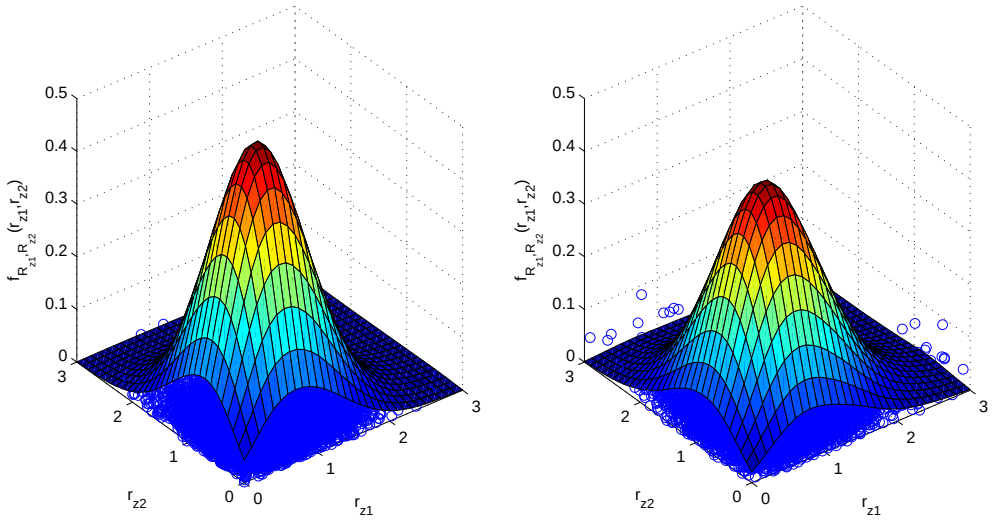

Figure 4.3: Joint densities of R_{z_1} and R_{z_2} for the actual PPP model (left) and under the independence assumption (right). R_{z_1} and R_{z_2} are the distances of the mobiles to their respective BSs in two neighboring Voronoi cells.

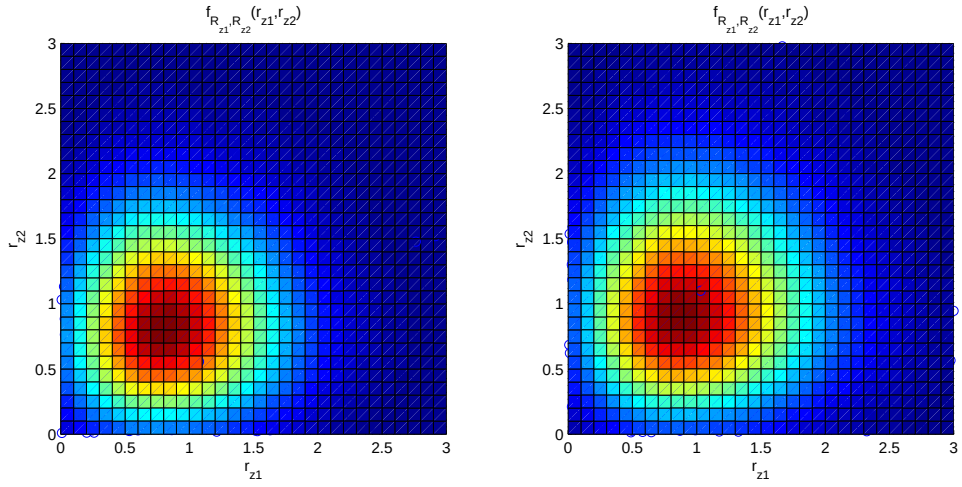

Figure 4.4: Top view of the joint densities of R_{z_1} and R_{z_2} for the actual PPP model (left) and under the independence assumption (right). R_{z_1} and R_{z_2} are the distances of the mobiles to their respective BSs in two neighboring Voronoi cells.

two random variables R_{z_1} and R_{z_2}, which are the distances of the mobiles to their respective BSs in two neighboring Voronoi cells. Since the dependence is expected to be strongest for the neighboring cells, this study can be thought of as a worst case study. We numerically compute the joint PDF $f_{R_{z_1},R_{z_2}}(r_{z_1}, r_{z_2})$ for the actual PPP model and compare it with the joint PDF derived under the independence assumption in Fig. 4.3. It should be noted that the joint PDF under the independence condition follows directly from (4.19) and is given by:

$$f_{R_{z_1},R_{z_2}}(r_{z_1}, r_{z_2}) = (2\pi\lambda)^2 r_{z_1} r_{z_2} e^{-\lambda\pi(r_{z_1}^2 + r_{z_2}^2)}, r_{z_1} \geq 0, r_{z_2} \geq 0. \tag{4.20}$$

From Fig. 4.3, we note that the two joint densities are surprisingly similar, with the PDF slightly more dispersed in the case of the independence assumption, which is the expected direct result of independence. For better visualization, we also provide the top view of the joint densities in Fig. 4.4, which leads to the same conclusion. The correlation coefficient $\rho_{R_{z_1},R_{z_2}}$ is numerically computed to be .07 for this simulation setup.

After validating the independence assumption, we now use the density of R_z, given by (4.19), to derive the Laplace transform of interference for the PPP case, which is given by:

$$\mathscr{L}_{I_z}(s) \exp\left(-2\pi\lambda \int_r^\infty \left(1 - \int_0^\infty \frac{1}{1 + su^{\frac{\alpha\epsilon}{2}} x^{-\alpha}} \pi\lambda e^{-\lambda\pi u} \mathrm{d}u\right) x \mathrm{d}x\right). \tag{4.21}$$

We plot the uplink coverage probability using this expression of the Laplace transform and compare it with the numerically computed coverage probability for a simulated PPP under true power control (without independence assumption) in Fig. 4.5(a) and Fig. 4.5(b) with no noise and $\lambda = .25$ for $\alpha = 4$, $\epsilon = 1$ and $\alpha = 3.25$, $\epsilon = .75$ respectively. We note that the analytical result derived under the independence

assumption closely approximates the true power control result for a PPP as well as the results based on simulations utilizing a set of actual BS locations compared to a regular grid.

The results in Fig. 4.5(a) and Fig. 4.5(b) are also further compared with two other analytical models. The first is the Wyner model which gives a single value for the interference and SIR $\equiv \frac{1}{2\gamma}$ where γ is a function of the pathloss exponent α [115] and as a result cannot model the typical performance in the same manner as the PPP-based model. The second approximates inter-cell interference as a log-normal random variable with parameters determined through a numerical fit of the grid model. The log-normal approximation provides a complete CCDF of the SINR, however it does not capture the shape of the SINR distribution as well as the PPP-based model. Additionally, since these approaches combine the interference into a single term that must be empirically estimated they cannot be easily parameterized as a function of key network features such as pathloss exponent, BS/user density, or fractional power control. However, since our model is a function of these system parameters we show in Sec. 4.3 it can be used to give insights into system design and performance trends.

4.2.2 Comments on Regular (Grid) Model

Grid models are used to model more "regular" BS locations. The most popular model used in prior work places the BSs on a hexagonal grid. While this model has been extremely helpful in the numerical studies of macro-cellular networks, it does not provide analytical tractability. In this subsection, we show that the random spatial model for the mobile user locations along with an appropriately chosen distribution of R_z enables us to derive analytical expression for the coverage probability that closely approximates the numerically computed results for the hexagonal grid model.

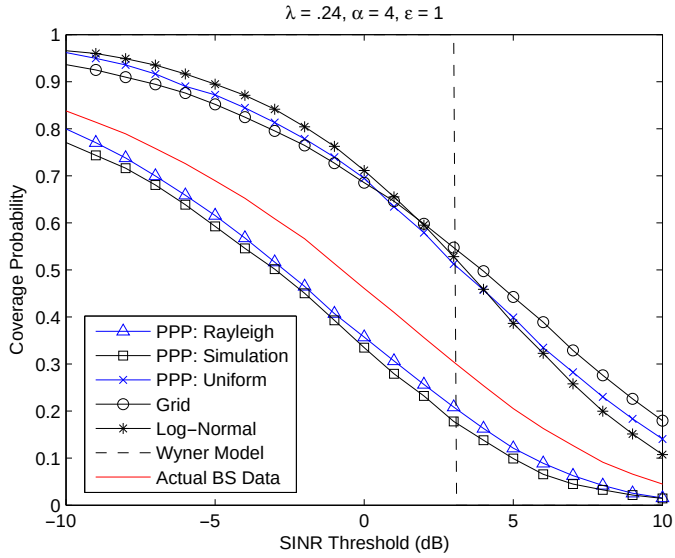

(a) $\alpha = 4,\ \epsilon = 1$

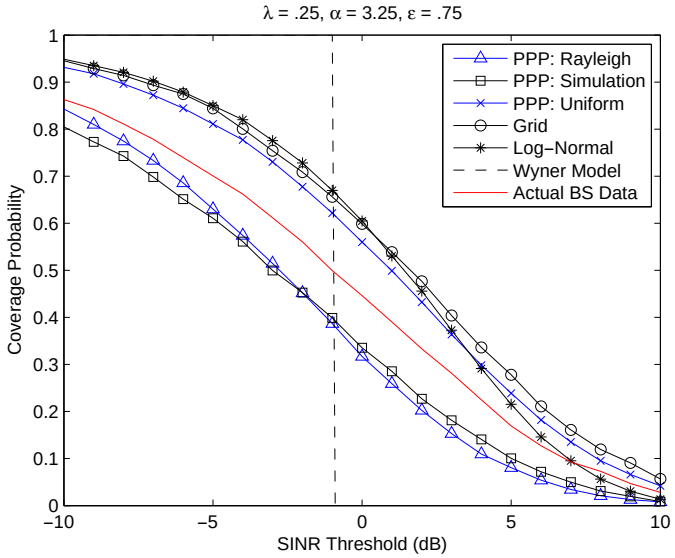

(b) $\alpha = 3.25,\ \epsilon = .75$

Figure 4.5: Coverage comparisons of the models with Rayleigh and Uniform-distributed R_z with simulations for the grid, PPP model, actual BS locations, a log-normal interference approximation, and the Wyner model, for (a) $\alpha = 4, \epsilon = 1$ and (b) $\alpha = 3.25, \epsilon = .75$.

Approximating hexagons as circles with the same area λ^{-1}, we assume that each BS is located uniformly in a circle of radius $\frac{1}{\sqrt{\pi\lambda}}$ around its corresponding mobile [17]. The radius value is evaluated from the density of the mobile users assuming there is one base station per mobile user. It is important to note that the only difference between this and the original PPP model is the distribution of R_z, which is assumed to be uniform in $\left[0, \frac{1}{\sqrt{\pi\lambda}}\right]$ to emulate more regular networks. The density of R_z can be easily evaluated as:

$$f_{R_z}(r_z) = 2\pi\lambda r_z, r_z \in \left[0, \frac{1}{\sqrt{\pi\lambda}}\right]. \tag{4.22}$$

As shown in Fig. 4.2, this closely approximates the distribution of R_z in a grid model. Using this density of R_z, we can now compute the Laplace transform of interference which can be expressed as:

$$\mathscr{L}_{I_z}(s) = \exp\left(-2\pi\lambda \int_r^\infty \left(1 - \int_0^\infty \frac{1}{1 + su^{\alpha\epsilon}x^{-\alpha}} 2\pi\lambda u \mathrm{d}u\right) x \mathrm{d}x\right). \tag{4.23}$$

In the case of $\alpha = 4$ and $\epsilon = 1$ the expression for the Laplace transform can be found in closed-form as $\mathscr{L}_{I_z}(T) =$

$$\exp\left(-\frac{\pi\lambda}{2\sqrt{T}}\left(\pi\lambda \arctan\left(\frac{\sqrt{T}}{\pi\lambda r^2}\right) r^4 - \frac{T}{\pi\lambda}\arctan\left(\frac{\pi\lambda r^2}{\sqrt{T}}\right) - \frac{r^2}{\sqrt{T}} + \frac{T}{2\lambda}\right)\right). \tag{4.24}$$

We compare the coverage probability derived using this Laplace transform with the numerically computed coverage probability using true power control in a grid model in Fig. 4.5(a) and Fig. 4.5(b) with $\lambda = .25$ and $\sigma^2 = 0$ for $\alpha = 4$, $\epsilon = 1$ and $\alpha = 3.25$, $\epsilon = .75$. Surprisingly, we note that the analytical result derived using a random spatial model under the independence assumption in both cases closely approximates the true power control result for a hexagonal grid model even compared to the log-normal interference approximation. As with the PPP model, a crucial step

is to appropriately choose the the distribution of R_z. Thus, while utilizing the same underlying random spatial model for the mobile user locations, we are able to "tune" the results to fit a range of highly non-uniform to very regular network topologies.

4.3 System Design Applications

Based on the framework developed in Sec. 4.2, we analyze performance metrics in the context of realistic parameters for modern networks and gain insight into the system design. Here we primarily focus on the scenario of Sec. 4.2.1 where the BS is located uniformly in the Voronoi cell of its corresponding mobile user and the nearest base station distance in this case is Rayleigh distributed. This is useful in capturing the non-uniform topology of many modern network deployments, although similar analysis could be performed using the uniform-distribution based power control approach.

4.3.1 Average rate

The use of link-adaptive algorithms in modern cellular networks allows the average SINR to be directly related to average data rate for mobile users. A straightforward application of the results of Sec. 4.2 is to determine analytical expressions for user rate under different stochastic power control models as a function of the key uplink parameters, something previously not possible with deterministic network topology models.

Assuming adaptive modulation and coding, we define the average data rate based upon the Shannon capacity expression, $\bar{\tau}(\lambda, \alpha, \epsilon) = \mathbb{E}[\ln(1 + \text{SINR})]$, integrating over the SINR and fading distributions. For the sake of convenience, we give the

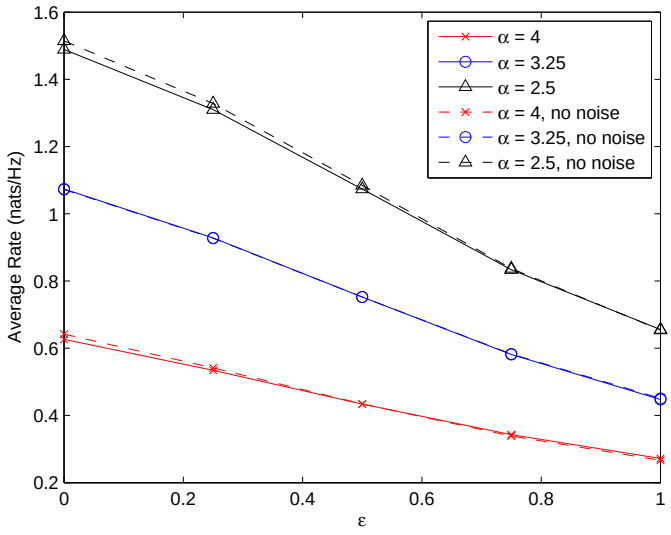

Figure 4.6: Average user rate as a function fractional power control parameter ϵ for pathloss exponents $\alpha = 2.5, 3.25$, and 4 and $\lambda = .24$ and with no noise or with $\sigma^2 = -104$dBm.

results in units of nats/Hz, where 1 bit $= \log_e(2)$ nats.

Theorem 13 (Uplink average rate)**.** *The average rate of a randomly chosen uplink user is given by*

$$\bar{\tau}(\lambda, \alpha, \epsilon) \;=\; \int_{r>0} 2\pi\lambda r e^{-\pi\lambda r^2} \int_{t>0} e^{-\left(e^t-1\right) r^{\alpha(1-\epsilon)}\sigma^2} \mathscr{L}_{I_z}\left(\left(e^t-1\right) r^{\alpha(1-\epsilon)}\right) \mathrm{d}t\mathrm{d}r,$$

where $\mathscr{L}_{I_z}(s)$ *is given by* (4.17).

Proof. Starting from the definition of $\bar{\tau}$ and SINR,

$$\begin{aligned}
\bar{\tau}(\lambda,\alpha,\epsilon) &= \mathbb{E}\left[\ln\left(1+\text{SINR}\right)\right] \\
&= \int_{r>0}\int_{t>0}\mathbb{P}\left[\ln\left(1+\text{SINR}\right)>t\right]\mathrm{d}t f_R(r)\mathrm{d}r \qquad (4.25)\\
&= \int_{r>0} 2\pi\lambda r e^{-\pi\lambda r^2}\int_{t>0}\mathbb{P}\left[\ln\left(1+\frac{g\left(r^{\alpha(\epsilon-1)}\right)}{\sigma^2+I_{\mathcal{Z}}}\right)>t\right]\mathrm{d}t\mathrm{d}r \\
&= \int_{r>0} 2\pi\lambda r e^{-\pi\lambda r^2}\int_{t>0}\mathbb{P}\left[g>\frac{\left(e^t-1\right)\left(\sigma^2+I_{\mathcal{Z}}\right)}{r^{\alpha(\epsilon-1)}}\right]\mathrm{d}t\mathrm{d}r \\
&= \int_{r>0} 2\pi\lambda r e^{-\pi\lambda r^2}\int_{t>0} e^{-\left(e^t-1\right)r^{\alpha(1-\epsilon)}\sigma^2}\mathbb{E}_{I_z}\left[e^{-\left(e^t-1\right)r^{\alpha(1-\epsilon)}I_z}\right]\mathrm{d}t\mathrm{d}r \\
&= \int_{r>0} 2\pi\lambda r e^{-\pi\lambda r^2}\int_{t>0} e^{-\left(e^t-1\right)r^{\alpha(1-\epsilon)}\sigma^2}\mathscr{L}_{I_z}\left(\left(e^t-1\right)r^{\alpha(1-\epsilon)}\right)\mathrm{d}t\mathrm{d}r,
\end{aligned}$$

where the derivation of $\mathscr{L}_{I_z}(s)$ follows Theorem 12 and has either the form of (4.21) or (4.23) depending on whether the Rayleigh or uniform assumption on the distribution of R_z is made. □

In Fig. 4.6 we plot the average user rate expressions using the Rayleigh assumption for R_z as a function of ϵ for pathloss values of $\alpha = 2.5$, 3.25, and 4 and no noise or $\sigma^2 = -104$dBm. The average rate increases with α as well as the range values over all values of ϵ. Since the computed average rates are for a randomly chosen user anywhere in the network, the effects of power control on the high, medium, and low SINR users is combined into a single value. Thus as ϵ increases, the rate decreases due to the loss in rate for some users whose transmit power is reduced on average not being overcome by the reduction in interference and increased rate for some users, especially those near the cell-edge. We also note that for a dense deployment with $\lambda = .24$ in an area of 100km^2 the no noise approximation is very tight.

Table 4.1: System Parameters

Bandwidth	10 MHz
BS density	.24 BS/km^2
User distribution	uniform
Pathloss (dB)	$37\log(d)$, d = distance in meters
Downlink Tx Power	45 dBm (30 W)
Uplink Max Tx Power	23 dBm (200 mW)
FPC ϵ	0.6, 0.8, 1.0
Noise Power Density	-174 dBm/Hz

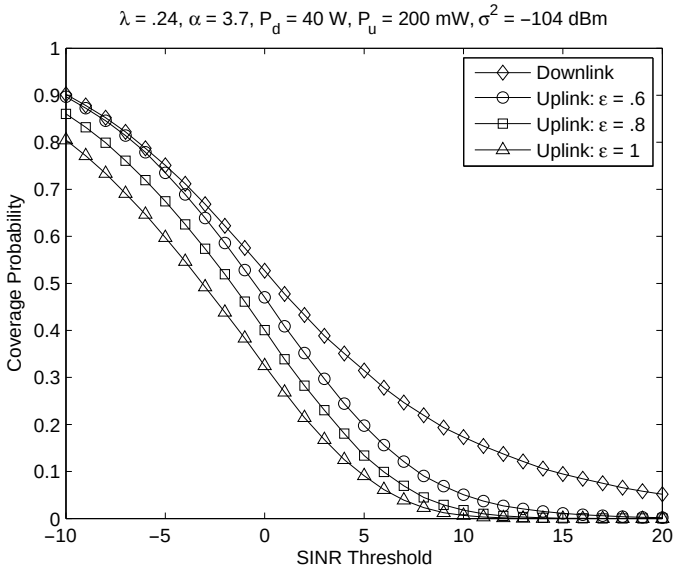

Figure 4.7: A comparison of the coverage probability for the downlink with 40W transmit power and the uplink utilizing fractional power control with $\epsilon = .6, .8$ and 1, and a max transmit power of 200 mW.

4.3.2 Downlink vs. Uplink Coverage

Another immediate application of the model is to consider the difference in coverage between the downlink and the uplink for the same network topology. We consider the randomly chosen user's SINR distribution in the downlink based on the

model presented in [10] for a network whose BSs are distributed according to a PPP with density λ. The coverage probability is

$$p_c(T, \lambda, \alpha) = \pi\lambda \int_0^\infty e^{-\pi\lambda v(1+\rho(T,\alpha))-\mu T \frac{\sigma^2}{P} v^{\alpha/2}} \mathrm{d}v, \tag{4.26}$$

where

$$\rho(T, \alpha) = T^{2/\alpha} \int_{T^{-2/\alpha}}^\infty \frac{1}{1+u^{\alpha/2}} \mathrm{d}u. \tag{4.27}$$

Some insight can be obtained by comparing (4.26) expression with the uplink expressions based on the model of Section 4.2.1. The downlink which assumes constant power transmissions across the network, has two major terms, the first term based on $\rho(T, \alpha)$ is not dependent on transmit power and represents the interference-limited contribution to the SINR while the second term depends on the noise power σ^2 and transmit power P, representing the noise-limited part of the SINR. However, the use of fractional power control in the uplink significantly changes the shape of the distribution of the interference power. This can be seen in both the noise-limited term with σ^2 and the Laplace transform of the interference, which are dependent on ϵ and the distribution of R_z since the transmit powers of the mobiles throughout the network are not constant, but highly variable unlike the downlink.

Fig. 4.7 plots the two cases with the system parameters given in Table 4.1, which are standard assumptions for a LTE-based cellular network [28, 45]. We note the disparity between the SINR distributions, especially for large SINR values. One reason for the uplink's lower coverage is due to the mismatch in transmit power compared to the downlink. Additionally at the high SINR values, the use of larger ϵ values also impacts the coverage probability since the users closest to their serving base stations greatly reduce their transmit power relative to the users at the edge of the cell. The impact of ϵ is investigated in further detail in the following section.

The notion of disparate uplink and downlink coverage regions has fundamental consequences on the system design of these cellular networks, different from those of wireless LANs for example which have much smaller coverage regions and typically do not have as significant hardware distinctions between the different network devices. For example scenarios wherein the mobile user may be able to decode the downlink transmissions, but unable to connect via the uplink will impact handoff algorithms between base stations. One advantage of having a unified framework for uplink and downlink coverage is the ability to evaluate and optimize as function of the relevant system parameters. The aim may be to determine network and system parameters such that the uplink and downlink are balanced or investigating tradeoffs between capacity and coverage enhancements at the base station and mobile terminal respectively.

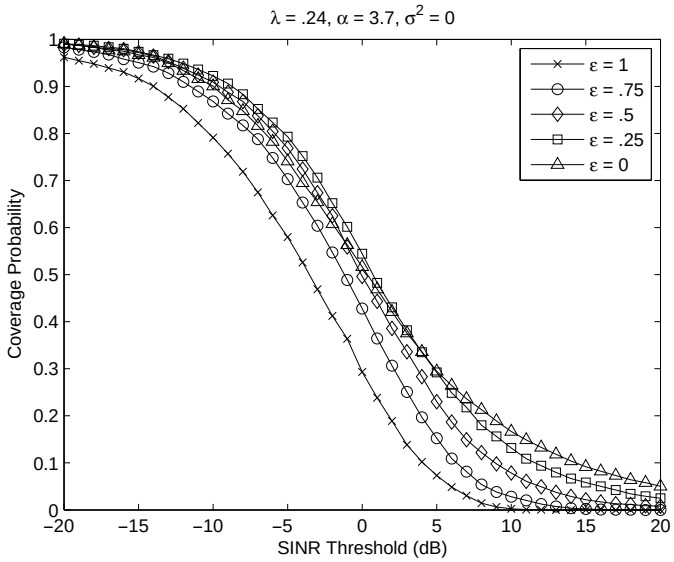

Figure 4.8: A plot of the uplink coverage probability for a PPP network with stochastic fractional power control and a range of ϵ values.

4.3.3 Fractional Power Control

As mentioned previously, the primary motivations for fractional power control in the cellular uplink are to provide beneficial coverage improvements for the lowest-percentile users, who are typically at the cell-edge, and to manage average transmit powers of battery-powered mobile devices. Fig. 4.8 gives the coverage probability distributions as a function of the fractional power control factor ϵ for a network topology given by Table 4.1. The baseline case of fixed transmit power ($\epsilon = 0$) does not provide the lowest overall coverage probabilities, but does provide the greatest probability for the highest SINR thresholds. Both $\epsilon = .25$ and $\epsilon = .5$ provide greater coverage gains for the lowest percentile users than fixed transmit power before crossing below the $\epsilon = 0$ curve at 5 and 0 dB respectively. As ϵ increases, the coverage probability curves shift lower with $\epsilon = .75$ providing much lower coverage probability than fixed transmit power, especially for SINR thresholds > 5 dB. Full-inversion, $\epsilon = 1$ power control shows an even more significant reduction in coverage.

In Fig. 4.9 we plot the coverage maximizing value of ϵ for a given SINR target T, denoted as $\hat{\epsilon}$ as a function of the SINR threshold for $\alpha = 2.5, 3.2$, and 3.7 by numerically computing the coverage probability expressions. This gives insight into the selection of ϵ based on solely on a coverage probability maximizing basis. An interesting observation is that there are two distinct regions denoted in each plot by plateaus of near constant $\hat{\epsilon}$. For users with low SINR a moderate value of $\epsilon = .25 - .3$ provides the greatest gains while for users with high SINR, the SINR is maximized by transmitting with the maximum power and $\epsilon = 0$. In all three cases, the transition between the two regions is fairly steep in its slope, with an approximately 5 dB range, while as α increases the $\hat{\epsilon}$ for the low SINR region decreases while the SINR

transition threshold between the two regions increases slightly. Additionally, this dual-regime behavior for fractional power control in uplink cellular networks differs from the behavior of power control in other classes of wireless networks, notably ad-hoc wireless networks, which were shown to have an optimal value of $\epsilon = .5$ [58, 109].

This observed effect of fractional power control can be understood by focusing on the gains perceived by users close to their desired base station relative to those at the edge and their interdependency. Cell-interior users typically experience good RF conditions and are not as susceptible to interference, but are more limited by the reduction in their transmit power under power control. Cell-edge users, however, are more fundamentally interference limited, and an increase in their transmit power with high ϵ benefits their SINR. As a result, there is a trade off in the reduction of interference from neighboring cell-center users and increased interference by mobiles at the cell edge. In effect, full-inversion power control performs a reordering of SINRs between cell-edge and cell-interior users which does not provide system-wide gains.

Fig. 4.10 gives the overall transmit power utilization of mobiles in the network as a function of ϵ with a maximum transmit power of 23 dBm and an average transmit power of $\mu^{-1} = 10$ dBm. Clearly the transmit powers of the mobile users are greatly reduced with the introduction of power control. For high values of ϵ we note that 10-15% of the users have transmit power less than 0 dBm, which is a 23 dB reduction in power compared to the maximum transmit power. For this reason, proposed system guidelines for the uplink may wish to choose ϵ to balance the metrics of coverage and battery utilization.

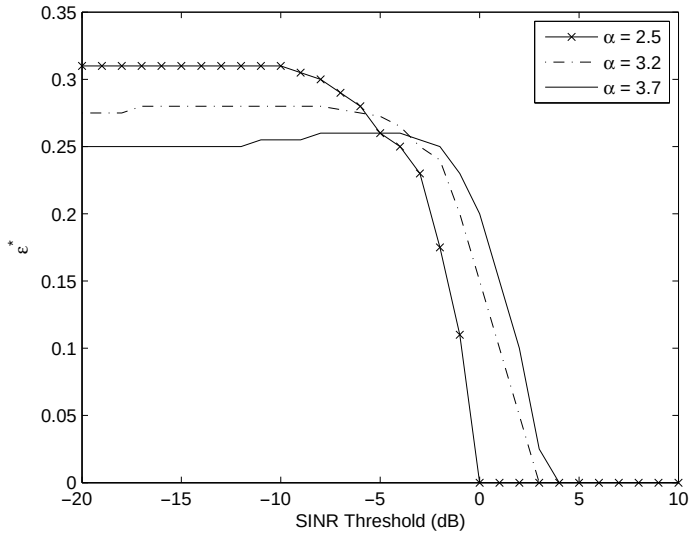

Figure 4.9: A plot of the coverage-maximizing $\hat{\epsilon}$ for a given SINR threshold value, $\lambda = .24$, and $\alpha = 2.5, 3.2$, and 3.7.

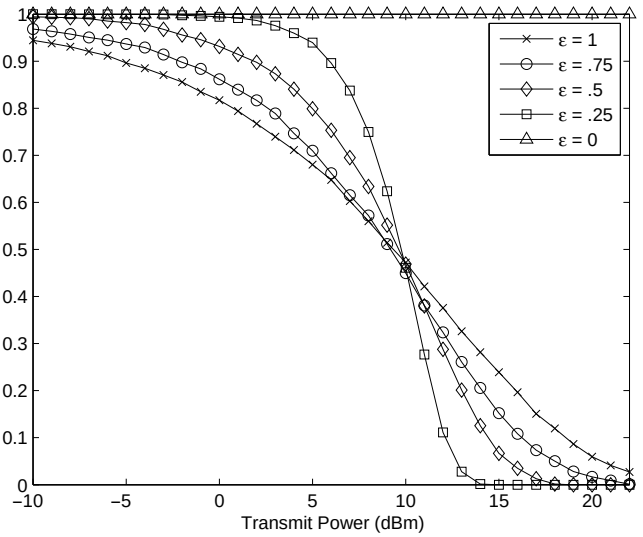

Figure 4.10: The CCDF of the average transmit power per mobile as a function of ϵ with $\lambda = .24$, $P_{max} = 23$dBm, $\mu^{-1} = 10$dBm, and $\alpha = 3.7$ pathloss factor.

4.4 Conclusion

This chapter has presented tractable expressions for the coverage probability and average rate in the cellular uplink which are applicable to uniform and irregular network topologies. The expressions are based on a novel analytical model utilizing the spatial Poisson process and are solely a function of the network topology and system design parameters including SINR targets, base station density, and fractional power control parameters. The presented results provide insight into the differences of downlink and uplink performance expectations and the tradeoff between using fractional power control to benefit cell-edge users and reducing overall power utilization by mobiles.

In the next chapter the analytical model for the cellular uplink is extended to consider the use of FFR techniques and determine the subsequent impact on edge and interior user SINR, average rate, transmit power utilization, and other system design guidelines.

Chapter 5

Analytical Evaluation of Uplink Fractional Frequency Reuse

Just as in the cellular downlink, ICIC resource allocation strategies are critical for balancing interference management with overall spectral efficiency. The development of a tractable analytical approach for evaluating FFR in the uplink faces new challenges compared to the downlink in the modeling of the interference generated throughout the network by distributed mobile devices with significant transmit power limits and highly variable transmit power due to power control. This section provides background on the use of FFR in the uplink of cellular networks, followed by a discussion of the new analytical model extending the results of Chapter 4 based upon the Poisson model, and concludes with discussion of the impact of system design parameters on coverage probability, average rate, and transmit power utilization.

5.1 Related Work

Several semi-analytical approaches for Strict FFR have been proposed for the cellular uplink. In [35] the authors consider a hexagonal network with two tiers of interference. A unique feature is the use of Markov chains to model the loads of the different base stations which allows them to iteratively calculate the total interference in the center cell. They then provide numerical simulation results to illustrate the tradeoff a static FFR strategy makes between improvement in the edge user outage,

and sum-rate loss compared to universal reuse. In [85] the authors model the network as a hexagonal grid and empirically evaluate the SINR of users as a function of their location, with the co-channel interference approximated as arising from users in the centers of adjacent cells. In [41], simulations are used to evaluate the throughput gain of FFR in the uplink of an LTE network with a focus on the performance relationship between Strict FFR and frequency selective scheduling (FSS).

Several studies on the performance of SFR in the uplink have been conducted using system simulations based upon a hexagonal grid network with consideration for transmit power limitations [4, 72, 106]. The results show a range of gains that are dependent on the underlying set of FFR and network parameters chosen including user distribution and the number of tiers of interfering mobiles considered.

A traffic-adaptive SFR strategy for the uplink presented in [91] shows gains for interior and edge user throughput analogous to those originally found for a similar approach in the downlink [103]. The authors illustrate the performance gains through detailed system simulations using a hexagonal base station grid and simulation guidelines outlined by the 3GPP standards body.

5.2 Contributions

The main contribution of this chapter is the analytical evaluation of uplink cellular networks utilizing fractional power control and FFR through the derivation of the SINR distribution of cell-edge and cell-interior users as a function of network and FFR system parameters. Our model in this chapter takes the locations of the mobile users from a spatial PPP instead of a deterministic model, which leads to tractable expressions that also capture the non-uniformity of modern deployments.

We then develop general insights into coverage probability, average rate, resource allocation, transmit power, and the interdependence of system design parameters. From the derived expressions we quantify the coverage probability gains achieved with Strict FFR for edge users relative to universal reuse and SFR, as well as the tradeoff SFR can achieve in terms of coverage performance for edge and inner users through greater frequency efficiency than Strict FFR and selection of a power control factor. We additionally present expressions for average rate and provide results illustrating how the analytical model can be related to traffic load or coverage requirements and used to allocate frequency subbands under Strict FFR and SFR to achieve capacity gains over standard full frequency reuse. Finally we discuss differences between downlink and uplink FFR approaches, especially the implications on power control and transmit power which is especially important for battery-limited mobiles. In the following section, we provide a detailed description of the system model and comment on our underlying assumptions.

5.3 System Model and Relevant Tools

We consider the uplink of an OFDMA-based cellular network where mobile users locations are based upon a spatial Poisson Point Process (PPP) with density λ [104]. Users connect to their closest BS, which is uniformly located in the user's corresponding Voronoi cell at a distance R which is Rayleigh distributed according to the null probability of the PPP. Interfering mobiles are given by the set $\mathcal{Z}_k$, and the distance between an interfering mobile and the serving BS is denoted as D_z while the distance of an interfering mobile to its serving BS is denoted by R_z. Since the network is OFDMA-based we assume that each time/frequency subband is allocated to a single user per cell and therefore $R_z > R$. In enforcing this condition R_z becomes

at least slightly correlated, however as shown in Chapter 4 this correlation is weak and instead assume R_z is nearly an i.i.d random variable, which we take to be Rayleigh distributed, the same as R. We utilize the distance proportional pathloss model of $|x|^{-\alpha}$, with pathloss exponent $\alpha > 2$. Each subband experiences i.i.d. exponentially distributed fast-fading power with mean μ and Gaussian noise with power σ^2.

The transmit power utilized by mobiles is based upon fractional pathloss-inversion of the form $Pr^{\alpha\epsilon}$, where $\epsilon \in [0, 1]$ is the power control exponent and P is the received power target that is fixed for all mobiles and typically based upon a minimum desired SINR at the base station, max transmit power limit, and estimated noise and interference power [97]. In the case of $\epsilon = 0$, all mobiles transmit with constant power $P = P_{\max}$, while at the other extreme, selecting $\epsilon = 1$ leads to a desired signal's received power at the base station of gP regardless of the user's location. Since users closer to the base station can invert their pathloss with a lower transmit power than at the cell edge, the selection of ϵ also has implications on battery utilization as well as link performance. The primary metric of interest is the SINR measured at the typical base station's receiver at the origin, given by (4.1).

The application of Strict FFR and SFR requires classification of *edge* and *interior* users. Unlike the hexagonal grid model for BS locations edge or interior user terms do not have simple geographic intuition since the underlying topology is based upon a PPP and cells are defined by a Voronoi tessellation with random area. Rather than a fixed radius for determining edge and interior partitions [78], we assume that base stations utilize a pre-determined SINR threshold T_{FR} wherein users with average SINR greater than the threshold are classified as interior users and users below the threshold as edge users, which is the proposed approach utilized by wireless standards

bodies such as IEEE 802.16 or 3GPP [45, 52].

For Strict FFR, inner and edge users transmit only on their reserved subbands. In the case of SFR, the inter-cell interference term $I_{\mathcal{Z}}$ comes from both interior and edge users, the primary difference is the power allocation applied to the subbands. The power control factor $\beta \leq 1$ is applied to interior users on the reserved subband, resulting in transmit power given by $P_{\text{int}} = \beta P r^{\alpha\epsilon}$ such that their transmit power is less than a mobile at a similar location classified as an edge user, whose transmit power on the reserved subband is given by $P_{\text{edge}} = P r^{\alpha\epsilon}$. Although β can be theoretically chosen arbitrarily, a practical range for β is typically assumed to be between .01 and .5, although this is most often related to dynamic transmit power range limitations of the mobile as well as the impact on the interference experienced by interior and edge users [4, 33].

In the following section we will derive the distribution of the SINR for cell-edge and cell-interior users as a function system parameters including network topology, power control and FFR parameters.

5.4 Coverage probability

In this section, we derive coverage probability for a mobile in the uplink utilizing fractional power control and Strict FFR or SFR. The definition of coverage is the probability that at the serving BS the uplink SINR as defined by (4.1) is larger than a SINR threshold T given by (2.6). This is equivalently the complementary cumulative distribution function (CCDF) of the SINR denoted as $\bar{F}(T)$.

5.4.1 Strict FFR

Our first result using the model introduced in Sec. 5.3 is for cell edge users in the case of Strict FFR. These are mobiles with SINR $< T_{\mathrm{FR}}$ as given in (4.1) on the common set of subbands reused in all cells and as a result are allocated a new reserved subband which is reused between cells with factor Δ.

Theorem 14 (Uplink Strict FFR, edge user)**.** *An uplink user allocated a Strict FFR subband has a probability of coverage* $\bar{F}_{\mathrm{FFR,e}}(T)$ *given by*

$$\begin{aligned} &= \mathbb{P}\left(\frac{\hat{g_y}Pr^{-\alpha(1-\epsilon)}}{\sigma^2+\hat{I_{\mathcal{Z}}}} > T \;\middle|\; \frac{g_yPr^{-\alpha(1-\epsilon)}}{\sigma^2+I_{\mathcal{Z}}} < T_{\mathrm{FR}}\right) \\ &= \frac{1}{1-p_c(T_{\mathrm{FR}},\lambda,\alpha,\epsilon)}\int_0^\infty 2\pi\lambda r e^{-\pi\lambda\left(r^2+2\upsilon(T,\alpha,\Delta,\epsilon)-\frac{\mu T\sigma^2}{Pr^{\alpha(1-\epsilon)}}\right)} \\ &\quad \left(1-e^{-\pi\lambda\left(r^2+2\upsilon(T_{\mathrm{FR}},\alpha,1,\epsilon)-\frac{\mu T_{\mathrm{FR}}\sigma^2}{Pr^{\alpha(1-\epsilon)}}\right)}\right)\mathrm{d}r, \end{aligned} \tag{5.1}$$

where $\upsilon(t,\alpha,\Delta,\epsilon) =$

$$\int_r^\infty \left[1-\frac{1}{\Delta}\int_0^\infty \frac{2\pi\lambda y e^{-\pi\lambda y^2}}{1+tr^{\alpha(1-\epsilon)}y^{\alpha\epsilon}x^{-\alpha}}\mathrm{d}y\right] x\mathrm{d}x, \tag{5.2}$$

and $p_c(T_{\mathrm{FR}},\lambda,\alpha,\epsilon)$ *is given by* (4.6)*.*

Proof. Given mobile y with SINR $< T_{\mathrm{FR}}$, a new subband δ_y is allocated with uniform probability $\frac{1}{\Delta}$ from Δ available FFR subbands. Subband δ_y experiences fading power $\hat{g_y}$ interference $\hat{I_{\mathcal{Z}}}$ from mobiles allocated the same subband. The CCDF of the SINR distribution $\bar{\mathrm{F}}_{\mathrm{FFR,e}}(T)$ for the user in question is conditioned on the previous SINR which was affected by previous fading power g_y and inter-cell interference power $I_{\mathcal{Z}}$, and is given by

$$\bar{\mathrm{F}}_{\mathrm{FFR,e}}(T) = \mathbb{P}\left(\frac{\hat{g_y}Pr^{-\alpha(1-\epsilon)}}{\sigma^2+\hat{I_{\mathcal{Z}}}} > T \;\middle|\; \frac{g_yPr^{-\alpha(1-\epsilon)}}{\sigma^2+I_{\mathcal{Z}}} < T_{\mathrm{FR}}\right). \tag{5.3}$$

Applying Bayes' rule we have,

$$\bar{\mathrm{F}}_{\mathrm{FFR,e}}(T) = \frac{\mathbb{P}\left(\frac{\hat{g_y} Pr^{-\alpha(1-\epsilon)}}{\sigma^2+\hat{I_{\mathbb{Z}}}} > T \ , \frac{g_y Pr^{-\alpha(1-\epsilon)}}{\sigma^2+I_{\mathbb{Z}}} < T_{\mathrm{FR}}\right)}{\mathbb{P}\left(\frac{g_y Pr^{-\alpha(1-\epsilon)}}{\sigma^2+I_{\mathbb{Z}}} < T_{\mathrm{FR}}\right)}. \tag{5.4}$$

Given that $\hat{g_y}$ and g_y are i.i.d. exponentially distributed with mean of μ, this gives

$$\begin{aligned}
&\frac{\mathbb{P}\left(\frac{\hat{g_y} Pr^{-\alpha(1-\epsilon)}}{\sigma^2+\hat{I_{\mathbb{Z}}}} > T \ , \frac{g_y Pr^{-\alpha(1-\epsilon)}}{\sigma^2+I_{\mathbb{Z}}} < T_{\mathrm{FR}}\right)}{\mathbb{P}\left(\frac{g_y Pr^{-\alpha(1-\epsilon)}}{\sigma^2+I_{\mathbb{Z}}} < T_{\mathrm{FR}}\right)} \\
= \ &\frac{\mathbb{E}\left[e^{\left(-\mu \frac{T}{P} r^{\alpha(1-\epsilon)}(\sigma^2+\hat{I_{\mathbb{Z}}})\right)}\left(1 - e^{\left(-\mu \frac{T_{\mathrm{FR}}}{P} r^{\alpha(1-\epsilon)}(\sigma^2+I_{\mathbb{Z}})\right)}\right)\right]}{\mathbb{E}\left[\left(1 - e^{\left(-\mu \frac{T_{\mathrm{FR}}}{P} r^{\alpha(1-\epsilon)}(\sigma^2+I_{\mathbb{Z}})\right)}\right)\right]}.
\end{aligned}$$

First we focus on the terms in the numerator and proceed by conditioning on r, which is the distance of the mobile to its serving BS. Assuming independent noise and interference, we can write the numerator as the product of expectations such that

$$\varsigma(T) \exp\left(-\mu \frac{r^{\alpha(1-\epsilon)}}{P} T \hat{I_{\mathbb{Z}}}\right)\left(1 - \varsigma(T_{\mathrm{FR}}) \exp\left(-\mu \frac{r^{\alpha(1-\epsilon)}}{P}\left(T\hat{I_{\mathbb{Z}}} + T_{\mathrm{FR}} I_{\mathbb{Z}}\right)\right)\right)$$

where $\varsigma(t)$ represents the noise terms given by

$$\varsigma(t) = e^{-\mu\sigma^2 \frac{t}{P} r^{\alpha(1-\epsilon)}} \tag{5.5}$$

By definition this is the same as the Laplace transform of $\hat{I_{\mathbb{Z}}}$ and $I_{\mathbb{Z}}$ denoted as $\mathscr{L}(s_1, s_2)$ jointly evaluated at $(s_1 = \mu r^{\alpha(1-\epsilon)} \frac{T}{P}, s_2 = \mu r^{\alpha(1-\epsilon)} \frac{T_{\mathrm{FR}}}{P})$. Thus we have

$$\begin{aligned}
&\mathbb{E}_{\hat{I_{\mathbb{Z}}}, I_{\mathbb{Z}}}\left[\varsigma(T) e^{-s_1 \hat{I_{\mathbb{Z}}}}\left(1 - \varsigma(T_{\mathrm{FR}}) e^{-s_2 I_{\mathbb{Z}}}\right)\right] \\
&= \mathbb{E}_{\hat{I_{\mathbb{Z}}}, I_{\mathbb{Z}}}\left[\varsigma(T) e^{-s_1 \sum_{z\in\hat{Z}} P\hat{G_z}\hat{R_z}^{\alpha\epsilon}\hat{D_z}^{-\alpha}\mathbf{1}(\delta_z=\delta_y)} \varsigma(T_{\mathrm{FR}})\left(1 - e^{-s_2 \sum_{z\in Z} P G_z R_z^{\alpha\epsilon} D_z^{-\alpha}}\right)\right] \\
&= \mathbb{E}_{\hat{I_{\mathbb{Z}}}, I_{\mathbb{Z}}} \varsigma(T)\left[\prod_{z\in\hat{Z}} e^{-s_1 P\hat{G_z}\hat{R_z}^{\alpha\epsilon}\hat{D_z}^{-\alpha}\mathbf{1}(\delta_z=\delta_y)}\left(1 - \varsigma(T_{\mathrm{FR}}) \prod_{z\in Z} e^{-s_2 P G_z R_z^{\alpha\epsilon} D_z^{-\alpha}}\right)\right] \\
&= \mathbb{E}_{\hat{I_{\mathbb{Z}}}}\left[\varsigma(T) \prod_{z\in\hat{Z}} \mathbb{E}\left[\mathbf{1}(\delta_z = \delta_y)\right] e^{-s_1 P\hat{G_z}\hat{R_z}^{\alpha\epsilon}\hat{D_z}^{-\alpha}}\right]\left(1 - \mathbb{E}_{\hat{I_{\mathbb{Z}}}}\left[\varsigma(T_{\mathrm{FR}}) \prod_{z\in Z} e^{-s_2 P G_z R_z^{\alpha\epsilon} D_z^{-\alpha}}\right]\right),
\end{aligned}$$

where the indicator function $\mathbf{1}(\delta_y = \delta_z)$ takes the value 1 to mark interfering mobiles that are utilizing thee same subband δ as user y. We can further evaluate the expression using the fact that $\hat{G}_z$ and G_z are both exponentially distributed with mean μ, giving

$$\mathbb{E}_{\hat{D}_z,\hat{R}_z}\left[\varsigma(T)\frac{1}{\Delta}\prod_{z\in\hat{Z}}\frac{\mu}{\mu+s_1\hat{R}_z{}^{\alpha\epsilon}P\hat{D}_z{}^{-\alpha}}\right]\left(1-\mathbb{E}_{D_z,R_z}\varsigma(T_{\mathrm{FR}})\left[\prod_{z\in Z}\frac{\mu}{\mu+s_2R_z^{\alpha\epsilon}PD_z^{-\alpha}}\right]\right). \tag{5.6}$$

Now, taking the expectation on R_z which is assumed to be Rayleigh distributed we have

$$\begin{aligned}
&= \mathbb{E}_{\hat{D}_z}\left[\varsigma(T)\frac{1}{\Delta}\prod_{z\in\hat{Z}}\mathbb{E}_{\hat{R}_z}\left[\frac{\mu}{\mu+s_1\hat{R}_z{}^{\alpha\epsilon}P\hat{D}_z{}^{-\alpha}}\right]\right]\\
&\quad\left(1-\mathbb{E}_{D_z}\left[\varsigma(T_{\mathrm{FR}})\prod_{z\in Z}\mathbb{E}_{R_z}\left[\frac{\mu}{\mu+s_2R_z^{\alpha\epsilon}PD_z^{-\alpha}}\right]\right]\right)\\
&= \mathbb{E}_{\hat{D}_z}\left[\varsigma(T)\frac{1}{\Delta}\prod_{z\in\hat{Z}}\int_0^\infty\frac{2\pi\lambda\hat{y}e^{-\pi\lambda\hat{y}^2}}{1+\frac{s_1}{\mu}\hat{y}^{\alpha\epsilon}P\hat{D}_z{}^{-\alpha}}\mathrm{d}\hat{y}\right]\\
&\quad\left(1-\mathbb{E}_{D_z}\left[\varsigma(T_{\mathrm{FR}})\prod_{z\in Z}\int_0^\infty\frac{2\pi\lambda ye^{-\pi\lambda y^2}}{1+\frac{s_2}{\mu}y^{\alpha\epsilon}PD_z^{-\alpha}}\mathrm{d}y\right]\right)
\end{aligned}$$

The probability generating functional (PGFL) of the PPP [104] allows us to obtain

$$\mathscr{L}(s_1,s_2) =$$
$$\varsigma(T)e^{-2\pi\lambda\int_r^\infty\left[1-\frac{1}{\Delta}\frac{2\pi\lambda\hat{y}e^{-\pi\lambda\hat{y}^2}}{1+\frac{s_1}{\mu}P\hat{y}^{\alpha\epsilon}x^{-\alpha}}\mathrm{d}\hat{y}\right]x\mathrm{d}x}\left(1-\varsigma(T_{\mathrm{FR}})e^{-2\pi\lambda\int_r^\infty\left[1-\int_0^\infty\frac{2\pi\lambda ye^{-\pi\lambda y^2}}{1+\frac{s_2}{\mu}Py^{\alpha\epsilon}x^{-\alpha}}\mathrm{d}y\right]x\mathrm{d}x}\right).$$

Substituting for $s_1,\ s_2$ we have $\mathscr{L}(\mu r^{\alpha(1-\epsilon)}\frac{T}{P},\mu r^{\alpha(1-\epsilon)}\frac{T_{\mathrm{FR}}}{P}) =$

$$e^{-\pi\lambda\int_r^\infty\left[1-\frac{1}{\Delta}\int_0^\infty\frac{2\pi\lambda\hat{y}e^{-\pi\lambda\hat{y}^2}}{1+Tr^{\alpha(1-\epsilon)}\hat{y}^{\alpha\epsilon}x^{-\alpha}}\mathrm{d}\hat{y}\right]x\mathrm{d}x}\left(1-\varsigma(T_{\mathrm{FR}})e^{-2\pi\lambda\int_r^\infty\left[1-\int_0^\infty\frac{2\pi\lambda ye^{-\pi\lambda y^2}}{1+T_{\mathrm{FR}}r^{\alpha(1-\epsilon)}Py^{\alpha\epsilon}x^{-\alpha}}\mathrm{d}y\right]x\mathrm{d}x}\right).$$

De-conditioning on r and substituting $\varsigma(T)$ and $\varsigma(T_{\mathrm{FR}})$, we have for the numerator

$$\int_0^\infty 2\pi\lambda re^{-\pi\lambda\left(r^2+2\upsilon(T_{\mathrm{FR}},\alpha,\Delta,\epsilon)-\frac{\mu T\sigma^2}{Pr^{\alpha(1-\epsilon)}}\right)}\left(1-e^{-\pi\lambda\left(r^2+2\upsilon(T,\alpha,1,\epsilon)-\frac{\mu T_{\mathrm{FR}}\sigma^2}{Pr^{\alpha(1-\epsilon)}}\right)}\right)\mathrm{d}r, \tag{5.7}$$

where $\upsilon(t,\alpha,\Delta,\epsilon) =$

$$\int_r^\infty \left[1 - \frac{1}{\Delta}\int_0^\infty \frac{2\pi\lambda y e^{-\pi\lambda y^2}}{1 + t r^{\alpha(1-\epsilon)} y^{\alpha\epsilon} x^{-\alpha}} \mathrm{d}y\right] x \mathrm{d}x.$$

Now we consider the denominator of (5.5),

$$\mathbb{E}\left[\left(1 - e^{\left(-\mu \frac{T_{\mathrm{FR}}}{P} r^{\alpha(1-\epsilon)} (\sigma^2 + I_{\mathcal{Z}})\right)}\right)\right],$$

noting that this expression is the same as the complement of the probability that the mobile user has SINR $> T_{\mathrm{FR}}$ on the full-reuse subband. As a result this can be directly obtained from (2.7) from [79] as

$$1 - p_c(T_{\mathrm{FR}}, \lambda, \alpha, \epsilon) \tag{5.8}$$

Plugging (5.7) and (5.8) back into (5.5) and substituting $r^2 = v$ gives the final result of (5.1). □

Users allocated FFR subbands experience a new distribution of interference $\hat{I_{\mathcal{Z}}}$ on the new subband coming from a different set of users than on the previous subband. This means that not only have the distances between the serving BS and the interfering mobiles changed, but also their transmit power, which is accounted for by the $\upsilon(t,\alpha,\Delta,\epsilon)$ terms. Additionally interdependence of the pathloss between the typical mobile and its serving BS is taken into account in 5.1 since it is assumed that during the subband transition the mobile is stationary although it experiences an independent fading power on the new subband.

Fig. 5.1 plots these coverage probability expressions for Strict FFR for $T_{\mathrm{FR}} =$ 1dB and fractional power control parameter ϵ values of 0, .6, and 1 along with the comparable expressions for full-reuse and SFR. Edge subband frequency reuse leads a

large increase in SINR for edge users compared to no FFR for all values of ϵ, although we also observe that ϵ greatly impacts the shape of those curves. Interestingly, $\epsilon = .6$ is the best performing over most SINR thresholds except for the highest values where no power control slightly outperforms. This is due to the fact that mobiles capable of achieving the highest SINR values are with high probability very close-in to their serving base station and the reduction in transmit power caused by fractional power control limits their achievable gains in this mostly noise-limited regime. This is also seen in the cross-over point between full-pathloss inversion ($\epsilon = 1$) and the no power control curves, which occurs around 6 dB for Strict FFR.

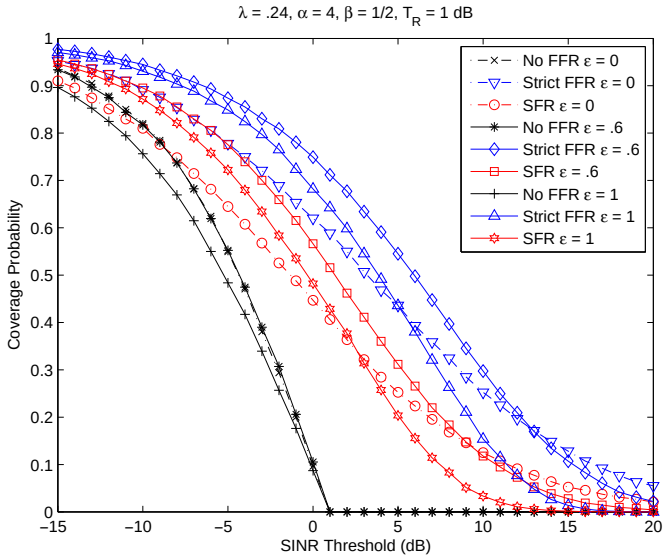

Figure 5.1: A plot of edge user coverage probability with fractional power control for full-reuse, SFR $\beta = 1/2$, and Strict FFR with a range of ϵ values.

Next we consider coverage for interior users under Strict FFR. Interior users by definition have SINR $> T_{\text{FR}}$ and the reuse factor Δ does not impact them since their subband allocation comes from a set shared by users in all cells.

Theorem 15 (Uplink Strict FFR, interior user)**.** *An interior user with Strict FFR has coverage probability given by*

$$\bar{\mathrm{F}}_{\mathrm{FFR,i}}(T) = \frac{p_c(\max\{T, T_{\mathrm{FR}}\}, \lambda, \alpha, 1, \epsilon)}{p_c(T_{\mathrm{FR}}, \lambda, \alpha, 1, \epsilon)},$$

where $p_c(t, \lambda, \alpha, \epsilon)$ is given by (4.6).

Proof. From the definition of (2.7) and applying Bayes' rule we have

$$\begin{aligned}
\bar{\mathrm{F}}_{\mathrm{FFR,i}}(T) &= \mathbb{P}\left(\frac{\hat{g_y} Pr^{-\alpha(1-\epsilon)}}{\sigma^2 + I_{\mathcal{Z}}} > T \;\middle|\; \frac{g_y Pr^{-\alpha(1-\epsilon)}}{\sigma^2 + I_{\mathcal{Z}}} > T_{\mathrm{FR}}\right) \\
&= \frac{\mathbb{P}\left(\frac{\hat{g_y} Pr^{-\alpha(1-\epsilon)}}{\sigma^2 + I_{\mathcal{Z}}} > \max\{T, T_{\mathrm{FR}}\}\right)}{\mathbb{P}\left(\frac{g_y Pr^{-\alpha(1-\epsilon)}}{\sigma^2 + I_{\mathcal{Z}}} > T_{\mathrm{FR}}\right)} \\
&= \frac{p_c(\max\{T, T_{\mathrm{FR}}\}, \lambda, \alpha, 1, \epsilon)}{p_c(T_{\mathrm{FR}}, \lambda, \alpha, 1, \epsilon)}. \qquad (5.9)
\end{aligned}$$

□

The $\max\{T, T_{\mathrm{FR}}\}$ term in the numerator is a result of interior users having SINR $\geq T_{\mathrm{FR}}$ by definition. Since interior users share the same subband in all cells, the SINR distribution can be expressed in terms of (4.6) from [79].

5.4.2 SFR

In the case of SFR, all subbands are reused in each cell, but $1/\Delta$ subbands are reserved for edge users to transmit on with higher power than interior users. This coarse power control factor $\beta \leq 1$ is applied to the SFR subbands when they are allocated to interior users. As a result the SINR of (4.1) differs from Strict FFR due to the new form of the interference power which is given as

$$I_{\mathcal{Z}} = \sum_{z \in \mathcal{Z}_{\mathrm{edge}}} g_z P \left(R_z^{\alpha}\right)^{\epsilon} {D_z}^{-\alpha} + \sum_{z \in \mathcal{Z}_{\mathrm{int}}} g_z \beta P \left(R_z^{\alpha}\right)^{\epsilon} {D_z}^{-\alpha}. \qquad (5.10)$$

The two sets of interfering mobiles $\mathcal{Z}_{\text{edge}}$ and $\mathcal{Z}_{\text{int}}$ consist of edge and interior mobiles respectively. Since $\frac{(\Delta-1)}{\Delta}$ of the interfering mobiles are given the β power control factor we can denote an effective interference power factor which consolidates the two classes of users in to a single term $\eta = (\Delta - 1 + (1/\beta)) / (\Delta/\beta)$ and the overall interference power becomes $\eta P I_{\mathcal{Z}}$. We now consider the SINR distribution for users under SFR starting again with the case for cell-edge users.

Theorem 16 (Uplink SFR, edge user)**.** *The coverage probability of an SFR edge user whose initial* SINR *is less than* T_{FR} *is* $\bar{\text{F}}_{\text{SFR,e}}(T)$

$$\begin{aligned} &= \mathbb{P}\left(\frac{\hat{g_y} P r^{-\alpha}}{\sigma^2 + \eta \hat{I_{\mathcal{Z}}}} > T \;\middle|\; \frac{g_y \beta P r^{-\alpha}}{\sigma^2 + \eta I_{\mathcal{Z}}} < T_{\text{FR}}\right) \\ &= \frac{1}{1 - p_c(\frac{\eta T_{\text{FR}}}{\beta}, \lambda, \alpha, \epsilon)} \int_0^\infty 2\pi\lambda r e^{-\pi\lambda r^2 (1 + 2\upsilon(\eta T, \alpha, 1, \epsilon)) - \frac{\mu \eta T \sigma^2}{P} r^{\alpha(1-\epsilon)}} \\ &\quad \left(1 - e^{-\pi\lambda r^2 (1 + 2\upsilon(\frac{\eta T_{\text{FR}}}{\beta}, \alpha, 1, \epsilon)) - \frac{\mu \eta T_{\text{FR}} \sigma^2}{\beta P} r^{\alpha(1-\epsilon)}}\right) \mathrm{d}r, \end{aligned} \tag{5.11}$$

where $\upsilon(t, \lambda, \alpha, \Delta, \epsilon) =$ *is given by* (5.2) *and* $p_c(t, \lambda, \alpha, \epsilon)$ *by* (4.6)*.*

Proof. A mobile user y with SINR $< T_{\text{FR}}$ is allocated a SFR subband δ, where $\delta \in \{1, ..., \Delta\}$, transmit power $P r^{\alpha(1-\epsilon)}$ instead of $\beta P r^{\alpha(1-\epsilon)}$ and experiences new fading and interference power $\hat{g_y}$ and $\eta \hat{I_z}$ respectively as opposed to g_y and ηI_z. The SINR CCDF $\bar{\text{F}}_{\text{SFR,e}}(T)$ is given conditioned on the SINR on the subband allocated prior to the SFR subband,

$$\bar{\text{F}}_{\text{SFR,e}}(T) = \mathbb{P}\left(\frac{\hat{g_y} P r^{-\alpha(1-\epsilon)}}{\sigma^2 + \eta \hat{I_z}} > T \;\middle|\; \frac{g_y \beta P r^{-\alpha(1-\epsilon)}}{\sigma^2 + \eta I_z} < T_{\text{FR}}\right). \tag{5.12}$$

Applying Bayes' rule,

$$\bar{\text{F}}_{\text{SFR,e}}(T) = \frac{\mathbb{P}\left(\frac{\hat{g_y} P r^{-\alpha(1-\epsilon)}}{\sigma^2 + \eta \hat{I_z}} > T \;, \frac{g_y \beta P r^{-\alpha(1-\epsilon)}}{\sigma^2 + \eta I_z} < T_{\text{FR}}\right)}{\mathbb{P}\left(\frac{g_y \beta P r^{-\alpha(1-\epsilon)}}{\sigma^2 + \eta I_z} < T_{\text{FR}}\right)}. \tag{5.13}$$

Following the method of Theorem 2 and using the fact that $\hat{g_y}$ and g_y are exponentially distributed with mean μ, we have

$$\bar{\mathrm{F}}_{\mathrm{SFR,e}}(T) = \frac{\mathbb{E}\left[e^{\left(-\mu\frac{T}{P}r^{\alpha(1-\epsilon)}(\sigma^2+\eta\hat{I}_z)\right)}\left(1-e^{\left(-\mu\frac{T_{\mathrm{FR}}}{\beta P}r^{\alpha(1-\epsilon)}(\sigma^2+\eta I_z)\right)}\right)\right]}{1-p_c(\frac{\eta T_{\mathrm{FR}}}{\beta},\alpha,1)}. \tag{5.14}$$

Next we consider the numerator and condition on r, which is the distance from the mobile to the serving BS. We can evaluate the expectation as the joint Laplace transform $\mathscr{L}(s_1,s_2)$ of $\hat{I}_z$ and I_z evaluated at $(\mu r^{\alpha(1-\epsilon)}\frac{\eta T}{P}, \mu r^{\alpha(1-\epsilon)}\frac{\eta T_{\mathrm{FR}}}{\beta P})$. Similar steps are taken with respect to Theorem 2, however the fundamental structure of the interference terms given by (4.2) are quite different since for SFR subbands are fully reused with $\Delta = 1$ in all cells such that $\hat{I}_z$ and I_z include mobiles from all cells and not just those considered to be edge users on subband δ_y. Thus we write $\mathscr{L}(s_1,s_2)$

$$\begin{aligned}
&= \mathbb{E}_{D_z}\left[\varsigma(T)\prod_{z\in\hat{Z}}\mathbb{E}_{\hat{R}_z}\left[\frac{\mu}{\mu+s_1\hat{R}_z{}^{\alpha\epsilon}P\hat{D}_z{}^{-\alpha}}\right]\right] \\
&\quad\left(1-\mathbb{E}_{D_z}\left[\varsigma\left(\frac{T_{\mathrm{FR}}}{\beta}\right)\prod_{z\in Z}\mathbb{E}_{R_z}\left[\frac{\mu}{\mu+s_2R_z^{\alpha\epsilon}PD_z^{-\alpha}}\right]\right]\right) \\
&= \mathbb{E}_{D_z}\left[\varsigma(T)\prod_{z\in\hat{Z}}\int_0^\infty\frac{2\pi\lambda\hat{y}e^{-\pi\lambda\hat{y}^2}}{1+\frac{s_1}{\mu}\hat{y}^{\alpha\epsilon}\hat{D}_z{}^{-\alpha}}\mathrm{d}\hat{y}\right] \\
&\quad\left(1-\mathbb{E}_{D_z}\left[\varsigma\left(\frac{T_{\mathrm{FR}}}{\beta}\right)\prod_{z\in Z}\int_0^\infty\frac{2\pi\lambda ye^{-\pi\lambda y^2}}{1+\frac{s_2}{\mu}y^{\alpha\epsilon}D_z^{-\alpha}}\mathrm{d}y\right]\right).
\end{aligned}$$

We simplify the Laplace transform using the PGFL of the PPP as $\mathscr{L}(s_1,s_2) =$

$$\varsigma(T)e^{-2\pi\lambda\int_r^\infty\left[1-\frac{2\pi\lambda e^{-\pi\lambda y^2}}{1+\frac{s_1}{P}\hat{y}^{\alpha\epsilon}x^{-\alpha}}\mathrm{d}y\right]x\mathrm{d}x}\left(1-\varsigma\left(\frac{T_{\mathrm{FR}}}{\beta}\right)e^{-2\pi\lambda\int_r^\infty\left[1-\int_0^\infty\frac{2\pi\lambda ye^{-\pi\lambda y^2}}{1+\frac{s_2}{P}y^{\alpha\epsilon}x^{-\alpha}}\mathrm{d}y\right]x\mathrm{d}x}\right).$$

Hence $\mathscr{L}\left(\mu r^{\alpha(1-\epsilon)}\frac{\eta T}{P}, \mu r^{\alpha(1-\epsilon)}\frac{\eta T_{\mathrm{FR}}}{\beta P}\right) =$

$$\varsigma(T)\,e^{-2\pi\lambda\int_r^\infty\left[1-\int_0^\infty\frac{2\pi\lambda\hat{y}e^{-\pi\lambda\hat{y}^2}}{1+\eta Tr^{\alpha(1-\epsilon)}\hat{y}^{\alpha\epsilon}x^{-\alpha}}\mathrm{d}\hat{y}\right]x\mathrm{d}x}\left(1-\varsigma\left(\frac{T_{\mathrm{FR}}}{\beta}\right)e^{-2\pi\lambda\int_r^\infty\left[1-\int_0^\infty\frac{2\pi\lambda ye^{-\pi\lambda y^2}}{1+\frac{\eta T_{\mathrm{FR}}}{\beta}r^{\alpha(1-\epsilon)}y^{\alpha\epsilon}x^{-\alpha}}\right]\mathrm{d}x}\right).$$

Lastly, after de-conditioning on r and substituting for the noise terms we have

$$\int_0^\infty 2\pi\lambda r e^{-\pi\lambda r^2(1+2\upsilon(\eta T,\alpha,1,\epsilon))-\frac{\mu\eta T\sigma^2}{P}r^{\alpha(1-\epsilon)}}\left(1-e^{-\pi\lambda r^2(1+2\upsilon(\frac{\eta T_{\mathrm{FR}}}{\beta},\alpha,1,\epsilon))-\frac{\mu\eta T_{\mathrm{FR}}\sigma^2}{\beta P}r^{\alpha(1-\epsilon)}}\right)\mathrm{d}r,$$

where $\upsilon(t,\alpha,\Delta,\epsilon)$ is given by (5.2).

The denominator of (5.14) again follows from Theorem 14 and equation (4.6) and is given as $1-p_c(\frac{T_{\mathrm{FR}}}{\beta},\lambda,\alpha,\epsilon)$. Substituting the numerator and denominator back into (5.14) gives the full result of (5.11). □

The expressions primarily differ from Strict FFR in that edge subbands are fully reused instead of with reuse factor Δ and the introduction of η and β which effectively reshape the SINR and FFR thresholds $\frac{\eta T}{\beta}$ and ηT_{FR} respectively.

Fig. 5.1 plots the coverage probability achieved with SFR for $T_{\mathrm{FR}} = 1\mathrm{dB}$ and $\beta = 1/2$ with fractional power control parameter ϵ taking values of 0, .6, and 1 along with the comparable expressions for full-reuse and Strict FFR. As expected due to the tradeoff between allowing interior users to share subbands with edge users the coverage gains are not has high as with Strict FFR. Additionally while $\epsilon = .6$ provides the highest coverage values for most SINR thresholds as was the case for Strict FFR, the crossover point between full-pathloss inversion ($\epsilon = 1$) and no power control is lower than Strict FFR at 3 dB.

Fig. 5.2 gives edge user coverage probability expressions as a function of the SFR coarse power control factor β for $\epsilon = .7$, $\alpha = 3.8$, and $T_{\mathrm{FR}} = 1\mathrm{dB}$. As β decreases, the gains begin to approach those of Strict FFR, while utilizing all subbands unlike Strict FFR, although with diminishing gains as $\beta < 1/4$. However since lower β implies a reduction of transmit power for subbands used by interior users, we next consider the impact on interior user SINR.

Theorem 17 (Uplink SFR, interior user)**.** *For the interior user under SFR the* SINR *CCDF* $\bar{\mathrm{F}}_{\mathrm{i}}(T)$ *is given by the following*

$$\bar{\mathrm{F}}_{\mathrm{SFR,i}}(T) = \frac{p_c(\eta \max\{T, T_{\mathrm{FR}}\}, \alpha, \epsilon)}{p_c(\eta T_{\mathrm{FR}}, \alpha, \epsilon)}.$$

Proof.

$$\begin{aligned}
\bar{\mathrm{F}}_{\mathrm{SFR,i}}(T) &= \mathbb{P}\left(\frac{g_y \beta P r^{-\alpha(1-\epsilon)}}{\sigma^2 + \eta I_z} > T \;\middle|\; \frac{g_y \beta P r^{-\alpha(1-\epsilon)}}{\sigma^2 + \eta I_z} > T_{\mathrm{FR}}\right) \\
&= \frac{\mathbb{P}\left(\frac{g_y \beta P r^{-\alpha(1-\epsilon)}}{\sigma^2 + \eta I_z} > \max\{T, T_{\mathrm{FR}}\}\right)}{\mathbb{P}\left(\frac{g_y \beta P r^{-\alpha(1-\epsilon)}}{\sigma^2 + \eta I_z} > T_{\mathrm{FR}}\right)} \\
&= \frac{p_c(\max\{T, T_{\mathrm{FR}}\}, \lambda, \alpha, \epsilon)}{p_c(T_{\mathrm{FR}}, \lambda, \alpha, \epsilon)}.
\end{aligned}$$

□

This result follows very closely from the Strict FFR expressions. However, unlike edge users whose SINR increases with smaller β, we see from the above expressions that this results in a degradation. The impact of this degradation is shown in Fig. 5.3 for β values of 1/2, 1/8, and 1/30, $\epsilon = .6$, $\alpha = 4$ and $T_{\mathrm{FR}} = 0$dB. We see that $\beta = 1/2$ leads to only minor degradation compared to the no FFR case and importantly we note much less than the corresponding gain for edge users that we observed in Fig. 5.2. As β becomes smaller the degradation increases up to a maximum of 15% at SINR threshold of 5 dB although there is a saturation effect, with only a slight decrease between $\beta = 1/8$ and $\beta = 1/30$ despite the almost 6 dB decrease in transmit power.

5.4.3 SINR Distribution

So far we have considered the impact of FFR on edge and interior users separately. However it is also interesting to consider the distribution of the overall SINR

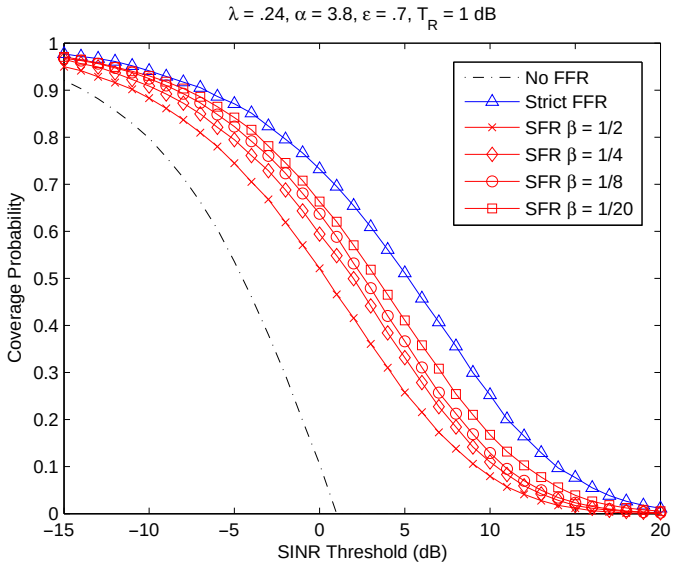

Figure 5.2: A plot of edge user coverage probability with fractional power control with $\alpha = 3.8$, $\epsilon = .7$ for full-reuse, Strict FFR, and SFR with a range of β values.

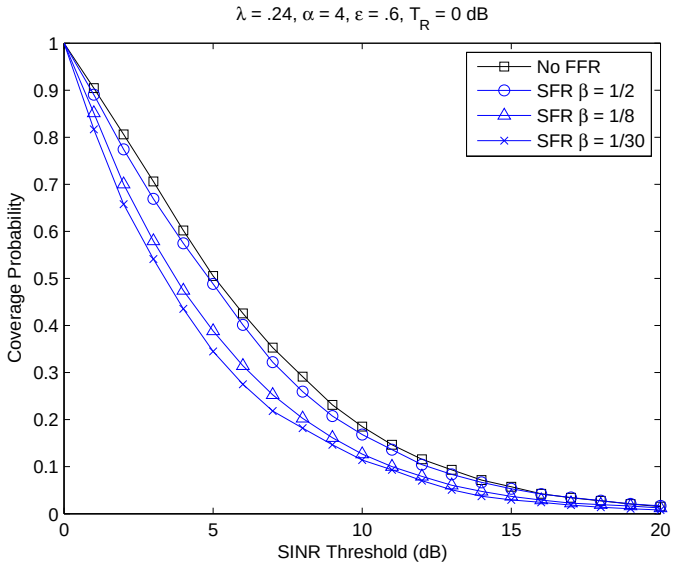

Figure 5.3: Interior user coverage probability with $\epsilon = .6$ for SFR with $\beta = \{1/2, 1/8, 1/30\}$ compared to full reuse.

of all users. In Fig. 5.4(a) and Fig. 5.4(b) we plot the overall SINR PDFs for no FFR, Strict FFR, and SFR with $\beta = .25$ for network parameters of $\lambda = .24$, $\alpha = 3.75$, $T_R = 1$ dB, and $\epsilon = \{0,\ .75\}$.

Our first observation is the skewing of the distributions of Strict FFR and SFR around 1 dB which is the value of the reuse threshold T_R. The disjointed behavior differs from the no FFR curves and is a result of the superposition of interior and edge user distributions induced by utilizing FFR. Below T_R we observe that Strict FFR and SFR have lower densities than the no FFR case, while above T_R they have higher densities which is directly related to the edge user distributions. Strict FFR and SFR reshape the SINR distributions of the typical user, moving a given percentage of them based on selection of T_R from low to high SINR, with Strict FFR showing the strongest gains.

Also Fig. 5.4(a) and Fig. 5.4(b) give insight into the effect of fractional power control. The overall behavior of Strict FFR and SFR is the same with respect to no FFR, but the curves do not have the same shape. The case of $\epsilon = 0$, no power control, has a much more dispersed distribution with a relatively lower peak than is the case with $\epsilon = .75$. In that case the power control has a strong impact on the distribution, creating a much stronger peak to the densities in the -5 to 5 dB range and lower densities above 10 dB. However Strict FFR is not as affected as SFR and no reuse at the highest SINR thresholds, due to the removal of edge and interior users from their respective sets of interfering users.

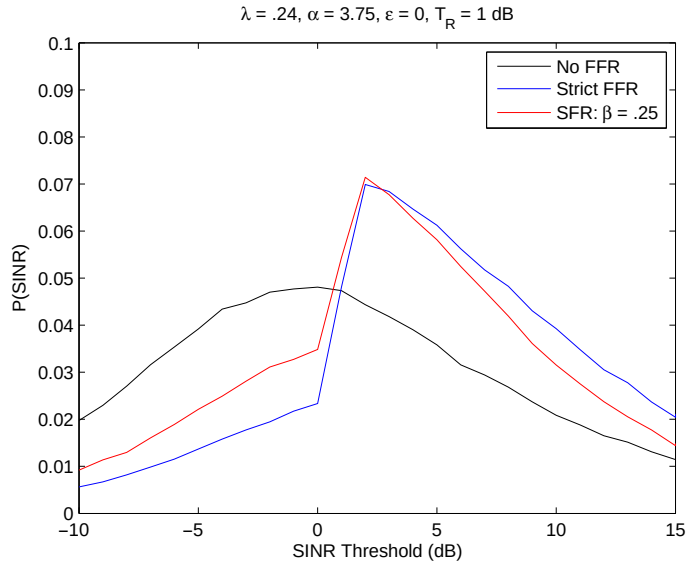

(a) $\epsilon = 0$

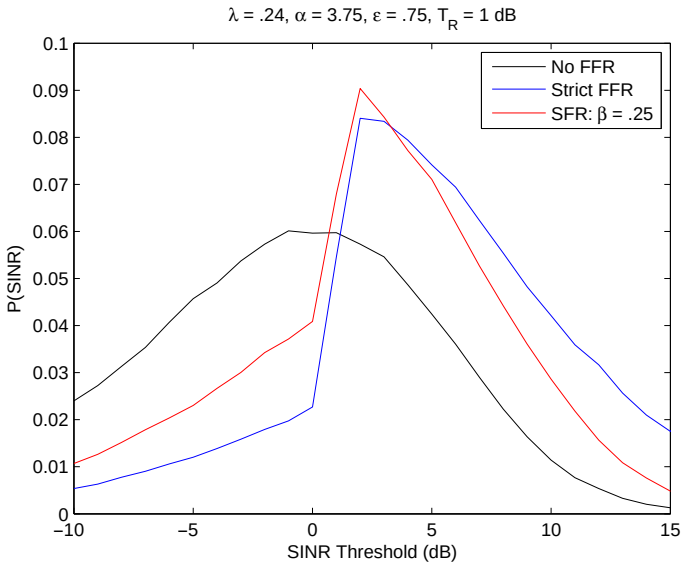

(b) $\epsilon = .75$

Figure 5.4: PDFs of the total user SINR for No FFR, Strict FFR, and SFR with $\beta = 1/4$, $\lambda = .24$, $T_{\text{FR}} = 1\text{dB}$, $\Delta = 3$, $\sigma^2 = 0$, and $\alpha = 3.75$ for fractional power control values of (a) $\epsilon = 0$ and (b) $\epsilon = .75$.

5.4.4 Comparison with Grid Model

In this section we compare coverage probability expressions obtained using our model with simulations based of (i) traditional hexagonal grid of base stations and, (ii) an actual urban cellular deployment with the same density λ.

Figs. 5.5(a) and 5.5(b) compare SINR distributions for Strict FFR and SFR respectively. The grid model serves as an upper bound compared to the PPP model due to its well-defined fixed-sized tiers effectively constraining interference and providing a buffer especially at the cell-edge [19]. Despite the random nature of the distances between interfering mobiles and their respective base stations, the analytical expressions for Strict FFR and SFR have a similar slope and shape compared to the results using actual base station locations and are actually a closer fit, especially in the case of Strict FFR.

5.5 System Design Implications

In this section we consider applications of the analytical framework developed in Sec. 5.4 for evaluating important system design metrics such as average rate, resource allocation, and transmit power.

5.5.1 Average rate

Besides its use for determining coverage in a network, SINR can be used to derive the average data rate due to the use of modern channel-adaptive modulation and coding. We now provide expressions for Strict FFR and SFR using the definition of average data rate based upon the Shannon capacity expression for a communications

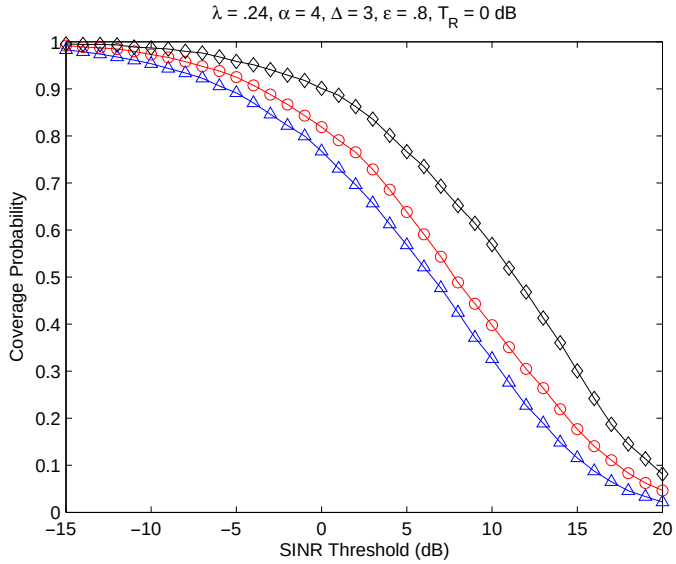

(a) Strict FFR

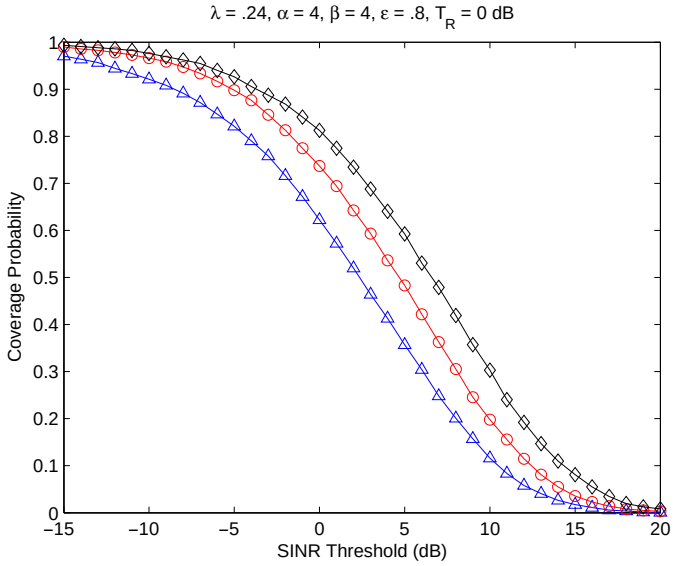

(b) SFR

Figure 5.5: Edge user coverage probability comparison between Poisson-model, grid model, and actual base station locations for (a) Strict FFR and (b) SFR with $\beta = 1/4$, $\epsilon = .8$, $T_{\text{FR}} = 0\text{dB}$, $\Delta = 3$, $\sigma^2 = 0$, and $\alpha = 4$.

channel,

$$\bar{\tau}\left(\lambda,\alpha,\epsilon\right)=\mathbb{E}\left[\ln\left(1+\mathrm{SINR}\right)\right], \tag{5.15}$$

taking the expectation over the SINR distributions given in Sec. 5.4. These results given in units of nats/Hz wherein 1 bit $=\log_e(2)$ nats.

5.5.1.1 Strict FFR

We first derive results for Strict FFR typical edge users.

Theorem 18 (Uplink Strict FFR, average edge user rate)**.** *The average rate under Strict FFR for a typical edge user is given by* $\bar{\tau}_{FFR}(T_{\mathrm{FR}},\lambda,\alpha,\epsilon,\Delta)=$

$$\int_{t>0}\frac{p_c\left((e^t-1),\lambda,\alpha,\epsilon,\Delta\right)-\upsilon\left(e^t-1,T_{\mathrm{FR}},\alpha,\Delta\right)}{1-p_c(T_{\mathrm{FR}},\lambda,\alpha,1)}\mathrm{d}t \tag{5.16}$$

where $\upsilon\left(e^t-1,T_{\mathrm{FR}},\alpha,\Delta\right)=$

$$\int_{t>0}\frac{1}{1-p_c(T_{\mathrm{FR}},\lambda,\alpha,\epsilon)}\int_0^{\infty}2\pi\lambda r e^{-\pi\lambda\left(r^2+2\upsilon(e^t-1,\alpha,\Delta,\epsilon)-\frac{\mu T\sigma^2}{Pr^{\alpha(1-\epsilon)}}\right)}\left(1-e^{-\pi\lambda\left(r^2+2\upsilon(T_{\mathrm{FR}},\alpha,1,\epsilon)-\frac{\mu T_{\mathrm{FR}}\sigma^2}{Pr^{\alpha(1-\epsilon)}}\right)}\right)\mathrm{d}r\mathrm{d}t, \tag{5.17}$$

and $p_c\left((e^t-1),\lambda,\alpha,\Delta\right)$ *is given by* (2.7)*.*

Proof. Starting from (5.15) the average rate of a user allocated a Strict FFR subband is $\bar{\tau}_{FFR}(T_{\mathrm{FR}},\lambda,\alpha,\Delta)$

$$\begin{aligned}&=\mathbb{E}\left[\ln\left(1+\mathrm{SINR}\right)\right]\\&=\int_{r>0}e^{-\pi\lambda r^2}\mathbb{E}\left[\ln\left(1+\frac{\hat{g_y}Pr^{-\alpha(1-\epsilon)}}{\sigma^2+\hat{I_{\mathcal{Z}}}}\right)\right]2\pi\lambda r\mathrm{d}r,\end{aligned}$$

where we used the fact that $E[\tau]=\int_{t>0}P(\tau>t)\mathrm{d}t$ since $\tau=\ln(1+\mathrm{SINR})$ is a positive random variable. Next, conditioning the new SINR based on its prior value

gives

$$\bar{\tau}_{FFR}(T_{\mathrm{FR}},\lambda,\alpha,\Delta)=\int_{r>0}2\pi\lambda re^{-\pi\lambda r^2}\int_{t>0}\mathbb{P}\left[(*)\right]\mathrm{d}t\ \mathrm{d}r.$$

Bayes' rule applied to $\mathbb{P}\left[(*)\right]$ gives,

$$\begin{aligned}\mathbb{P}\left[(*)\right] &= \mathbb{P}\left[\ln\left(1+\frac{\hat{g_y}Pr^{-\alpha(1-\epsilon)}}{\sigma^2+\hat{I_{\mathcal{Z}}}}\right)>t\ \middle|\ \frac{g_yPr^{-\alpha(1-\epsilon)}}{\sigma^2+I_{\mathcal{Z}}}<T_{\mathrm{FR}}\right]\\ &= \frac{\mathbb{P}\left[\ln\left(1+\frac{\hat{g_y}Pr^{-\alpha(1-\epsilon)}}{\sigma^2+\hat{I_{\mathcal{Z}}}}\right)>t\ ,\frac{g_yPr^{-\alpha(1-\epsilon)}}{\sigma^2+I_{\mathcal{Z}}}<T_{\mathrm{FR}}\right]}{\mathbb{P}\left[\frac{g_yPr^{-\alpha(1-\epsilon)}}{\sigma^2+I_{\mathcal{Z}}}<T_{\mathrm{FR}}\right]}\end{aligned}\tag{5.18}$$

The remainder of the theorem can then directly follow the method of Theorem 14 with appropriate substitutions of e^t-1 for T into (5.7) and (5.8), giving the final result of (5.17). □

Note that due to the integration over all possible rates t, for a given set of values (5.17) gives a single value and not a distribution of the rate. Although slightly more involved than the coverage probability expressions given in Theorem 14, they can still be simply evaluated using basic numerical integration techniques.

5.5.1.2 SFR

Determining average rate in the case of SFR closely follows Theorem 18.

Theorem 19 (Uplink SFR, edge user)**.** *The average rate of an edge user under SFR is*

$\bar{\tau}_{SFR}(T_{\mathrm{FR}},\lambda,\alpha,\eta,\beta)=$

$$\int_{t>0}\frac{1}{1-p_c(\frac{\eta T_{\mathrm{FR}}}{\beta},\lambda,\alpha,\epsilon)}\int_0^{\infty}2\pi\lambda re^{-\pi\lambda r^2(1+2\upsilon(\eta e^t-1,\alpha,1,\epsilon))-\frac{\mu\eta T\sigma^2}{P}r^{\alpha(1-\epsilon)}}\left(1-e^{-\pi\lambda r^2(1+2\upsilon(\frac{\eta T_{\mathrm{FR}}}{\beta},\alpha,1,\epsilon))-\frac{\mu\eta T_{\mathrm{FR}}\sigma^2}{\beta P}r^{\alpha(1-\epsilon)}}\right)\mathrm{d}r\mathrm{d}t,\tag{5.19}$$

where $\upsilon\left(t,\alpha,\Delta,\epsilon\right)=$ *is given by* (5.2) *and* $p_c\left(t,\lambda,\alpha,\epsilon\right)$ *is given by* (2.7)*.*

Proof. Beginning with (5.15) and integrating over the SFR edge user SINR distribution we have $\bar{\tau}_{SFR}(T_{\mathrm{FR}}, \lambda, \alpha, \eta, \beta)$

$$\begin{aligned} &= \mathbb{E}\left[\ln\left(1+\mathrm{SINR}\right)\right] \\ &= \int_{r>0} 2\pi\lambda r e^{-\pi\lambda r^2} \mathbb{E}\left[\ln\left(1+\frac{\hat{g_y} P r^{-\alpha}}{\sigma^2+\eta\hat{I_{\mathcal{Z}}}}\right)\right] \mathrm{d}r \\ &= \int_{r>0} 2\pi\lambda r e^{-\pi\lambda r^2} \int_{t>0} \mathbb{P}\left[(*)\right] \mathrm{d}t \ \mathrm{d}r. \end{aligned}$$

where

$$\mathbb{P}\left[(*)\right] = \mathbb{P}\left[\ln\left(1+\frac{\hat{g_y} P r^{-\alpha(1-\epsilon)}}{\sigma^2+\eta\hat{I_{\mathcal{Z}}}}\right) > t \;\middle|\; \frac{g_y \beta P r^{-\alpha(1-\epsilon)}}{\sigma^2+\eta I_{\mathcal{Z}}} < T_{\mathrm{FR}}\right].$$

Following the approaches of Theorems 16 and 18 and substituting $e^t - 1$ for T in (5.14) gives (5.19). □

5.5.2 Resource Allocation for FFR

One observation made from the subband allocations is the advantage SFR achieves compared to Strict FFR since fully 100% of the subbands can be utilized. However, when comparing their respective SINR distributions in the previous section it was noted that SFR trades relative coverage improvement for edge users with this resource efficiency compared to Strict FFR.

The analytical expressions from Sec. 5.4 can be used to determine the size of the subband partitions and the value of the reuse threshold T_{FR} with the goal of improving overall capacity for Strict FFR and SFR over the full-reuse, no FFR default strategy. Given a reuse threshold T_{FR}, N_{edge} is proportional to the SINR distribution $\bar{\mathrm{F}}(T_{\mathrm{FR}})$ for Strict FFR or SFR at T_{FR} according to the following

$$N_{\mathrm{edge}} = \lfloor \left(1 - \bar{\mathrm{F}}(T_{\mathrm{FR}})\right) N_{band} \rfloor. \tag{5.20}$$

This resource allocation framework directly connects the threshold T_{FR} to the other system parameters and gives freedom in choosing its value based upon coverage requirements or potentially based upon network load. For example, a small value of T_{FR} may correspond to a situation with few edge users and resources are skewed primarily to the cell center users, and a large value of T_{FR} represents a scenario where there is a large amount of traffic coming from the cell-edge. The overall average per-cell spectral efficiency computed using the results of Theorem 18 and Theorem 19 as well as equations (2.3), (2.4), and (5.20) is given as

$$\hat{\mathrm{SE}} = \frac{BN_{\mathrm{edge}}}{\log(2)}\bar{\tau}_{\mathrm{edge}}\left(\lambda, \alpha, \Delta, \epsilon\right) + \frac{BN_{\mathrm{int}}}{\log(2)}\bar{\tau}_{int}\left(\lambda, \alpha, \Delta, \epsilon\right), \tag{5.21}$$

where B is the per-subband bandwidth, N_{edge} and N_{int} are given by (2.3)-(5.20) in the case of Strict FFR and SFR respectively.

Fig. 5.6 gives the results for the SINR-proportional allocation for $\Delta = 3$ as function of the reuse threshold T_{FR} by comparing the spectral efficiency relative to full-reuse. The total number of subbands $N_{\mathrm{band}} = 50$, analogous to a 10MHz LTE deployment and the BS density is given by $\lambda = .24$. The interesting shape of the curves reflect the underlying tradeoffs of both SFR and Strict FFR. Strict FFR gives moderate gains of 5-20% at low and moderate reuse threshold values due to the signficant increase in SINR afforded to the edge users, but then drops below the performance achieved without FFR due to the loss of available subbands which approaches $N_{\mathrm{band}}/3$, which is the same as the conventional per-cell frequency reuse strategy. SFR initially underperforms both Strict FFR and full-reuse due to the more moderate increase in edge user SINR and slight degradation for interior users. However when $T_{\mathrm{FR}} > -6$ dB, SFR outperforms full-reuse and Strict FFR when $T_{\mathrm{FR}} \geq 3$ dB due to the ability to tradeoff the SINR improvement for edge users

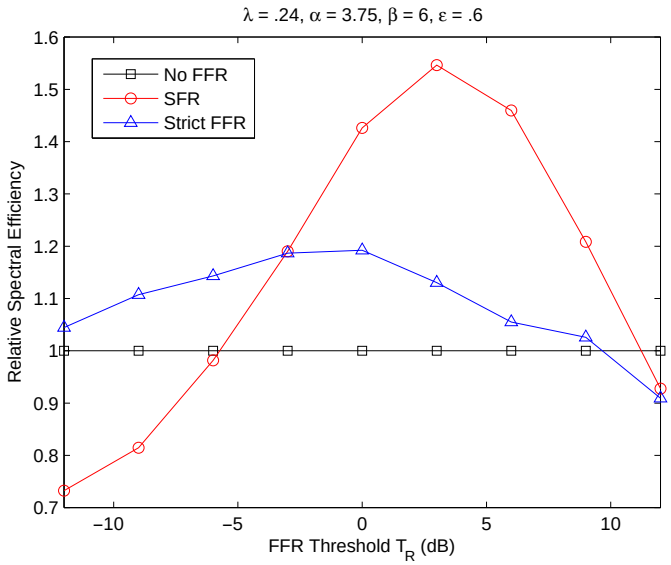

Figure 5.6: Average sum capacity for different reuse strategies using SINR-proportional sub-band allocation as a function of the SINR threshold T_{FR}.

with greater spectral resource efficiency than Strict FFR and produces larger gains of 40-50% at moderate threshold values. However as T_{FR} increases further, the gains under SFR decrease, due to the saturation in the number of subbands that can be allocated to edge users at who make up the vast majority of users $N_{\text{band}}/3$ combined with the reduction in users who are able to utilize the subbands reserved for interior users.

5.5.3 Downlink vs. Uplink Comparison

Next we compare coverage in the uplink with the downlink which was previously derived in Chap. 2. In that network model BSs are distributed according to a PPP with density $\lambda = .24$ base stations per km^2 and constant transmit power is assumed. Fig. 5.7 plots the two cases for a 10 MHz bandwidth, maximum transmit power of 40W in the downlink and 200mW in the uplink with $\epsilon = .75$, the pathloss

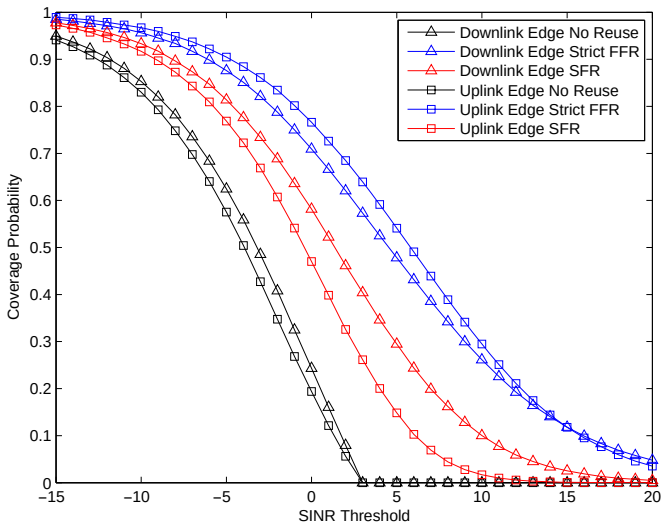

Figure 5.7: A comparison of uplink and downlink edge user coverage probability with full-reuse, SFR with $\beta = 1/2$, and Strict FFR. The downlink transmit power is 30W and the uplink utilizes fractional power control with $\epsilon = 1$, and a max transmit power of 200 mW.

exponent $\alpha = 3.8$, and the noise power spectral density σ^2 is -174 dBm/Hz, which are standard assumptions for LTE-based network deployments [45].

For both the No FFR and SFR cases downlink coverage probability is greater for all values of SINR up to the reuse threshold of $T_{\text{FR}} = 3$dB. In fact the disparity is quite large for SFR, with the limited uplink transmit power and impact of the fractional power control both shaping the SINR distribution. Interestingly in the case of Strict FFR, uplink coverage actually exceeds the downlink for this set of system parameters. Also, relative to full-reuse, SFR provides similar gains in the uplink and downlink, while Strict FFR provides slightly larger gains in the uplink.

Determining system parameters such that the uplink and downlink are balanced allows operators to provide an overall quality experience for mobile users. Ad-

ditionally to provide better data rates, increasing the SINR is useful in improving mobile handovers between base stations. Utilizing FFR techniques would allow for users at the edge of coverage to extend their connection time, which is an important metric in the development of handover algorithms for moderate to high mobility scenarios. Potentially the analytical framework developed in Sec. 5.4 can be related to the relevant parameters, giving greater insight into performance trends.

5.5.4 Fractional Power Control

The impact of fractional power control on uplink coverage is a function of the different gains achieved by users depending on whether users are in a heavily interference-limited regime at the cell-edge or whether they are in a more mixed, interference/noise-limited regime closer to the BS [79]. One benefit of analysis of Strict FFR and SFR is that it effectively distills these two regions into different sets which can be analyzed independently. Focusing on edge users allocated a Strict FFR or SFR subband in Fig. 5.1 for example, we noted that the value of $\epsilon = .6$ was coverage maximizing for most SINR values which is a much larger than result than the $\epsilon = .2 - .3$ range that was found in prior analysis focusing on full-reuse networks [79]. This can be explained by understanding that edge users benefit from an increase in their transmit power with high ϵ relative to interfering cell-interior users. This raises the question of whether FFR strategies for the uplink can also benefit from giving users a new ϵ value in addition to a reserved subband based on the reuse threshold.

The SINR expressions for Strict FFR and SFR given by (5.1) and (5.11) can be modified to accommodate this strategy wherein cell-interior users utilize ϵ_1 for their power control, but are switched to ϵ_2 if they are given an edge subband.

Fig. 5.8 shows the SINR distribution for three sets of ϵ_1, ϵ_2 pairs: $\{\epsilon_1 = 0, \epsilon_2 = .1\}$, $\{\epsilon_1 = .6, \epsilon_2 = .7\}$, $\{\epsilon_1 = 1, \epsilon_2 = 1\}$. In the case of Strict FFR, the increase in ϵ_2 for the first two cases produces moderate gains compared to that of Fig. 5.1. However, the gains are much more significant in the SFR cases, with coverage almost approaching that of Strict FFR, even for a low value of $\beta = 1/2$. This is due to the fact that SFR subbands are shared with interior users who are still utilizing the lower ϵ_1 value and thus given a boost in their overall transmit power by utilizing the higher ϵ value and inverting a greater portion of their pathloss.

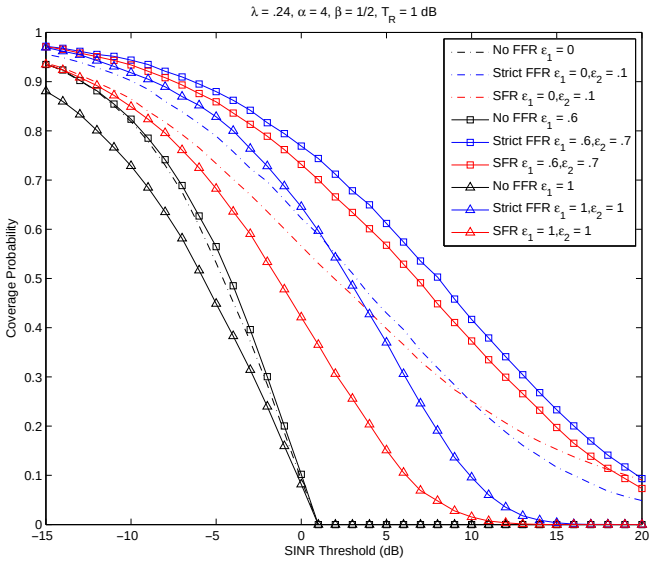

Figure 5.8: A plot of edge user coverage probability with fractional power control for full-reuse, SFR $\beta = 1/2$, and Strict FFR with a range of ϵ_1 and ϵ_2 values.

5.5.5 Transmit Power

One major benefit of fractional power control is the ability to reduce transmit power for mobile users, especially those close to their associated BS. As defined in

the model of Sec. 5.3 this mechanism is controlled by the system parameters ϵ and the generalized power target P. In this section we focus on a specific formulation of P that is utilized by 3GPP standards such as LTE and is a function of ϵ, the max per-subband transmit power P_{max} and the noise power σ^2 [36]. In this case P is given as

$$P = \epsilon \left(\text{SNR}_o + \sigma^2 \right) + P_{max} \left(1 - \epsilon \right), \tag{5.22}$$

where SNR_o is a target threshold in dB above the noise power σ^2 to ensure successful signal decoding at the receiver. Typical ranges for SNR_o are between 0-20 dB [45, 97].

Based on this model for the transmit power target, we now consider the impact on the distribution of the transmit power by utilizing FFR in conjunction with fractional power control. Fig. 5.9 presents the CDF of the typical mobile's transmit power, $\mathbb{P}\left[Pr^{\alpha\epsilon}\right]$, under Strict FFR and a maximum transmit power of 200 mW as a function of ϵ. The shape of the curves highlight the impact of the fractional power control parameter ϵ on the range of the transmit power. For example, with $\epsilon = .2$ the majority of mobiles transmit between 10 and 20 dBm, while for $\epsilon = 1$ the range is 40 dBm. From the point of view for balancing coverage maximization and transmit power utilization, $\epsilon = .6$ provides the largest coverage gains for Strict FFR and SFR and from Fig. 5.9 we see that in this case 50% of the users are 10 dB below the maximum transmit power limit of 23 dBm.

5.6 Uplink FFR for multi-tier networks

An important extension of the analytical model presented in this chapter for a single tier cellular network is to one consisting of multiple tiers of access points with which mobile users can pottentially connect. However while Chapter 3 provided this

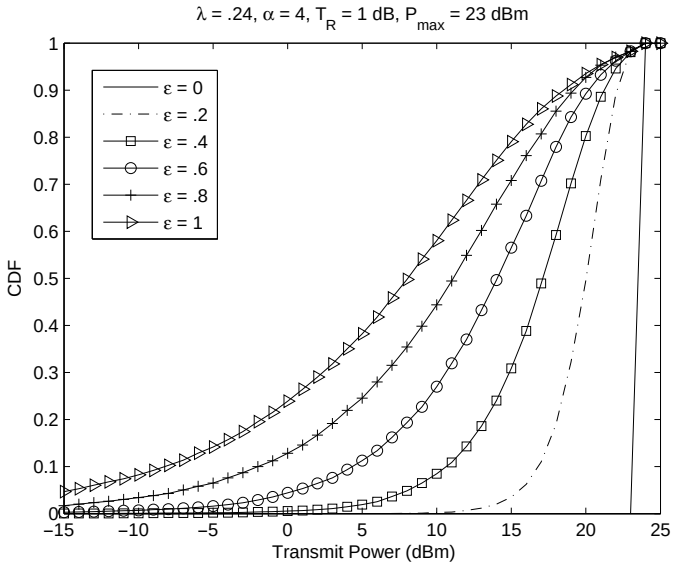

Figure 5.9: The CCDF of the average transmit power per mobile as a function of ϵ with $P_{max} = 23$dBm, $TR = 1$dB, and $\alpha = 4$ pathloss factor.

extension for the downlink of heterogeneous networks, in the uplink the extension is not as straightforward. This is primarily due to the dependence between user and base station locations in the uplink analysis compounded by the introduction of multiple tiers and association policies. This section does not present a comprehensive model for all possible approaches but instead focuses on a specific two-tier scenario relevant to 3GPP standardization efforts for advanced 4G cellular networks.

5.6.1 Multi-tier system model

We consider an OFDMA cellular uplink with 2-tiers of access points (macrocells and picocells for example). Assuming closed access between the tiers, the locations of the users of each tier are modeled as independent spatial Poisson point processes (PPP) of density λ_k. We focus on a typical first-tier macrocell at the origin

and compute the received SINR. The mobile user connected to this typical BS is at a distance r_k and is Rayleigh distributed, the same as Sec. 5.3, and the same pathloss and power control model is assumed. The resulting SINR is given by

$$\text{SINR} = \frac{gPr^{\alpha(\epsilon-1)}}{\sigma^2 + I_{\mathcal{Z}} + I_{\mathcal{Z}}}, \tag{5.23}$$

where for a given set of interfering mobiles $\mathcal{Z}$,

$$I_{\mathcal{Z}} = \sum_{z \in \mathcal{Z}} g_z P_k \left(R_z^{\alpha}\right)^{\epsilon_k} {D_z}^{-\alpha}. \tag{5.24}$$

Thus we see that the SINR at the macro base station is impacted by both macro user interference $I_{\mathcal{Z}}$ and second-tier interference $I_{\mathcal{Z}}$. Each tier can set different received power targets P_k and ϵ_k in addition to the relevant FFR parameters.

As with single-tier modeling, one key question arises from the selection of the distribution of the interfering users' transmit power which is dependent on R_z, the distance to their associated base station. As presented in Chap. 4, two possible choices are Rayleigh or uniform distributions. The Rayleigh distribution is attractive for modeling outdoor macro base station users since it roughly corresponds to uniformly distributed users in the network. However an important practical consideration for heterogeneous networks is the introduction of second-tier access points like picocells into areas with high user concentration often termed 'hotspots'. For these second-tier users located in hotspots the distribution of the distance to their serving base station is taken to be uniform over the area of a circle whose radius is defined as the extent of the hotspot.

5.6.2 Coverage comparison

Based on this model we present the coverage probability for macro users in this two-tier network as a function of the different FFR strategies. The network consists of macro users with density $\lambda_1 = .2$ and hotspot users with density $\lambda_2 = 8\lambda_1$ with pathloss exponent $\alpha = 3.8$, fractional power control exponent $\epsilon = .8$, and σ^2 = -104 dBm. In the case of Strict FFR, first-tier edge users are given subbands that are not allocated to any users of the second-tier, thus completely removing the cross-tier interference. However SFR, utilizes a more efficient allocation strategy in which macro edge users are allocated subbands with higher transmit power than inner macro users by a factor of β_1 and are also subbands utilized by the second-tier users but with lower power by a factor of β_2.

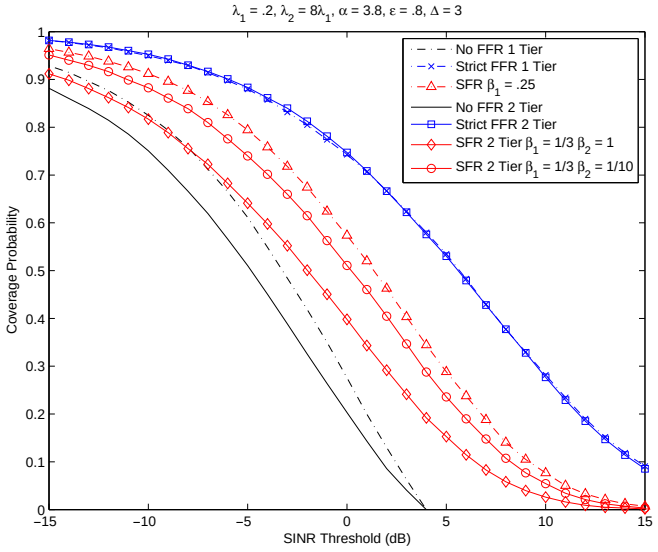

Figure 5.10: Coverage probability comparison between a 1-tier and 2-tier uplink network with universal reuse, Strict FFR, and SFR. In the 2-tier case, the first tier users (macro) have Rayleigh distributed R_z while second tier users have a R_z distribution with a hotspot radius of 200m.

The comparison of this two tier network with a single tier network is given in Fig. 5.10. We note that there is significantly lower coverage probability for no FFR and SFR users in the two-tier network compare to the single-tier network due to the cross-tier interference, however since it is not present, macro edge users under Strict FFR achieve the exact same performance in both networks. However, as mentioned previously in Chapter 3, this strict partitioning of inter and intra-tier resources can be problematic in some practical deployment scenarios where bandwidth resources are expensive and limited, necessitating higher reuse. Interestingly we observe that the two-tier network with SFR for $\beta_2 = 1/10$ greatly improves the performance relative to not applying SFR on the second tier ($\beta_2 = 1$) and in fact almost completely negates the impact of the cross-tier interference to a degree that it achieves similar performance as a single-tier network. Although a single result, this gives insight into motivation for utilizing FFR techniques especially in the context of heterogeneous networks where even strategies requiring static or minimal coordination overhead can achieve significant performance improvements for the users with the worst performance while balancing overall network capacity [29].

5.7 Conclusion

This chapter has presented a new analytical framework for analyzing rate and coverage in the uplink of cellular networks utilizing FFR techniques. These expressions based on the spatial PPP model and are relevant for deployments with irregular topologies and lead to tractable expressions which are a function of the underlying system design parameters. Resulting applications for system design showed how increased coverage and system capacity can be achieved through selection of reuse factor and thresholds in conjunction with power control parameters than a standard

approach not utilizing FFR. Overall SFR was shown to provide the highest capacity gains through high resource efficiency, but the Strict FFR provides better fairness and coverage gains to users at the cell-edge.

Chapter 6

Conclusion

6.1 Summary

This dissertation has presented research on the modeling and analytical evaluation of fractional frequency reuse strategies for multi-tier cellular networks. While these techniques are very relevant for modern networks faced with managing the significant impact of inter-tier and cross-tier interference, developing a fully tractable analytical model is challenging primarily because of the intractability of the hexagonal grid model of base station locations and the inability to capture the nature of non-uniform deployments, with most prior work resorting to simulations to evaluate the performance.

Chapter 2 presented a new tractable, analytical framework that is a function of relevant system parameters for the two principal FFR strategies, Strict FFR and SFR in the cellular downlink based on a spatial Poisson distribution for access point locations. Through a comparison with actual urban base station deployments, the Poisson model was shown to be at least as good and in some cases a better performance predictor compared to the grid model which idealizes real network geometry. In addition, by considering a special case relevant to interference-limited networks, the analytical expressions for the SINR distributions reduce to simple expressions, from which we develop system guidelines which show that while Strict FFR provides better coverage probability for edge users than SFR for low power control factors, a SFR

system can improve its coverage performance by increasing the cell-edge user power control factor, without the loss in spectral efficiency that is inherent in Strict FFR. A strategy for allocating frequency sub-bands to edge users for SFR and FFR based on a chosen threshold T_{FR}, which can be related to network traffic load or coverage requirements was also presented.

Next in Chapter 3 we extended the work to general K-tier cellular network downlinks with closed access and to two-tiers networks for open access. Performance analysis of these networks is much more involved than for a single-tier network because of the need to account for inter-cell and cross-tier interference and the non-uniformity of the access point deployments arising from both topographic and economic reasons. A further complication in heterogeneous network analysis arises from different user association policies. The analytical framework allowed for the evaluation the coverage probability and average rate for users connected to any of tiers as a function of system parameters. As a result, the models give insight into how the FFR parameters and resource partitions can be adapted based on the densities, transmit powers, and resource allocation strategies of the tiers.

Next, in order to extend the framework to the uplink of cellular networks as well, uplink coverage probability for networks using fractional power control, which is a general power control framework used in modern cellular systems, was first derived in Chapter 4. The uplink analysis is significantly more involved than its downlink counterpart because the transmit power of a mobile in the uplink depends upon the distance to its associated base station due to the fractional power control. This dependence is not easy to model accurately and hence leads to some technical challenges in the derivation of the coverage probability. However, this dependence was shown to

be is weak and instead independence between users is assumed which improves the tractability of the system model with minimal impact on the accuracy of the results. Using the same model for the user locations, coverage probability for "regular" BS deployments was also derived, where it is assumed that a BS is uniformly distributed in a circle around its corresponding mobile (independent of other BSs) instead of being uniformly distributed in its Voronoi cell. Interestingly, this analytical result closely approximates the coverage probability computed numerically for the traditional grid model.

Finally, in Chapter 5 the analytical model of the previous chapter was extended to allow the evaluation of uplink cellular networks utilizing fractional power control and FFR through the derivation of the SINR distribution of cell-edge and cell-interior users as a function of network and FFR system parameters. General insights are presented for the metrics of coverage probability, average rate, resource allocation, transmit power, and the interdependence of system design parameters. From the derived expressions the coverage probability gains achieved with Strict FFR for edge users relative to universal reuse and SFR can be quantified, as well as the tradeoff SFR can achieve in terms of coverage performance for edge and inner users through greater frequency efficiency than Strict FFR and selection of a power control factor and contrasted with their performance in the downlink. Expressions for average rate were provided, illustrating how the analytical model can be related to traffic load or coverage requirements and used to allocate frequency subbands under Strict FFR and SFR to achieve capacity gains over standard full frequency reuse. The chapter concluded with an extension to the uplink of two-tier networks with closed access.

6.2 Future Work

Building on this framework, future research using the Poisson model can move towards evaluating ICIC strategies using base station cooperation to implement FFR techniques dynamically alongside resource allocation strategies to adapt to different channel conditions and user traffic loads in each cell [20, 25, 48, 101]. Self-organizing networks are an important component of future wireless standards such as 3GPP LTE-Advanced as the complexity of operating them increases with the number of active access points. Efficient operation which can adapt to traffic or deployment scenarios is not only important from an economic perspective, but is also critical to developing networks which are natural or man-made disaster-tolerant. A cohesive framework would allow for research into the dynamics and implications of FFR along with other important cellular network research including handoffs, base station cooperation, and FFR in conjunction with relays and/or femtocells. Besides developing tractable analytical tools, one advantage of utilizing a network model based on a Poisson or other random model is that it is more relevant for non-uniform deployments since the location and size of coordinating clusters of base stations has a large impact on achievable results, something which cannot be captured with a regular grid model for locations [65, 71].

Another interesting application of FFR is in the context of carrier aggregation, in which multiple bandwidth partitions located at different center carrier frequencies (even if they are not contiguous) are simultaneously utilized, increasing potential data rates for users in the uplink or downlink [94, 107]. This is very practical for operators who desire to utilize all of their different spectrum holdings in as flexible a manner as possible. However challenges arise in determining how to optimally

aggregate the different bandwidth partitions. The different bandwidth partitions may have greatly different pathloss characteristics depending on how far separated the center frequencies are and some partitions may be better suited for interior uses instead of at the cell edge or restricted to only certain tiers of access points. Applying FFR techniques could potentially lead to greater flexibility for operators by extending the range of applicability for different carrier aggregation modes and different FFR parameters could be optimized based on the carrier frequency or size of the bandwidth partition.

Bibliography

[1] 3GPP. TS 36.331: Radio resource control (RRC) protocol specification. March 2008.

[2] 3GPP. TR 36.902: Evolved universal terrestrial radio access network (E-UTRAN) self-configuring and self-optimizing network (SON) use cases and solutions (release 9). Jun. 2010.

[3] A. Agrawal, J.G. Andrews, J.M. Cioffi, and T. Meng. Iterative power control for imperfect successive interference cancellation. *IEEE Transactions on Wireless Communications*, 4(3):878–884, May 2005.

[4] M. Al-Shalash, F. Khafizov, and Zhijun C. Interference constrained soft frequency reuse for uplink ICIC in LTE networks. In *Proc. IEEE Intl. Symp. on Personal Indoor and Mobile Radio Communications*, pages 1882–1887, Istanbul, Turkey, Sept. 2010.

[5] Alcatel-Lucent. R4-115702: Release 11 FeICIC work scope. *3GPP TSG RAN WG4 Meeting #41*, Nov. 2011.

[6] S.H. Ali and V.C.M. Leung. Dynamic frequency allocation in fractional frequency reused OFDMA networks. *IEEE Trans. on Wireless Communications*, 8(8):4286–4295, August 2009.

[7] A. Alsawah and I. Fijalkow. Optimal frequency-reuse partitioning for ubiquitous coverage in cellular systems. In *Proc. European Signal Processing Conf.*,

Lausanne, Switzerland.

[8] J. G. Andrews, F. Baccelli, and R. K. Ganti. A new tractable model for cellular coverage. In *Proc. Allerton Conf. on Communication, Control, and Computing*, pages 1204–1211, Monticello, Illinois, Oct. 2010.

[9] J.G. Andrews. Interference cancellation for cellular systems: a contemporary overview. *IEEE Wireless Communications Magazine*, 12(2):19–29, Apr. 2005.

[10] J.G. Andrews, F. Baccelli, and R.K. Ganti. A tractable approach to coverage and rate in cellular networks. *IEEE Transactions on Communications*, 59(11):3122–3134, Nov. 2011.

[11] M. Andrews, V. Capdevielle, A. Feki, and P. Gupta. Autonomous spectrum sharing for mixed LTE femto and macro cells deployments. In *IEEE Conference on Computer Communications Workshops*, pages 1–5, March 2010.

[12] M. Assad. Optimal fractional frequency reuse (FFR) in multicellular OFDMA system. In *Proc. IEEE Vechicular Technology Conf.*, pages 1–5, Calgary, Alberta, September 2008.

[13] M. Assad and N.U.L. Hassan. Optimal fractional frequency reuse (FFR) and resource allocation in multiuser OFDMA system. In *Proc. Intl. Conf. on Information and Communication Technologies*, pages 88–92, August 2009.

[14] F. Baccelli, M. Klein, M. Lebourges, and S. Zuyev. Stochastic geometry and architecture of communication networks. *J. Telecommunication Systems*, 7(1):209–227, 1997.

[15] K. Begain, G.I. Rozsa, A. Pfening, and M. Telek. Performance analysis of GSM networks with intelligent underlay-overlay. In *Proc. Intl. Symp. on Computers and Communications*, pages 135–141, Taormina, Italy, July 2002.

[16] F.F. Bernardo, R.R. Agusti, J.J. Perez-Romero, and O.O. Sallent. Intercell interference management in OFDMA networks: A decentralized approach based on reinforcement learning. *IEEE Transactions on Systems, Man, and Cybernetics*, 41(6):968–976, Nov. 2011.

[17] Zubin Bharucha and Harald Haas. The distribution of path losses for uniformly distributed nodes in a circle. *Rec. Lett. Commun.*, 2008:1–4, 2008.

[18] G. Boudreau, J. Panicker, N. Guo, R. Chang, N. Wang, and S. Vrzic. Interference coordination and cancellation for 4G networks. *IEEE Communications Magazine*, 47(4):74–81, Apr. 2009.

[19] T.X. Brown. Cellular performance bounds via shotgun cellular systems. *IEEE Journal on Sel. Areas in Communications*, 18(11):2443–2455, Nov. 2000.

[20] H. Sun C. Chen. Adaptive frequency reuse in IEEE 802.16m. *IEEE C802.16m-08/702*, 2008.

[21] C.U. Castellanos, D.L. Villa, C. Rosa, K.I. Pedersen, F.D. Calabrese, P.-H. Michaelsen, and J. Michel. Performance of uplink fractional power control in UTRAN LTE. In *IEEE Vehicular Technology Conference*, pages 2517–2521, May 2008.

[22] V. Chandrasekhar and J. Andrews. Spectrum allocation in tiered cellular networks. *IEEE Transactions on Communications*, 57(10):3059 –3068, Oct.

2009.

[23] V. Chandrasekhar, J. Andrews, and A. Gatherer. Femtocell networks: a survey. *IEEE Communications Magazine*, 46(9):59–67, Sept. 2008.

[24] R.Y. Chang, Z. Tao, J. Zhang, and C. Kuo. A graph approach to dynamic fractional frequency reuse (FFR) in multi-cell OFDMA networks. In *Proc. IEEE Intl. Conf. on Communications*, pages 1–6, Dresden, Germany, June 2009.

[25] C. Chen. Proposed text for interference mitigation in IEEE 802.16m AWD. *IEEE C802.16m-09-1022r2*, 2009.

[26] L. Chen and D. Yuan. Generalizing FFR by flexible sub-band allocation in OFDMA networks with irregular cell layout. In *Proc. IEEE Wireless Communications and Networking Conf.*, pages 1–5, Sydney, Australia, April 2010.

[27] W. Choi and J.G. Andrews. The capacity gain from intercell scheduling in multi-antenna systems. *IEEE Transactions on Wireless Communications*, 7(2):714–725, Feb. 2008.

[28] M. Coupechoux and J.M. Kelif. How to set the fractional power control compensation factor in LTE? In *Proc. IEEE Sarnoff Symposium*, pages 1–5, May 2011.

[29] A. Dalal, Hailong Li, and D.P. Agrawal. Fractional frequency reuse to mitigate interference in self-configuring LTE-femtocells network. In *IEEE International Conference on Mobile Adhoc and Sensor Systems*, pages 49–54, Oct. 2011.

[30] H. S. Dhillon, R. K. Ganti, F. Baccelli, and J. G. Andrews. Modeling and analysis of K-tier downlink heterogeneous cellular networks. *IEEE Journal on Selected Areas in Comm.*, Apr. 2012.

[31] H.S. Dhillon, R.K. Ganti, and J.G. Andrews. A tractable framework for coverage and outage in heterogeneous cellular networks. In *Proc., Information Theory and Applications Workshop (ITA)*, pages 1–6, Feb. 2011.

[32] S.N. Donthi and N.B. Mehta. Joint performance analysis of channel quality indicator feedback schemes and frequency-domain scheduling for LTE. *IEEE Transactions on Vehicular Technology*, 60(7):3096–3109, Sept. 2011.

[33] K. Doppler, C. Wijting, and K. Valkealahti. Interference aware scheduling for soft frequency reuse. In *Proc. IEEE Vehicular Technology Conf.*, pages 1–5, Barcelona, Apr. 2009.

[34] S.-E. Elayoubi, O. Ben Haddada, and B. Fourestie. Performance evaluation of frequency planning schemes in ofdma-based networks. *Wireless Communications, IEEE Transactions on*, 7(5):1623 –1633, may 2008.

[35] S.E. Elayoubi and O. Ben Haddada. Uplink intercell interference and capacity in 3G LTE systems. In *Proc. IEEE Intl. Conf. on Networks*, pages 537–541, Adelaide, Australia, November 2007.

[36] Ericsson. R1-074850: Uplink power control for E-UTRA - range and representation of P0. *3GPP TSG RAN WG1 Meeting #51*, Novemeber 2007.

[37] D.D. Falconer, F. Adachi, and B. Gudmundson. Time division multiple access methods for wireless personal communications. *IEEE Communications*

Magazine, 33(1):50–57, Jan. 1995.

[38] L. Fang and X. Zhang. Optimal fractional frequency reuse in OFDMA based wireless networks. In *Proc. Intl. Conf. on Wireless Communications, Networking and Mobile Computing*, pages 1–4, Crete Island, Greece, October 2008.

[39] Z.C. Fluhr and E. Nussbaum. Switching plan for a cellular mobile telephone system. *IEEE Transactions on Vehicular Technology*, 22(4):197–202, Nov. 1973.

[40] H. Fujii and H. Yoshino. Theoretical capacity and outage rate of OFDMA cellular system with fractional frequency reuse. In *Proc. IEEE Vehicular Technology Conf.*, pages 1676–1680, Singapore, May 2008.

[41] M. Fushiki, T. Ohseki, and S. Konishi. Throughput gain of fractional frequency reuse with frequency selective scheduling in SC-FDMA uplink cellular system. In *IEEE Vehicular Technology Conference*, pages 1–5, Sep. 2011.

[42] A. Galindo-Serrano and L. Giupponi. Distributed Q-Learning for interference control in OFDMA-based femtocell networks. In *IEEE Vehicular Technology Conference*, pages 1–5, May 2010.

[43] R. K. Ganti, Francois Baccelli, and J. G. Andrews. A new way of computing rate in cellular networks. In *Proc., IEEE International Conference on Communications*, Kyoto, Jun. 2011.

[44] R. K. Ganti and M. Haenggi. Spatial analysis of opportunistic downlink relaying in a two-hop cellular system, 2009. submitted.

[45] A. Ghosh, J. Zhang, J. G. Andrews, and R. Muhamed. *Fundamentals of LTE*. Prentice Hall, 2010.

[46] S. Govindasamy and D. H. Staelin. Asymptotic spectral efficiency of the uplink in spatially distributed wireless networks with multi-antenna base stations. *CoRR*, abs/1102.1232, 2011.

[47] M. Haenggi, J.G. Andrews, F. Baccelli, O. Dousse, and M. Franceschetti. Stochastic geometry and random graphs for the analysis and design of wireless networks. *IEEE Journal on Sel. Areas in Communications*, 27(7):1029–1046, Sept. 2009.

[48] S. Hamouda, C. Yeh, J. Kim, S. Wooram, and D. Se. Kwon. Dynamic hard fractional frequency reuse for mobile WiMAX. pages 1–6, Galveston, Texas, March 2009.

[49] P. Hatrack and J.M. Holtzman. Reduction of other-cell interference with integrated interference cancellation/power control. In *IEEE Vehicular Technology Conference*, volume 3, pages 1842–1846, May 1997.

[50] J.D. Herdtner and E.K.P. Chong. Analysis of a class of distributed asynchronous power control algorithms for cellular wireless systems. *IEEE Journal on Selected Areas in Communications*, 18(3):436–446, Mar. 2000.

[51] A. Hernandez, I. Guio, and A. Valdovinos. Interference management through resource allocation in multi-cell OFDMA networks. In *Proc. IEEE Vehicular Technology Conf.*, pages 1–5, Barcelona, April 2009.

[52] N. Himayat, S. Talwar, A. Rao, and R. Soni. Interference management for 4G cellular standards [WIMAX/LTE update]. *IEEE Communications Magazine*, 48(8):86 –92, 2010.

[53] H. Holma and A. Toskala. *WCDMA for UMTS: Radio Access for Third Generation Mobile Communications, Revised Edition.* Wiley, 2001.

[54] K. Huang, V.K.N. Lau, and Y. Chen. Spectrum sharing between cellular and mobile ad hoc networks: transmission-capacity trade-off. *IEEE Journal on Selected Areas in Communications*, 27(7):1256–1267, Sept. 2009.

[55] Huawei. R1-050507: Soft frequency reuse scheme for UTRAN LTE. *3GPP TSG RAN WG1 Meeting #41*, May 2005.

[56] R. Irmer, H. Droste, P. Marsch, M. Grieger, G. Fettweis, S. Brueck, H.P. Mayer, L. Thiele, and V. Jungnickel. Coordinated multipoint: Concepts, performance, and field trial results. *IEEE Communications Magazine*, 49(2):102 –111, Feb. 2011.

[57] S.A. Jafar, G.J. Foschini, and A.J. Goldsmith. PhantomNet: exploring optimal multicellular multiple antenna systems. In *IEEE Vehicular Technology Conference*, volume 1, pages 261 – 265 vol.1, Sept. 2002.

[58] N. Jindal, S. Weber, and J.G. Andrews. Fractional power control for decentralized wireless networks. *IEEE Transactions on Wireless Communications*, 7(12):5482 –5492, Dec. 2008.

[59] H. Jo, P. Xia, and J. G. Andrews. Downlink femtocell networks: Open or closed? In *Proc., IEEE International Conference on Communications*, Kyoto,

Jun. 2011.

[60] M.K. Karakayali, G.J. Foschini, and R.A. Valenzuela. Network coordination for spectrally efficient communications in cellular systems. *IEEE Wireless Communications Magazine*, 13(4):56 –61, Aug. 2006.

[61] J.M. Kelif and M. Coupechoux. Impact of topology and shadowing on the outage probability of cellular networks. In *Proc. IEEE International Conference on Communications*, pages 1–6, June 2009.

[62] D. Kim. On the convergence of fixed-step power control algorithms with binary feedback for mobile communication systems. *IEEE Transactions on Communications*, 49(2):249–252, Feb. 2001.

[63] S. G. Kim, K. Cho, D. Yoon, Y. J. Ko, and J. K. Kwon. Performance analysis of downlink inter cell interference coordination in the LTE-Advanced system. In *Proc. Fourth International Conference on Digital Telecommunications*, pages 30–33, July20–25, 2009.

[64] C. A. Kin, A. Maaref, and J. Zhang. Opportunistic cell edge selection in multi-cell OFDMA networks. In *IEEE Global Telecommunications Conference*, pages 1–6, Dec. 2009.

[65] D. Lee, H. Seo, B. Clerckx, E. Hardouin, D. Mazzarese, S. Nagata, and K. Sayana. Coordinated multipoint transmission and reception in LTE-advanced: deployment scenarios and operational challenges. *IEEE Communications Magazine*, 50(2):148–155, Feb. 2012.

[66] H.C. Lee, D.C. Oh, and Y. H. Lee. Mitigation of inter-femtocell interference with adaptive fractional frequency reuse. In *Proc., IEEE International Conference on Communications*, pages 1 –5, May 2010.

[67] J. Lee, S. Bae, Y. Kwon, and M. Chung. Interference analysis for femtocell deployment in OFDMA systems based on fractional frequency reuse. *IEEE Communications Letters*, 2011.

[68] T. Lee, J. Yoon, S. Lee, and J. Shin. Interference management in OFDMA femtocell systems using fractional frequency reuse. In *Proc. International Conference on Communications, Circuits and Systems*, pages 176 –180, 2010.

[69] N. Levy and S. Shamai. Information theoretic aspects of users' activity in a Wyner-like cellular model. *IEEE Transactions on Information Theory*, 56(5):2241–2248, May 2010.

[70] J. Li, N.B. Shroff, and E.K.P. Chong. A reduced-power channel reuse scheme for wireless packet cellular networks. *IEEE/ACM Trans. on Networking*, 7(6):818–832, Dec. 1999.

[71] R. Madan, J. Borran, A. Sampath, N. Bhushan, A. Khandekar, and Tingfang Ji. Cell association and interference coordination in heterogeneous LTE-A cellular networks. *IEEE Journal on Selected Areas in Communications*, 28(9):1479–1489, Dec. 2010.

[72] X. Mao, A. Maaref, and K. H. Teo. Adaptive soft frequency reuse for inter-cell interference coordination in SC-FDMA based 3GPP LTE uplinks. In *Proc., IEEE Global Telecomm. Conference*, pages 1–6, Dec. 2008.

[73] M.M.S. Marwangi, N. Fisal, S.K.S. Yusof, R.A. Rashid, A.S.A. Ghafar, F.A. Saparudin, and N. Katiran. Challenges and practical implementation of self-organizing networks in lte/lte-advanced systems. In *International Conference on Information Technology and Multimedia*, pages 1–5, Nov. 2011.

[74] S. Mukherjee. Analysis of UE outage probability and macrocellular traffic offloading for WCDMA macro network with femto overlay under closed and open access. In *Proc., IEEE International Conference on Communications*.

[75] S. Mukherjee. UE coverage in LTE macro network with mixed CGS and open access femto overlay. In *Proc., IEEE International Conference on Communications*.

[76] S. Mukherjee. UE coverage in LTE macro network with mixed CSG and open access femto overlay. In *IEEE International Conference on Communications Workshops*, pages 1–6, Jun. 2011.

[77] R. Mullner, C.F. Ball, K. Ivanov, J. Lienhart, and P. Hric. Contrasting open-loop and closed-loop power control performance in UTRAN LTE uplink by UE trace analysis. In *Proc. IEEE International Conference on Communications*, pages 1–6, June 2009.

[78] T. Novlan, J. Andrews, I. Sohn, R.K. Ganti, and A. Ghosh. Comparison of fractional frequency reuse approaches in the OFDMA cellular downlink. In *Proc. IEEE Globecom*, pages 1–5, Miami, Florida, December 2010.

[79] T. D. Novlan, H. S. Dhillon, and J. G. Andrews. Analytical modeling of uplink cellular networks, 2012. submitted, *IEEE Transactions on Wireless Communications*.

[80] T.D. Novlan, R.K. Ganti, J.G. Andrews, and A. Ghosh. A new model for coverage with fractional frequency reuse in OFDMA cellular networks. In *Proc. IEEE Globecom*, Houston, Dec. 2011.

[81] T.D. Novlan, R.K. Ganti, A. Ghosh, and J.G. Andrews. Analytical evaluation of fractional frequency reuse for OFDMA cellular networks. *IEEE Transactions on Wireless Communications*, 10(12):4294–4305, Dec. 2011.

[82] O. Onireti, F. Heliot, and M.A. Imran. Closed-form approximation for the trade-off between energy efficiency and spectral efficiency in the uplink of cellular network. *Proc. European Wireless Conference*, pages 1 –6, Apr. 2011.

[83] P. Patel and J. Holtzman. Analysis of a simple successive interference cancellation scheme in a DS/CDMA system. *IEEE Journal on Selected Areas in Communications*, 12(5):796–807, Jun. 1994.

[84] Picochip. The case for home base stations. *white paper*, April 2007.

[85] M. Porjazoski and B. Popovski. Analysis of intercell interference coordination by fractional frequency reuse in LTE. In *Proc. International Conference on Software, Telecommunications and Computer Networks*, pages 160 –164, 2010.

[86] C. Prehofer and C. Bettstetter. Self-organization in communication networks: principles and design paradigms. *IEEE Communications Magazine*, 43(7):78–85, Jul. 2005.

[87] Qualcomm. LTE advanced: heterogeneous networks. *white paper*, Jan 2011.

[88] M. Rahman and H. Yanikomeroglu. Enhancing cell-edge performance: a downlink dynamic interference avoidance scheme with inter-cell coordination. *IEEE Trans. on Wireless Communications*, 9(4):1414–1425, April 2010.

[89] A.M. Rao. Reverse link power control for managing inter-cell interference in orthogonal multiple access systems. In *Proc. IEEE Vehicular Technology Conference*, pages 1837–1841, Oct. 2007.

[90] T. S. Rappaport. *Wireless Communications Principles and Practice, 2nd ed.* Prentice Hall, 2002.

[91] B. Rengarajan, A.L. Stolyar, and H. Viswanathan. Self-organizing dynamic fractional frequency reuse on the uplink of OFDMA systems. In *Annual Conference on Information Sciences and Systems*, pages 1–6, Mar. 2010.

[92] B. Sadiq, R. Madan, and A. Sampath. Downlink scheduling for multiclass traffic in LTE. *EURASIP Journal on Wireless Communications and Networking*.

[93] A. Saleh, A. Rustako, and R. Roman. Distributed antennas for indoor radio communications. *IEEE Transactions on Communications*, 35(12):1245–1251, December 1987.

[94] Z. Shen, A. Papasakellariou, J. Montojo, D. Gerstenberger, and Fangli Xu. Overview of 3GPP LTE-advanced carrier aggregation for 4G wireless communications. *Communications Magazine, IEEE*, 50(2):122–130, Feb. 2012.

[95] O. Simeone, O. Somekh, H.V. Poor, and S. Shamai. Local base station cooperation via finite-capacity links for the uplink of linear cellular networks. *IEEE Transactions on Information Theory*, 55(1):190–204, Jan. 2009.

[96] A. Simonsson. Frequency reuse and intercell interference co-ordination in E-UTRA. In *IEEE Vehicular Technology Conference*, pages 3091–3095, April 2007.

[97] A. Simonsson and A. Furuskar. Uplink power control in LTE - overview and performance, principles and benefits of utilizing rather than compensating for SINR variations. In *Proc. IEEE Vehicular Technology Conference*, pages 1 –5, Sept. 2008.

[98] C.Y. Sin and V.K.N. Lau. On the theoretical analysis of optimal cellular systems design with multi-user detection in slow flat fading channel - uplink analysis. In *Proc. IEEE Vehicular Technology Conference*, volume 1, pages 182–186, May 2006.

[99] O. Somekh and S. Shamai. Shannon-theoretic approach to a Gaussian cellular multiple-access channel with fading. *IEEE Transactions on Information Theory*, 46(4):1401–1425, July 2000.

[100] O. Somekh, O. Simeone, Y. Bar-Ness, A.M. Haimovich, and S. Shamai. Cooperative multicell zero-forcing beamforming in cellular downlink channels. *IEEE Transactions on Information Theory*, 55(7):3206–3219, Jul. 2009.

[101] K. Son, S. Chong, and G. de Veciana. Dynamic association for load balancing and interference avoidance in multi-cell networks. *IEEE Transactions on Wireless Communications*, 8(7):3566–3576, July 2009.

[102] M. Sternad, T. Ottosson, A. Ahlen, and A. Svensson. Attaining both coverage and high spectral efficiency with adaptive OFDM downlinks. In *Proc. IEEE*

Vehicular Technology Conf., volume 4, pages 2486–2490, Orlando, Florida, Oct. 2003.

[103] A.L. Stolyar and H. Viswanathan. Self-organizing dynamic fractional frequency reuse for best-effort traffic through distributed inter-cell coordination. In *IEEE INFOCOM*, pages 1287–1295, Apr. 2009.

[104] D. Stoyan, W. Kendall, and J. Mecke. *Stochastic Geometry and Its Applications, 2nd Edition*. John Wiley and Sons, 1996.

[105] S. Verdu. Optimum multiuser signal detection, Aug. 1986. Ph.D. diss., Univ. of IL, Urbana-Champaign.

[106] F. Wamser, D. Mittelsta, and D. Staehle. Soft frequency reuse in the uplink of an OFDMA network. In *Proc. IEEE Vehicular Technology Conf.*, pages 1–5, Taipei, Taiwan, May 2010.

[107] H. Wang, C. Rosa, and K. Pedersen. Performance of uplink carrier aggregation in LTE-advanced systems. In *IEEE Vehicular Technology Conference Fall*, pages 1–5, Sept. 2010.

[108] J.F. Whitehead. Signal-level-based dynamic power control for co-channel interference management. In *Proc. IEEE Vehicular Technology Conference*, pages 499 –502, may 1993.

[109] X. Wu, S. Tavildar, S. Shakkottai, T. Richardson, J. Li, R. Laroia, and A. Jovicic. FlashLinQ: A synchronous distributed scheduler for peer-to-peer ad hoc networks. In *Allerton Conference on Communication, Control, and Computing*, pages 514–521, Oct. 2010.

[110] A.D. Wyner. Shannon-theoretic approach to a Gaussian cellular multiple-access channel. *IEEE Transactions on Information Theory*, 40(6):1713–1727, Nov. 1994.

[111] P. Xia, V. Chandrasekhar, and J.G. Andrews. Open vs. closed access femtocells in the uplink. *IEEE Transactions on Wireless Communications*, 9(12):3798 – 3809, December 2010.

[112] H. Xiao and Z. Feng. A novel fractional frequency reuse architecture and interference coordination scheme for multi-cell OFDMA networks. In *procvtc*, pages 1 –5, May 2010.

[113] W. Xiao, R. Ratasuk, A. Ghosh, R. Love, Y. Sun, and R. Nory. Uplink power control, interference coordination and resource allocation for 3GPP E-UTRA. In *Proc. IEEE Vehicular Technology Conference*, pages 1–5, Sept. 2006.

[114] Z. Xie and B. Walke. Performance analysis of reuse partitioning techniques in OFDMA based cellular radio networks. In *Proc. IEEE International Conference on Telecommunications*, pages 272 –279, 2010.

[115] J. Xu, J. Zhang, and J.G. Andrews. On the accuracy of the Wyner model in cellular networks. *IEEE Transactions on Wireless Communications*, 10(9):3098–3109, Sep. 2011.

[116] G. Yanhui, A.Y.S. Lam, and V.O.K. Li. Performance bounds of opportunistic scheduling in wireless networks. In *IEEE Global Telecommunications Conference*, pages 1–5, Dec. 2010.

[117] R.D. Yates. A framework for uplink power control in cellular radio systems. *IEEE Journal on Selected Areas in Communications*, 13(7):1341–1347, Sep. 1995.

[118] J. Zhang and J. Andrews. Distributed antenna systems with randomness. *IEEE Transactions on Wireless Communications*, 7(9):3636 –3646, 2008.

[119] J. Zhang, R. Chen, J.G. Andrews, and R.W. Heath. Coordinated multi-cell MIMO systems with cellular block diagonalization. In *Asilomar Conference on Signals, Systems and Computers*, pages 1669–1673, Nov. 2007.

Vita

Thomas David Novlan was born in El Paso, Texas. He has been a recipient of the Virginia and Ernest Cockrell, Jr. Graduate Fellowship since 2007. He completed his B.S. with high honors at The University of Texas, Austin in 2007 and received his M.S. at The University of Texas, Austin in 2009. He was an intern at Qualcomm during the summer of 2008 working on a spectrum sensing cognitive radio prototype and at Intel in 2010 working on system-level and link-level simulators for IEEE 802.11af-based networks. His current research focuses on the modeling and analysis of frequency allocation strategies for heterogeneous cellular networks. His research is supported by AT&T Laboratories where he was an intern from May 2011 to May 2012 working on advanced interference management techniques for heterogeneous wireless networks.

Permanent address: 12706 Oro Valley Trail
Austin, Texas 78729

This dissertation was typeset with LaTeX[†] by the author.

[†]LaTeX is a document preparation system developed by Leslie Lamport as a special version of Donald Knuth's TeX Program.